PONTIFICIA UNIVERSIDAD CATOLICA DE CHILE

SCHOOL OF ENGINEERING

EVALUATION OF THE INFLUENCE OF SHEAR KEYS ON THE SEISMIC BEHAVIOR OF CHILEAN BRIDGES

JOSÉ DE JESÚS WILCHES ESTÁN

Thesis submitted to the Office of Graduate Studies in partial fulfillment of the requirements for the Degree of Doctor in Engineering Sciences

Advisors:

HERNÁN SANTA MARÍA OYANEDEL
ROBERTO T. LEON

Santiago de Chile, December, 2021

PONTIFICIA UNIVERSIDAD CATOLICA DE CHILE

SCHOOL OF ENGINEERING

EVALUATION OF THE INFLUENCE OF SHEAR KEYS ON THE SEISMIC BEHAVIOR OF CHILEAN BRIDGES

JOSÉ DE JESÚS WILCHES ESTÁN

Members of the Committee

HERNÁN SANTA MARÍA Hernan Santa Maria Pumenay

ROBERTO LEÓN Roberto Leon

JOSÉ RESTREPO Jose I. Restrepo

MATÍAS HUBE Matias Hube G.

MATÍAS VALENZUELA Matias Valenzuela Saavedra

YADRAN ETEROVIC Yadran Eterovic S.

Thesis submitted to the Office of Graduate Studies in partial fulfillment of the requirements for the Degree of Doctor in Engineering Sciences.

Santiago of Chile, December, 2021

DEDICATION

To God, to my parents José and Emilse for teaching me the value of perseverance, to my wife Marcela and my daughter Isabella who are my inspiration. To my sisters Frinia and Maria Jose and my niece Emily who taught me to love the differences.

ACKNOWLEDGMENTS

Many individuals and institutions have contributed to this research and my graduate studies. Although I certainly cannot fully thank them in few pages, I would like to recognize, at least briefly, their assistance and support.

Firstly, I wish to express my sincere gratitude to my advisors Dr. Hernán Santa María, and Dr. Roberto T. Leon for their continuous support, motivation, and knowledge. I am very thankful for the unique opportunity and the privilege of working on this remarkable research project that has become one of the best experiences in my professional career and my personal life.

I would also like to thank Professors Rafael Riddell and Carl Lüders (Professors Emeritus of the Pontificia Universidad Católica de Chile), for their insightful comments and dedication to this research. Additionally, I would like to thank the rest of the committee members, Doctors José I. Restrepo, Matías Hube, Matías Valenzuela and Gustavo Lagos.

I want to thank my whole family for believing in me at all times. In particular, my grandmother Frinia Delgado (RIP), my uncles Nelson Stanp (RIP) and Buenaventura Wilches (RIP).

A special thanks to my uncle Juan Wilches and my aunts Paulina and Policarpa Wilches for motivating me and helping me become an engineer. I am very thankful with the Quinchanegua Cubides family for their continued motivation.

I wish to acknowledge the funding provided by ANID (Chilean National Agency for Research and Development) through the ANID Doctorate Scholarship and the Research Center for Integrated Disaster Risk Management (CIGIDEN) ANID/FONDAP 15110017. ANID has funded my double doctoral studies at Pontificia Universidad Católica de Chile and Virginia Tech. I also want to thank the faculty of the Department of Structural and Geotechnical Engineering of the Pontificia Universidad Católica de Chile and of Virginia Tech University.

Finally, I want to take this opportunity to thank some special friends, William Castro, José Colombo, Jairo Montaño, and Carlos Arrate, who helped and supported me throughout this process.

TABLE OF CONTENTS

LIST OF TABLES

LIST OF FIGURES

1. CHAPTER 1

INTRODUCTION

1.1. Background and motivation

In recent decades, many regions of the world have been affected by earthquakes that have resulted in significant damage to transportation networks and to bridges in particular. Notable among these in the past three decades are the 1989 Loma Prieta [1] and 1994 Northridge [2] events in the USA, the 1995 Hyogo-ken Nanbu [3] and 2011 Tohoku [4] in Japan, the 1999 Chi-Chi [5] in Taiwan, and the 2011 Christchurch [6] in New Zealand.

Chile has not been an exception as it is located next to a 5,000 km long fault with a subduction rate of more than 7 cm/year, making it the most active subduction zone in the world [7]. Throughout its history, the country has been hit by severe earthquakes that has shown that road bridges designed under modern design codes are structures vulnerable to failures or collapses. This has been attributed to conceptual problems in the design codes and the lack of attention during the development of design projects. Table 1-1 shows the chronology of the most important earthquakes in Chile and their influence on the development of the Chilean seismic codes.

Tabla 1-1. Chronology of earthquakes and resulting code changes.

Date	M_w	Event and Resulting Code Changes
1570	~7.5	Epicenter on the high seas; destroyed Concepción; large tsunami.
1647	~8	Shook Santiago with extraordinary violence; demolished most major buildings and houses.
1730	~8.7	Considerable damage to the buildings between La Serena and Concepción.
1835	~8.5	Affected Concepción and Talcahuano with a combination of earthquake, tsunami, and volcanic activity.
1868	~9	Affected the Arica region and the Chilean coast as well as a large part of southern Peru.
1906	~8.2	Affected Valparaíso; intensity in the area close to the epicenter has been estimated as IX in the Mercalli Modified Intensity Scale (MMI). **Codes:** The government of Chile creates the first scientific commission for the study of earthquakes.
1922	~8.5	Affected Vallenar and Huasco, Atacama region; followed by a devastating tsunami.
1928	~8.3	Centered on the Maule region; destroyed Talca. **Codes:** The government passed a law that created a committee to propose regulations related to earthquakes. In 1935, a construction code known as the General Ordinance of Constructions and Urbanizations was made official.
1939	8.3	Affected Chillán; generated most human losses and material damage in Chilean history; felt strongly as far as Buenos Aires. **Codes:** The government appointed several committees to study the current seismic codes and propose modifications. These modifications came into force officially in 1949. Resulted in the creation of the Development and Reconstruction Corporation (CORFO) to start the industrialization of the country.
1943	8.2	Affected Ovalle; tsunami accompanied the earthquake.
1958	7	Significant damage in the highway infrastructure and hydroelectric plants in the metropolitan region of Santiago. **Codes:** A governmental body known as INDITECNOR, which eventually changed its name to the National Standards Institute (INN), began to review the design practices of the Ordinance of Construction.
1960	9.5	The largest earthquake ever recorded destroyed Valdivia. It generated tsunamis that devastated the coasts of Japan, Hawaii, the Philippines, and the west coast of the United States. **Codes:** Creation in 1963 of the Chilean Association of Seismology and Earthquake Engineering (ACHISINA).
1965	7.4	Affected the central zone of Chile. Major damage to adobe and masonry structures. **Codes:** Development of the first seismic design standard for buildings begins, issued in 1972.
1971	7.7	Affected Illapel. Many old adobe and brick buildings collapsed. **Codes:** Better construction techniques and materials are established in all types of buildings, such as reinforced masonry and reinforced concrete buildings.
1985	7.8	Considerable damage to adobe buildings, reinforced concrete and bridge failures in Algarrobo and the entire central zone of Chile. **Codes:** Improvement of seismic codes, especially in construction methods and details. Development of a new, modern seismic design code, which was issued in 1996.
1996	7.7	Affected the north of Chile, especially Antofagasta. Landslides were recorded, and communications collapsed.
2007	7.8	Damage to government buildings in Tocopilla, as well as essential road routes.
2010	8.8	Collapses of buildings and bridges in the Maule region. Damage in extensive areas due to soil liquefaction. **Codes:** Modifications to the design and construction codes. Greater use of isolated structures and seismic protection systems. Important changes were generated in the bridges design codes.
2015	8.5	Affected the Coquimbo region, produced displacements of more than 1 m west of Chile.

During Chilean earthquakes, many highway bridges have been damaged or destroyed. In the 1960 Valdivia earthquake (M_w 9.5) about 20 bridges were damaged [8]. The main damage were failures in the abutments due to the collapse of the embankments, failures in the concrete blocks at the ends of the cap-beams (today called shear keys) and tilting of the piles due to ground failure. In the 1985 Algarrobo earthquake (M_w 8.0) 40 highway bridges were damaged. The predominant failures were related to the settlement of abutments, failures in the external concrete shear keys and the settlement of highway fillings [9]. After the Maule earthquake in 2010 (M_w 8.8), about 300 highway bridges were damaged [10]. The most common types of damage [11, 12, 13, 14, 15] observed were: (a) transverse displacement and excessive rotation of the deck, (b) collapse of segments of bridges due to the loss of vertical support in abutments or bents, (c) failure of skewed highway bridges associated with insufficient seat support length, (d) damage to the seismic bars (e) damage to the precast girders due to pounding with the external shear keys, and (f) diagonal tension failure of the external shear keys (Fig. 1-1).

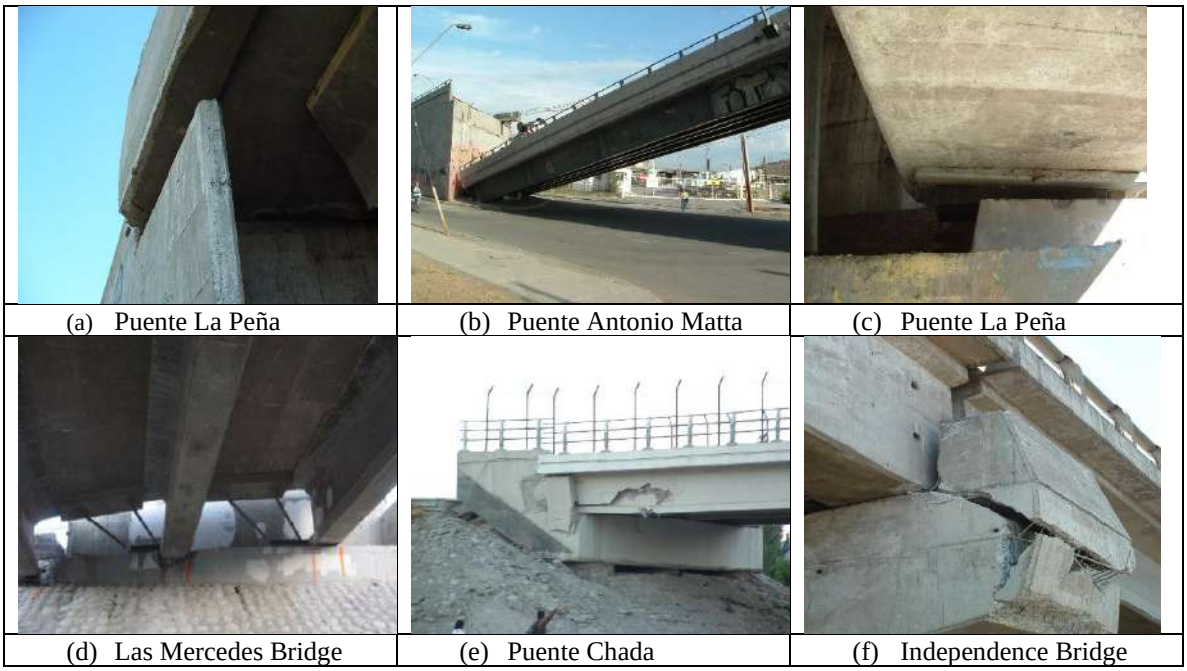

(a) Puente La Peña | (b) Puente Antonio Matta | (c) Puente La Peña

(d) Las Mercedes Bridge | (e) Puente Chada | (f) Independence Bridge

Fig. 1-1. Common types of damage observed during the 2010 Maule earthquake were

For a better understanding of the distribution of damage on Chilean bridges during the Maule earthquake 2010 (M_w 8.8), a description of the distribution of damage occurred in 80 bridges inspected after the 2010 earthquake is shown (Fig. 1-2). The most damaged bridges were simply supported bridges with precast girders and simply supported composite bridges, which represent 67% and 16% of all the damaged bridges, respectively (Fig. 1-2(a)). Fig. 1-2(b) shows the different types of damage that occurred in two seismic zones, having many bridges that often presented more than one type of damage. Of the inspected bridges, 50% were located in seismic zone 2 (A_0 = 0.3 g) and 50% in seismic zone 3 (A_0 = 0.4 g). Damage in shear keys, precast girders, seismic bars, and elastomeric bearings, and excessive displacement of the deck, appeared in 88%, 83%, 37%, 26% and 49% of the bridges for the seismic hazard zone 3, respectively. Similarly, for seismic hazard zone 2 the values were 33%, 17%, 50%, 50% and 33%, respectively.

It is important to mention that the damage observed during the 2010 Maule earthquake in the shear keys also has been reported in other earthquakes around the world [2, 5, 16, 17, 18, 19, 20, 21]. For these reasons, it is needed to evaluate the influence of shear keys on the seismic behavior of Chilean highway bridges.

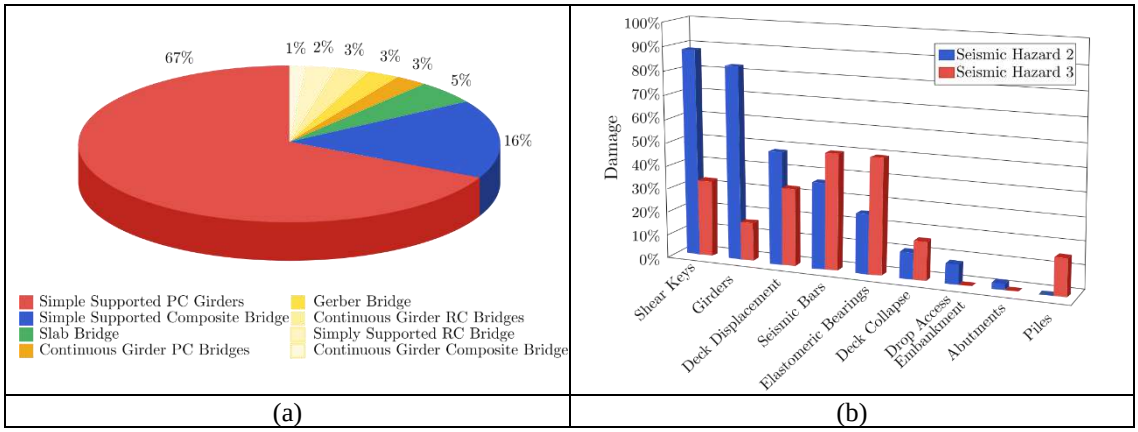

(a) (b)

Fig. 1-2. Damage distribution of Chilean bridges after the 2010 Maule earthquake (Mw 8.8): (a) by the type of bridge and (b) by the type of damage.

1.2. Problem definition

Sacrificial shear keys are used in the abutments and bents of bridges to restrict the transverse and rotational movement of the deck under extreme lateral displacement demands, preventing the deck from losing its vertical support and collapsing. During the maximum considered earthquake, it is expected that the shear keys will be severely damaged by the impacts of the superstructure [23, 24] before damage occurs on the walls of the abutment or in the columns of the bridge bents, and thus shear keys are characterized as sacrificial elements. Currently, to ensure that the shear keys function properly as sacrificial elements, some design codes state that the lateral load capacity of the shear keys must not exceed the greatest of 30% of the vertical reaction in the abutments and/or pile and 75% of the lateral capacity of the pile [24].

During the 2010 Maule earthquake a recurrent type of damage in abutments and bents was observed in the external shear keys, which showed diagonal shear failures [10, 14] (Fig. 1-3(a)). The typical observed damage included a diagonal tension crack, indicating that the ductile behavior of the shear keys [24, 25, 26] prevented excessive lateral displacements [10, 14], and thus prevented the deck collapse. It is important to mention that, although these external shear keys acted as sacrificial elements, wich is the desired behavior for this type of elements, the Chilean design code [27] does not establish a methodology for the design of such elements. In some cases, the shear keys failed completely but prevented the deck collapse (Fig. 1-3(b)). Fig. 1-3(c) shows damage to an internal shear key, which prevented the collapse of the superstructure. However, before the 2010 Maule earthquake, there were few bridges that had internal shear keys. Figures 1-3(d)-(f) show the damage to the shear keys in the abutments.

(a) Vespucion Independencia Bridge | (b) Perquilauquén Bridge | (c) Llacolen-North Access Bridge

(d) Underpass (2 km. North Ercilla) | (e) Underpass Rengo | (f) Overpass Hospital

Fig. 1-3. Damage to the shear keys on bridges.

In Chile, the shear keys must be designed considering a horizontal acceleration equal to A_0 (Maximum Effective Acceleration). Each shear key must be able to withstand all the transverse force of the deck divided by the number of interior shear keys [27]. The American Association of State Highway and Transportation Officials specifications [22] do not explicitly state about the design force to be applied to the shear keys. However, these specifications indicate that the design force for the superstructure-substructure connection is calculated as the product of the design seismic coefficient by the permanent load divided between a response modification factor. The Japan road bridges [28] design specifications state that the ultimate strength of the shear keys should be less than 1.5 times the dead load reaction. On the other hand, the Mexican standard [29] states that the design force for the shear keys is calculated as the seismic coefficient, multiplied by the dead load minus the seismic shear n-times the importance factor.

Several authors have theoretically and experimentally studied the seismic response of sacrificial shear keys [24, 25, 30, 31, 32, 33, 34, 35, 36]. Tassios et al. [30] experimentally investigated the behavior of the interfaces of smooth concrete and smooth and rough concrete under monotonic and cyclic displacements. The results obtained can be used to predict the friction behavior of reinforced concrete interfaces and to analytically model the shear sliding

behavior of reinforced concrete. Buyukozturk et al. [31] carried out tests to evaluate the shear resistance and deformation behavior of joints with prefabricated segmented bridge shear keys. They found that the resistance of epoxy joints with shear key was consistently higher than that of dry joints with shear keys, proposing formulas to evaluate the shear resistance of joints with shear keys. Kaneko et al. [32] proposed a simple design formula as a first step in the development of design aids for shear resistance of the shear keys and then validated their model based on fracture mechanics [33]. Megally et al. [25] performed an experimental campaign to study the seismic response of interior and exterior shear keys. In addition, they developed analytical models to estimate the capacity of the shear keys, as well as their post-peak performance under cyclic loads. Bozorgzadeh et al. [24] also conducted an experimental research program on external shear keys; unlike Megally et al. [25], they included the contribution of all the wall of the abutments. The results were used to develop an analytical model to estimate the lateral resistance of external and interior shear keys on abutments and cap beams. Also, recommendations for the detailing of the reinforcement of the external shear keys, as well as recommendations for their construction were made. Franco et al. [34] proposed an analytical procedure to estimate the maximum load capacity and post-peak load of the sacrificial interior shear keys based on the evaluation of the experimental results they carried out. Goel and Chopra [35] investigated analytically the role of shear keys in the earthquake-resistant behavior of bridges located on geological faults. A simplified force–deformation model for the behavior of shear keys, based on the experimental results obtained by Megally et al. [25], was proposed. They concluded that the seismic demands on a bridge with non-linear shear keys on geological faults are limited by the demands of a bridge with elastic shear keys.

Nailiang & Jianzhong [36] experimentally and analytically evaluated the seismic performance of highway bridges with different displacement control devices, including external shear keys. They proposed a simplified model for the hysteretic response of external shear keys with diagonal tension failure. The proposed model differs from the model proposed by Megally et al. [25] in that the stiffness associated with the unloading branches of the shear keys is equal to the initial loading stiffness of the element. Their results show that if the shear keys are well designed, the seismic demands of the piles can be effectively reduced, and the displacement of the elastomeric bearings can also be controlled to meet the

performance objectives.

After the previous discussion, it can be observed that experimental and analytic investigations have been carried out regarding the influence of shear keys on the seismic behavior of bridges and some codes have incorporated provisions for the seismic design of the shear keys. However, some uncertainties remain in the structural behavior of such elements, such as:

- What is the actual behavior of road bridges with sacrificial shear keys during an earthquake?
- What is the difference in hysterical behavior between an external and internal sacrificial shear key?
- What is the effect of considering soil nonlinearity and seismic threat in the seismic behavior of bridges with sacrificial shear keys have?
- How are sacrificial shear keys designed seismically?
- Could a new technique be defined for self-centering shear keys in highway bridges such that it eliminates residual displacements of the superstructure?

This research aims to address several of these problems mainly from an analytical point of view, for which it will be considered as a hypothesis that shear keys behave as a sacrificial element, that is, they fail before any other element of the infrastructure.

1.3.Objectives and methodology

The main objective of this research is to evaluate the influence of the use of shear keys on the seismic behavior of typical Chilean highway bridges.

The specific objectives are:

1) To numerically evaluate the influence of sacrificial external shear keys on the seismic response of typical Chilean highway bridges (Paper I - published).

2) To assess the effects of changes in seismic design criteria in the transverse and vertical response of Chilean highway bridges (Paper II - published).
3) To propose a new technique for self-centering shear keys in highway bridges (Paper III – Submitted).

Specific objectives are related to the following aspects:

a) The first objective is to evaluate the influence of shear keys on Chilean road bridges according to the seismic hazard zone and the type of foundation floor.

b) The second objective seeks to analyze the effect of regulatory changes on seismic design requirements on Maule 2010 post-earthquake shear keys. Due to the multiple damages observed after the Maule earthquake, new regulatory seismic criteria were incorporated to improve the seismic performance of bridges in Chile. It is intended to evaluate the effectiveness of the criteria related to shear keys for different types of seismic hazard and soil types. The criteria to be evaluated are increased strength in the design of shear keys (external and internal), effectiveness of rigid diaphragms and increased resistance in seismic bars. These criteria are evaluated only for straight bridges.

c) The third objective seeks to propose a new technique for self-centering shear keys in highway bridges, to prevent collapse and eliminate residual displacements of the

superstructure. The new technique for self-centering shear keys is developed by modifying conventional aspect ratios and considering soil movement. A case study is investigated to validate the effectiveness of the proposed shear keys compared to current shear keys.

The research methodology is presented in Table 1-2. The specific phases and objectives are related to the corresponding activities that are required to achieve the objectives described above.

Tabla 1-2. Investigation methodology.

Phase	Activity	Specific objectives
1	A bibliographic review was carried out in order to elaborate the theoretical and experimental state of the art regarding the seismic response of the shear keys, to identify the most common damages observed in bridges during recent earthquakes (for example, the 2010 Maule earthquake) and to compare them with what the Chilean regulations and other international regulations say.	1, 2 and 3
2	The most used bridge typologies in Chile were statistically analyzed; for this study the bridges were characterized according to their materiality, length, number of beams and bents, type of deck, interface between superstructure and infrastructure, shear keys, diaphragms, skew angle, among others.	1, 2 and 3
3	A seismic demand was defined, that is, the number of records used in the IDA (Incremental Dynamic Analysis) analyzes, identified and classified considering the type of soil and the seismic hazard. To avoid bias in the results, records of different Chilean earthquakes had to be included.	1, 2
4	Analytical models (2D and 3D) of the failure mechanism of the shear keys were developed and calibrated with finite element models (ANSYS, OPENSEES) and experimental results of scale models made by other researchers.	1, 2 and 3
5	The Non-Linear response of the analytical model developed in (4) were quantified, to obtain fragility curves from IDA curves.	1, 2
6	A new technique for self-centering shear keys in highway bridges to modify the seismic response of bridges, to prevent collapse and eliminate residual displacement of the superstructure in highway bridges.	3
7	The results were analyzed and discussed, aiming to give recommendations to the seismic design criteria for Chilean bridges.	1, 2 and 3

1.4. Dissertation outline

This thesis is written in the format of three independent articles, so each chapter is a self-contained paper that has been published or is in the process of being published [37, 38, 39]. This dissertation is organized into the following chapters:

Chapter 2 presents an evaluation of the influence of the use of external shear keys on the seismic behavior of Chilean highway bridges. For this evaluation, the representative typology of Chilean highway bridges is selected, and with this typology two analytical models are performed: (1) One with non-linear shear keys, which offers transverse constraint to displacement up to a maximum deformation of the sacrificial shear keys, and (2) other without sacrificial shear keys, which has no transverse displacement restriction. The results are expressed by fragility curves considering different soil conditions and seismic risk zones. The chapter corresponds to the article “Influence of the use of external shear keys on the seismic behavior of Chilean highway bridges” [37].

Chapter 3 discusses the effects of changes in seismic design criteria in the transverse and vertical response of Chilean highway bridges. This discussion is achieved by comparing the fragility curves of a typical bridge designed to Chilean standards before and after the 2010 Maule earthquake, considering soil type and seismic hazard. Four structural configurations of bridges were designed using the different design criteria and then modelled for the evaluation of their seismic behavior. The chapter corresponds to the article “Effects of changes in seismic design criteria in the transverse and vertical response of Chilean highway bridges” [38].

Chapter 4 presents a new technique for self-centering shear keys to modify the seismic response of bridges, to prevent collapse and eliminate residual displacements of the superstructure. The new technique for self-centering shear keys is developed by modifying conventional aspect ratios and considering soil movement. A case study is investigated to validate the effectiveness of the proposed shear key compared to the current design of shear keys, such as those evaluated in Chapters 2 and 3. This chapter corresponds to the article “New Technique for Self-Centering Shear Keys in Highway Bridges” [39].

Chapter 5 gives the general conclusions and recommendations obtained in this investigation.

Appendix A. Documents all the records used in this investigation classified by soil type and seismic hazard.

Appendix B. Summarizes the formulas and the main analytical results obtained in the proposed self-centering shear key model.

1.5. Original contributions

The present research project is distinctive in many ways. Some points that make this project unique are:

- It provides qualitative and quantitative recommendations to evaluate the effect of shear keys design on bridge seismic behavior.
- Improves analytical prediction of the strength and deformation of external and internal shear keys on bridges.
- Provides a new technique for self-centering shear keys in highway bridges
- Provides a database of records classified by soil type and seismic hazard.

In summary, this research provides a unique set of data that can and has been used to verify advanced computational models and provide support for the development of both simplified and advanced analysis techniques for the use of shear keys in highway bridges as an element of sacrifice.

Additionally, this research study is an effort to (1) develop new fundamental knowledge, (2) improve our understanding of the seismic behavior of shear keys, (3) extending design ranges, (4) provide calibration data, and (5) improve the accuracy of the seismic response prediction of shear keys as a sacrificial element.

The author expects that, based on the results and the conclusions obtained in this research project, the use of shear keys in highway bridges will have an immediate practical impact on the analysis, design and, as a consequence, on the construction of the road network for either constructing new structures or retrofitting old structures.

References

[1] Mitchell, D., Tinawi, R., and Sexsmith, R. G., 1991. Performance of bridges in the 1989 Loma Prieta earthquake lessons for Canadian designers. Canadian Journal of Civil Engineering, 18(4), 711–734. DOI: 10.1139/l91-085.

[2] Fenves, G. L., and Ellery, M., 1998. Behavior and failure analysis of a multiple-frame highway bridge in the 1994 Northridge earthquake. PEER 98/08. Pacific Earthquake Engineering Research Center.

[3] Kawashima, K., and Unjoh, S., 1997. The damage of highway bridges in the 1995 Hyogo-ken Nanbu earthquake and its impact on Japanese seismic design. Journal of Earthquake Engineering, 1(3), 505–541. DOI: 10.1080/13632469708962376.

[4] Takahashi, Y., and Hoshikuma, J.-I., 2013. Damage to road bridges induced by ground motion in the 2011 great east Japan earthquake. Journal of JSCE, 1(1), 398–410. DOI: 10.2208/journalofjsce.1.1_398.

[5] Chang, K.-C., Chang, D.-W., Tsai, M.-H., and Sung, Y.-C., 2000. Seismic performance of highway bridges. Earthquake Engineering and Engineering Seismology, 2(1), 55–77.

[6] Wood, J. H., Chapman, H. E., and Brabhaharan, P., 2012. Performance of highway structures during the darfield and christchurch earthquakes of 4 september 2010 and 22 february 2011. New Zealand Transport Agency. New Zealand Transport Agency.

[7] Lomnitz, C., 2004. Major Earthquakes of Chile: A Historical Survey, 1535-1960. Seismological Research Letters, 75(3), 368–378. DOI: 10.1785/gssrl.75.3.368.

[8] Steinbrugge, K. V., and Flores Álvarez, R., 1963. The chilean earthquakes of may, 1960: A structural engineering viewpoint. Bulletin of the Seismological Society of America, 53(2), 225–307.

[9] Willie, L., Bolt, B., Durhin, M., Gates, J., McCormick, D., Smith, P., Abrahamson, N. A., et al., 1986. The Chile Earthquake of March 3, 1985—Damage to Bridges and Highways. Earthquake Spectra, 2(2), 411–427. DOI: 10.1193/1.1585389.

[10] Buckle, I. G., Hube, M., Chen, G., Yen, W.-H., and Arias, J. G., 2012. Structural performance of bridges in the offshore Maule earthquake of 27 february 2010. Earthquake Spectra, 28(S1), S533–S552. DOI: 10.1193/1.4000031.

[11] Yashinsky, M., Oviedo, R., Ashford, S., Fargier-Gabaldon, L., and Hube, M., 2010. Performance of highway and railway structures during the february 27, 2010 Maule Chile earthquake. EERI/PEER/FHWA Bridge Team Report. EERI/PEER/FHWA Bridge Team Report.

[12] Elnashai, A. S., Gencturk, B., Kwon, O.-S., Hashash, Y. M. A., Kim, S. J., Jeong, S.-H., and Dukes, J., 2012. The Maule (Chile) earthquake of February 27, 2010: Development of hazard, site specific ground motions and back-analysis of structures. Soil Dynamics and Earthquake Engineering, 42(January 2011), 229–245. Elsevier. DOI: 10.1016/j.soildyn.2012.06.010.

[13] Kawashima, K., Unjoh, S., Hoshikuma, J.-I., and Kosa, K., 2011. Damage of Bridges due to the 2010 Maule, Chile, Earthquake. Journal of Earthquake Engineering, 15(7), 1036–1068. DOI: 10.1080/13632469.2011.575531.

[14] Schanack, F., Valdebenito, G., and Alvial, J., 2012. Seismic Damage to Bridges during the 27 February 2010 Magnitude 8.8 Chile Earthquake. Earthquake Spectra, 28(1), 301–315. DOI: 10.1193/1.3672424.

[15] Toro, F., Rubilar Moya, F. I., Hube, M., Santa María, H., and Cabrera, T., 2013. Statistical analysis of pedestrian bridges damaged during 2010 Chile earthquake. Seventh National Seismic Conference on Bridges and Highways (pp. 1–12).

[16] Booth, E., 1985. The Chile earthquake of march 1985. Disasters/9/3/1985.

[17] Lew HS. Performance of structures during the Loma Prieta earthquake of October 17, 1989. vol. 778; 1989.

[18] Priestley MJ, Seible F, Uang C-M. The Northridge earthquake of January 17, 1994: Damage analysis of selected freeway bridges. United States of America; 1994.

[19] [15] Li J, Peng T, Xu Y. Damage investigation of girder bridges under the Wenchuan earthquake and corresponding seismic design recommendations. Earthq Eng Eng Vib 2008;7:337–44. https://doi.org/10.1007/s11803-008-1005-6.

[20] Kawashima K, Takahashi Y, Ge H, Wu Z, Zhang J. Damage of bridges in 2008 Wenchuan, China, earthquake. J Earthq Eng 2009;13:965–96. https://doi.org/10. 1080/13632460902859169.

[21] Yashinsky M. Lessons learned from the March 11, 2011 M9.0 great Tohoku earthquake and tsunami; 2011. p. 1–15.

[22] American Association of State Highway and Transportation Officials, 2011. Guide Specifications for LRFD Seismic Bridge Design with 2012, 2014 interim revisions. 2th Edition (p. 266).

[23] California Department of Transportation, 2006. Standard specifications (pp. 1–872). United States of America: California Department of Transportation.

[24] Bozorgzadeh A, Megally SH, Ashford S, Restrepo JI. Capacity evaluation of exterior sacrificial shear keys of bridge abutments. J Bridge Eng 2007;11:555–65.

[25] Megally SH, Silva PF, Seible F. Seismic response of sacrificial shear keys in bridge abutments: Structural systems research report SSRP-2001/23. San Diego, La Jolla, California: Department of Structural Engineering, University of California; 2001.

[26] Xiang N, Li J. Seismic performance of highway bridges with different transverse unseating-prevention devices. J Bridg Eng 2016;21. https://doi.org/10.1061/ (ASCE)BE.1943-5592.0000909

[27] Ministerio de Obras Públicas. Manual de carreteras – Volumen No 3 – Instrucciones y criterios de diseño (in Spanish). Chile: MOP-DGOP-Direccion de Vialidad; 2017.

[28] Japan Road Association. Design specification for highway bridges – Part V: Seismic design. Japan: Japan Road Association; 2002

[29] Secretaria de Comunicaciones y Transporte. Proyectos de nuevos puentes y similares (in Spanish); 2001.

[30] Tassios, T. P., and Vintzeleou, E. N. (1987). "Concrete-to-concrete friction." J. Struct. Engrg., ASCE, 113(4), 832-849.

[31] Buyukozturk O, Bakhoum MM, Beattie SM. Shear behaviour of joints in precast concrete segmental bridges. J Struct Eng 1990;116:3380–401.

[32] Kaneko Y, Connor JJ, Triantafillou TC, Leung CK. Fracture mechanics approach for failure of concrete shear keys. I: Theory. J Eng Mech 1993;119:681–700.

[33] Kaneko Y, Connor JJ, Triantafillou TC, Leung CK. Fracture mechanics approach for failure of concrete shear keys. II: Verification. J Eng Mech 1993;119:701–19.

[34] Silva PF, Megally SH, Seible F. Seismic performance of sacrificial interior shear keys. ACI Struct J 2003;100:177–87.

[35] Goel RK, Chopra AK. Role of shear keys in seismic behavior of bridges crossing fault-rupture zones. J Bridge Eng 2008;13:398–408.

[36] Nailiang X, Jianzhong L. Seismic performance of highway bridges with different transverse unseating-prevention devices. J Bridge Eng 2016;21.

[37] Wilches Están, J. de J., Santa María, H., Riddell, R., and Arrate Letelier, C., 2017. Influence of the use of external shear keys on the seismic behavior of Chilean highway bridges. Engineering Structures, 147, 613–624. DOI: 10.1016/j.engstruct.2017.06.015

[38] Wilches Están, J. de J., Santa María, H., Riddell, R., and Arrate Letelier, C., 2019. Effects of changes in seismic design criteria in the transverse and vertical response of Chilean highway bridges. Engineering Structures, 191(August 2018), 370–385. Elsevier Ltd. DOI: 10.1016/j.engstruct.2019.04.064

[39] Wilches Están, J. de J., Santa María, H., Leon, R., Fernandez, C. Restrepo, Jose I., 2020. New Technique for Self-Centering Shear Keys in Highway Bridges. Engineering Structures, Submitted.

2. CHAPTER 2

INFLUENCE OF THE USE OF EXTERNAL SHEAR KEYS ON THE SEISMIC BEHAVIOR OF CHILEAN HIGHWAY BRIDGES

Abstract: The present study evaluates the influence of external sacrificial shear keys on the seismic behavior of bridges commonly found in Chile. The damages observed in the external sacrificial shear keys as a result of the Maule earthquake of 2010 led to the revision of this type of elements. The results of a statistical analysis of Chilean highway bridges were used to identify a representative typology of bridges. Two models were used for the evaluation of the seismic behavior of the selected typology, given different soil conditions and seismic hazard zones, as follows: (1) one without sacrificial shear keys, which has no transverse displacement restriction and (2) other with non-linear shear keys, which offers transverse constraint to displacement up to a maximum deformation of the sacrificial shear key. Fragility curves were generated using non-linear analytical models and a series of compatible records.

The comparison of the fragility curves for damage levels I (initial slip) and II (large residual displacement of the superstructure) shows that the most vulnerable bridges are bridges without external shear keys, regardless of the seismic hazard zone and the type of soil. For damage level III (collapse) it is irrelevant whether or not the bridge has external shear keys.

2.1. Introduction

The observation of the main seismic events since late 20th century until today, as in Chile (1985, 2010, 2014), USA (1994), Mexico (1995, 2003, 2010), Japan (2001), China (2008), and Haiti (2010), has shown that highway bridges designed under latest design codes are structures vulnerable to failure or collapse; this has been attributed to conceptual problems in the normative design and the lack of attention during the development of design projects. A common fault detected in the performance of highway bridges with external sacrificial shear keys is the one associated with the diagonal tension phenomenon [1–6]. Several authors have theoretically and experimentally studied the seismic response of shear keys [7–13]. Buyukozturk et al. [7] performed tests to evaluate the shear strength and deformation behavior of prefabricated segmented bridge joints. They found that the strength of the epoxy joints was consistently larger than that of the dry joints, and proposed formulas to evaluate the shear strength of the joints. Kaneko et al. [8] proposed a simple design formula as a first step in the development of design aids for shear resistance of the shear keys and then validated their model based on fracture mechanics [9]. Megally et al. [10] carried out an experimental campaign to study the seismic response of interior and exterior shear keys. In addition, they developed analytical models to evaluate the capacity of the shear keys, as well as their post-peak performance under cyclical loads. Bozorgzadeh et al. [11] also conducted an experimental research program on external shear keys; unlike Megally et al. [10], they included the contribution of all the wall of the abutments. The results were used to develop an analytical model to estimate the lateral resistance of external and interior shear keys on abutments and cap beams. Also, recommendations for the detailing of the reinforcement of the external shear keys, as well as recommendations for their construction were made. Goel and Chopra [12] investigated analytically the role of shear keys in the earthquake-resistant behavior of bridges located on geological faults. A simplified force–deformation model for the behavior of shear keys, based on the experimental results obtained by Megally et al. [10], was proposed. They concluded that the seismic demands on a bridge with non-linear shear keys on geological faults are limited by the demands of a bridge with elastic shear keys.
Nailiang & Jianzhong [13] experimentally and analytically evaluated the seismic performance of highway bridges with different displacement control devices, including external shear keys. They proposed a simplified model for the hysteretic response of external shear keys with diagonal tension failure. The proposed model differs from the model proposed by Megally et al. [10] in that the stiffness associated with the unloading branches of the shear keys is equal to the initial loading stiffness of the element. Their results show that if the shear keys are well designed, the seismic demands of the piles can be effectively reduced, and the displacement of the elastomeric bearings can also be controlled to meet the performance objectives. It is important to note that none of the previous investigations have assessed the variability of the seismic response of bridges with sacrificial external shear keys with the seismic hazard and the soil type. In Chile, extensive damage has been observed in highway bridges due to great magnitude seismic events. In the 2010 Maule earthquake (Mw

8.8) approximately 300 bridges, representing about 3% of the total number of the existing bridges in the country [6], were damaged. The most frequent damages observed were: transverse displacement and/or excessive rotation of the superstructure, the collapse of segments of bridges due to the loss of vertical support in abutments or piles, damage associated to dynamic effects caused in skewed bridges or due to insufficient length in the supporting structures, damage in prestressed concrete beams due to the impact of the beam against the external shear key. This chapter will be evaluated the influence of sacrificial external shear keys on the seismic behavior of highway bridges, considering different scenarios of analysis according to the soil type and hazard zone classification of the latest design code. In order to achieve the objective, the study of an intermediate pile of a typical Chilean bridge was carried out through the realization of a plane type model in OpenSees [14]. This model was elaborated by considering a typical structure obtained after a statistical analysis of the configuration of Chilean underpass and overpass highway bridges. A pushover analysis was conducted to determine the collapse characteristic; also, fragility curves were determined through an Incremental Dynamic Analysis (IDA) to establish the bridge performance and differences between considering or not the use of external shear keys. The model takes into account the non-linear behavior of sacrificial external shear keys, seismic bars, and elastomeric bearings. Regarding the characterization of the seismic demand, 42 accelerograms obtained from the Maule earthquake (Mw = 8.8, 2010), and 47 from the Algarrobo earthquake (Mw = 8.0, 1985) were used to define the expected seismic hazard as established by Riddell [15], for the soil type classifications I, II, and III (according to the Chilean Seismic Code [16]), modified by extending indefinitely the zone of velocity amplification; for the elaboration of the fragility curves accelerograms compatible with each hazard level were calculated.

2.2. Typology of highway bridges in Chile

According to the statistical study carried out in this research, the most used bridge type in Chile consists of a reinforced concrete deck, continuous or simply supported (with an average span of 26.0 m between supports in typical bridges), on prestressed concrete beams (with an average of 4 beams), supported on abutments and/or piles composed of a cap beam and simple or multiple columns. Additionally, elastomeric bearings are placed under each beam, constituting the interface between the beams and the intermediate abutments and/or piles. Sacrificial shear keys are used in piles and abutments (Fig. 2-1). The purpose of the outer sacrificial shear keys is to restrict the transverse movement of the superstructure under extreme lateral displacement demands, preventing the superstructure from losing its vertical support and collapse [17–19]. A typical detail of sacrificial external shear keys is shown in Fig. 2-2 on a cap beam in the pile of a bridge.

External shear keys with an appropriate design must be able to restrict the lateral displacement of the superstructure in the case of extreme seismic events, acting as sacrificial elements in which the damage is concentrated, avoiding damage to the infrastructure (cap beams, columns, piles, and abutments).

For example, to ensure that external shear keys function properly as sacrificial elements, CALTRANS [18] states that the lateral load-bearing capacity of the shear keys must not exceed the greatest of 30% of the vertical reaction in the abutments and/or pile and 75% of the lateral capacity of the pile.

Fig. 2-2. Typical Underpass Bridge in Chile.

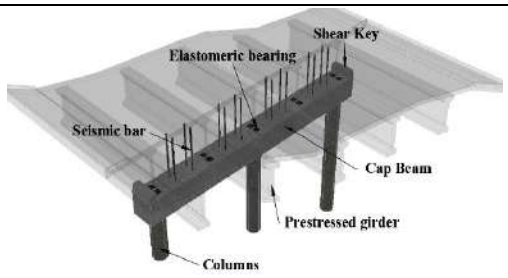

Fig. 2-1. Scheme of external shear keys in a bridge.

2.2.1. Damage observed on highway bridges after the Maule earthquake (2010, Mw 8.8)

Among the most frequently observed damage caused by the Maule earthquake was the sliding of the superstructure beams and support elastomers (Fig. 2-3(a)). In some cases, the superstructure collapsed as the result of excessive lateral displacement (Fig. 2-3(b)). Another type of damage frequently observed was that some sacrificial external shear keys presented shear failure of diagonal tension-type, as shown in Fig. 2-4. In all the observed cases of

ductile behavior of the sacrificial external shear keys, excessive lateral displacements were avoided, without loss of the vertical support of the superstructure and no damage in the abutments and intermediate piles. It is important to mention that, although these external shear keys acted as sacrificial elements, such is the desired behavior for this type of elements.

(a) Overpass of Independencia Highway Bridge. Excessive slip is shown in the picture.

(b) Underpass Los Pinos collapsed

Fig. 2-3. Frequent damages after Maule earthquake (2010).

(a) Independencia Highway Bridge

(b) Ruta 5 Sur Higway Bridge

(c) Costanera Norte Highway Bridge

Fig. 2-4. Typical damages of shear keys during the earthquake of Maule 2010, fault in diagonal tension

2.2.2. Changes in seismic-resistant design criteria of Chilean highway bridges, following the Maule earthquake (2010, Mw 8.8)

Due to the damages observed in the Maule earthquake, MOP [19] modified the criteria for the earthquake resistant design of highway bridges in the country [20]. The minimum resistance required for the design of external sacrificial shear keys was increased from 50% to 100% of the effective peak acceleration (EPA) specified for the seismic zone in which the bridge was located [19]. In addition, the use of diaphragm walls at the ends and the middle of a span of a bridge were incorporated as a requirement, with the aim of improving the interaction between the beams and the shear keys. The required strength for the diaphragm walls is the same as the design of external sacrificial shear keys. The minimum width of shear keys is 400 mm and the maximum is 700 mm. Also, in every shear key, a lateral neoprene pad of small thickness must be included to damp the impact on them.

2.3. Characterization of the bridge considered in this research

A representative structure of the Chilean highway bridges was selected for the development of the present study, as observed repeatedly throughout the country (Fig. 2-1). The bridge has two spans, symmetrical, with four runways, not skewed, and 26 m between supports (Fig. 2-5).

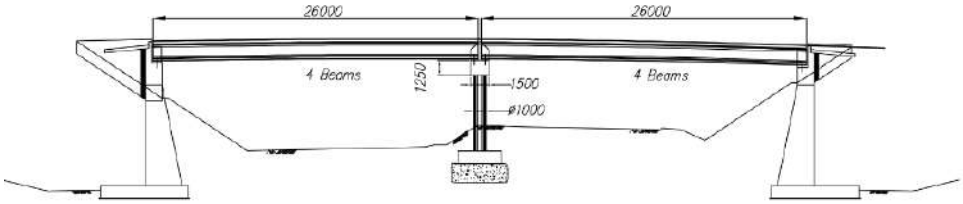

(a) Typical elevation

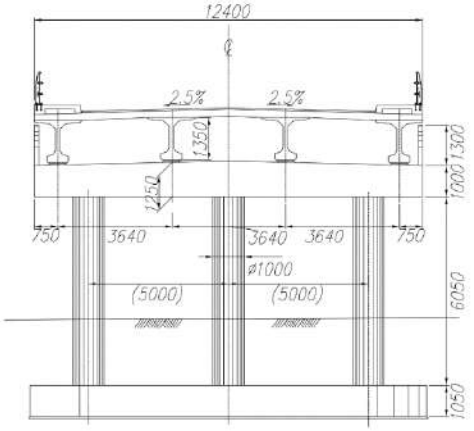

(a) Cross section at the pile

Fig. 2-5. General configuration and details of the prototype bridge used in the study.

The superstructure is simply supported on elastomeric bearings that in turn are supported on the abutments and a pile composed of a cap beam and three columns in the central part (Fig. 2-5). The structure of the abutments consists of reinforced concrete back walls, behind which there is an approach slab on top of compacted landfills. The structure of the intermediate pile consists of three columns 1 m in diameter spaced at 5 m, with 6 m of free height, on top of which rests a reinforced concrete cap beam 1.2 by 1.06 m cross section, and 14.2 m length. The superstructure of the bridge consists of two discontinuous sections, simply supported, whose structure consists of a 0.2 m thick and 11.75 m wide reinforced concrete slab, supported on four 1.35 m height prestressed concrete beams (Fig. 2-5). The selection of this configuration is the result of a characterization study of 120 highway bridges currently operating in Chile, that was carried out in this investigation but, because of its extension and a large amount of information, it is not presented in this document. The connection between the superstructure and the infrastructure is made by means of elastomeric bearings, 300 mm wide, 450 mm long and 34 mm high. The horizontal elastic stiffness (K_h) of the elastomeric

support is calculated with Eq. (2-1), resulting in a value of 7020 kN/m, while the vertical stiffness (K_v) is obtained from Eq. (2-2) and gives a value of 3,826,812 kN/m.

$$K_h = \frac{GA_b}{h_r} \qquad Eq.(2-1)$$

$$K_v = \frac{EcA_b}{h_r} \qquad Eq.(2-2)$$

where Ab is the loaded area of the bearing, h_r is the total thickness of rubber in the bearing, G is the shear modulus, and E_c is the instantaneous compression modulus of the rubber-steel composite under a specific level of vertical load. To prevent the superstructure from lifting during an extreme event, the interface between the superstructure and the infrastructure has seismic bars (Fig. 2-2), which are vertical steel bars embedded in the superstructure and infrastructure, in the spaces between the longitudinal beams. The structural design of the bridge is carried out using the Chilean codes for the seismic resistant design of Chilean Highway Bridges [19].

2.3.1. Analytical model of the failure mechanism in external shear keys

Different investigators [7–9] have identified and described two types of failure mechanisms for external shear keys. The first one is a frictional shear failure, which is associated with the formation of a horizontal crack that develops at the connection between the external shear key and the cap beam on which it is located. The second is associated with the formation of a diagonal crack that develops downwardly, perpendicular to the direction of the main tensile stresses. The latter was the failure mechanism of external shear keys observed in the Maule earthquake (Fig. 2-4), and therefore this is the case considered in this study. Megally et al. [10] developed a behavioral model for external reinforced concrete shear keys, based on strut end tie models [21]. The lateral resistance of external shear keys is calculated on the balance of shear forces along the diagonal crack that develops in the wall of the stirrup shaft or in the cap beam, according to Eq. (2-3):

$$V_n = V_c + V_s \qquad Eq.(2-3)$$

where V_n is the nominal shear strength of the external shear keys, V_c is the contribution of the concrete, and Vs is the contribution of the steel reinforcement. The strength of the concrete is calculated as:

$$V_c = 0.2\sqrt{f_c' dh} \qquad Eq.(2-4)$$

where f'_c c is the cylindrical compressive strength of the concrete at 28 days of setting, d is

the height of the wall of the abutments stem or the width of the cap beam, h is the height of the wall of the stem of the abutments or the height of the cap beam. The contribution to the resistance by the steel reinforcement Vs, is calculated using the following expression:

$$Vs = \left[T_1 h + T_2 d + n_h T_{i,h} \frac{h^2}{2\,s} + n_v T_{i,v} \frac{d^2}{2\,s} \right] \left(\frac{1}{h+a} \right) \qquad Eq.(2-5)$$

Where $T_1 = As_1 * fy_1$ is the strength developed by the traction tie, $T_2 = As_2 * fy_2$ is the strength developed in the first layer of steel reinforcement that crosses the interface of the shear key; n_h and n_v represent the number of layers of horizontal and vertical reinforcements inside the external shear key; $T_{i,h} = A_{s,h} * f_{y,h}$ and $T_{i,v} = A_{s,v} * f_{y,v}$ are the tensile strength of each horizontal bar i, h and each vertical bar I, v in the interior of the wall of the abutments or cap beam, where it crosses the diagonal crack, as shown in Fig. 2-6. Fig. 2-6 shows the internal forces through the diagonal failure crack in an external shear key.

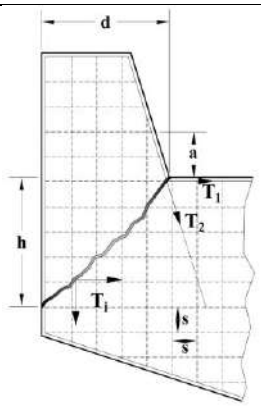

Fig. 2-6. Diagram of forces in external shear keys.

Megally et al. [10] and Bozorgzadeh et al. [11] proposed a simplified model to represent the hysteresis cycle in external shear keys (Fig. 2-7(a)); a trilinear approximation of the backbone curve can be used (Fig. 2-7(b)). Also, it can be assumed that the stiffness associated with unloading is equal to the initial stiffness of the element [13]. These simplifications of the models of the hysteresis cycle are consistent with Goel and Chopra [12]. The space between the outer beams and the outer shear keys has been incorporated directly into the force-displacement curve of the shear key, as shown in Fig. 2-7(c).

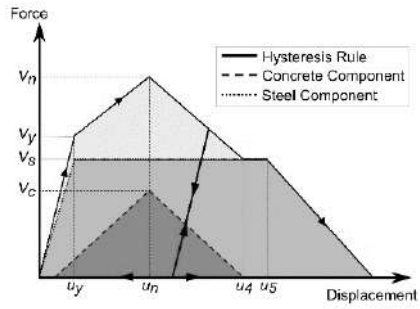

(a) Hysteretic Model (adapted from Megally et al. (2001)

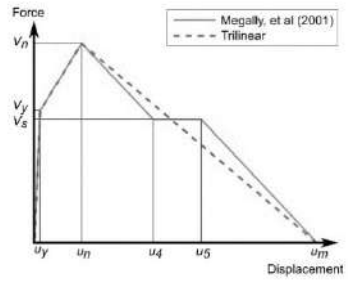

(b) Trilinear Model (adapted from Chopra et al. 2008)

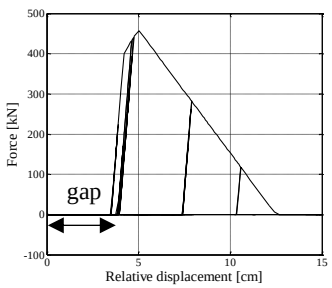

(c) Hysteretic response for various deformation levels

Fig. 2-7. Simplified model of hysteresis of external Shear Keys.

The characteristic displacements of the hysteresis cycle model of the shear keys, identified in Fig. 2-7a, can be determined using the following expressions [10]:

$$u_y = \sqrt{2}\,\varepsilon_y (L_d + L_a)\frac{h+d}{\sqrt{h^2+d^2}} \qquad Eq.(2-6(a))$$

$$u_n = \sqrt{2}\,\varepsilon_y (L_d + L_a)\frac{h+d}{s} \qquad Eq.(2-6(b))$$

$$u_4 = \sqrt{2}\,\varepsilon_{0,005} (L_d + L_a)\frac{h+d}{s} \qquad Eq.(2-6(c))$$

$$u_5 = \sqrt{2}\,\varepsilon_{0,007} (L_d + L_a)\frac{h+d}{s} \qquad Eq.(2-6(d))$$

where ε_y is the unit strain of the expected yield strength of the reinforcement steel, e0.005 is the unit strain of 0.005, e0.007 is the unit strain of 0.007, La is the width of the wall of the stem and/or cap beam, and L_d is the length of development of the reinforcement. The displacement um is obtained by assuming that the slope of the curve between u5 and um is the same as between u_n and u_4. Finally, the yield strength V_y is defined as:

$$V_y = V_s + V_c\frac{u_y}{u_n} \qquad Eq.(2-7)$$

2.3.2. Analytical model for studying the dynamic response of the standard bridge

Considering that the typical highway bridge in this study is not skewed, the transverse behavior of the bridge is studied through a plane 2D model of the central pile of the bridge. The structural analysis software OpenSees v2.5.0 [14] was used for the analyses, with the following considerations: the columns of the intermediate pile were considered to be embedded in the foundations, fixed at the base, neglecting the effect of the soil-structure interaction. The cap beam and the longitudinal beams of the superstructure were modeled as linear-elastic since in the Maule earthquake they showed elastic behavior. The columns of

the piles were modeled as linear-elastic, considering what is established by Scott and Fenves [22]. To model the seismic bars, a bilinear constitutive model defined by [23] (Fig. 2-8(a)) was considered, and a uniaxial material of hysteretic type was used according to [24].

Rubilar [25] tested elastomeric bearings, both for monotonic loading and for cyclic loading condition, in order to characterize their hysteretic behavior. It was concluded that the constitutive relationship of the elastomeric bearings can be considered as elastoplastic perfect behavior (Fig. 2-8(b)), which is consistent with results from previous investigations [26–28]. Two node link elements were used to model the bearings.

The shear keys were modeled as established by Megally et al. [10] (Fig. 2-7(a)) by adding two materials: the first associated with the properties of uniaxial concrete of hysteretic type [24], and the second associated with the initial gap between the outer longitudinal beams of the superstructure and the external shear keys, with the uniaxial material ElasticPPGap [24] (Fig. 2-8(c)).

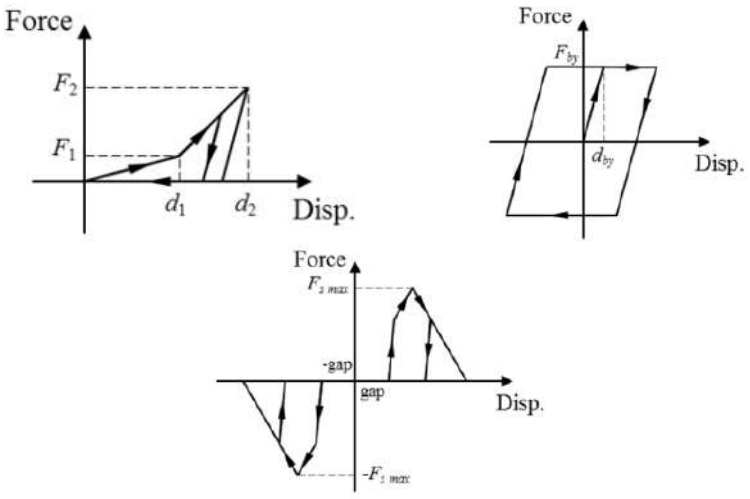

(a) Seismic bar (b) Elastomeric bearing (c) Shear Keys

Fig. 2-8. Hysteretic behavior of elements used in the model.

Two types of models of the pile were used, one with external sacrifice shear keys and the other without, see Fig. 2-9(a) and (b) respectively. For the case under study, it was not of interest the torsional effect of the superstructure, thus it was not considered in the model. Taking into account the above, and being consistent with the research objective, the vertical effect of the earthquake is also neglected in the analyses.

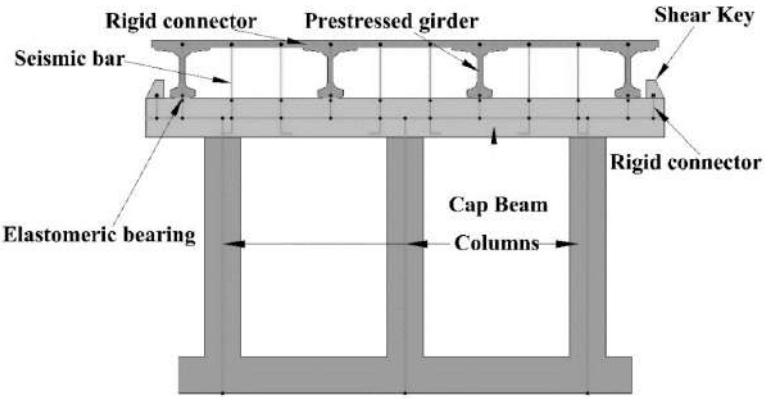

(a) Model with shear keys

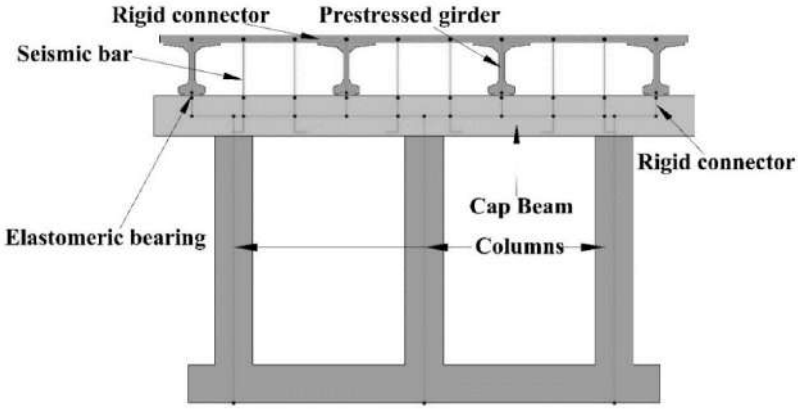

(b)Model without shear keys

Fig. 2-9. Analytical Model of the pile.

2.4. Characterization of the demand and seismic hazard

The study of the nonlinear response of structures is considerably sensitive to the characterization of the seismic demand used, as described in Saragoni [29]. Thus, a correct characterization is necessary in order to consider the main effects induced by the seismic events according to the location of each structure. In addition, it is important to determine the expected seismic hazard level, establishing seismic design demands in terms of displacement, velocity, and acceleration, which can determine the correct intensity of the expected seismic demand. The last is fundamental in the search to determine if the design of the shear keys, according to the design criteria established by MOP [19], offers a correct performance and if its use can generate an improvement of the structural behavior. To perform a correct characterization of the Chilean seismic demand, this research considered 47 horizontal accelerograms obtained in the Algarrobo earthquake (Mw 8.0, 1985) and 42 horizontal accelerograms obtained in the Maule earthquake (Mw 8.8, 2010), which include the characteristics of the country seismogenesis. The details of the accelerograms considered are shown in Tables 2-1 and 2-2.

Tabla 2-1. Summary of the horizontal records obtained in the Algarrobo earthquake [15].

Seismic Event: Algarrobo's Earthquake, March 3, 1985, Mw = 8.0											
	Accelerograms	Seismic zone	Location	Region	Soil's seismic classification		Accelerograms	Seismic zone	Location	Region	Soil's seismic classification
1	Los Vilos EW	3	Los Vilos	Coquimbo	I	3	Papudo S40E	3	Papudo	Valparaíso	I
2	Los Vilos NS					6	Quintay EW	3	Quintay	Valparaíso	I
4	Pichilemu EW	3	Pichilemu	Libertador General Bernardo O'Higgins	I	7	Quintay NS				
5	Pichilemu NS					8	Rapel EW	3	Rapel	Libertador General Bernardo O'Higgins	I
10	UTFSM N70E	3	Valparaíso	Valparaíso	I	9	Rapel NS				
11	UTFSM S20E					12	Zapallar EW	3	Zapallar	Valparaíso	I
14	Cauquenes EW	3	Cauquenes	Maule	II	13	Zapallar NS				
15	Cauquenes NS					16	Chillan Viejo N10W	3	Chillan	Biobío	II
18	Hualañe EW	3	Hualañe	Maule	II	17	Chillan Viejo N80E				
19	Hualañe NS					20	Illapel N20W	3	Illapel	Coquimbo	II
22	Iloca EW	3	Iloca	Maule	II	21	Illapel S70W				
23	Iloca NS					24	La Ligua N70W	3	La Ligua	Valparaíso	II
26	Las Tórtolas N26W	2	Colina	Metropolitana de Santiago	II	25	La Ligua S20W				
27	Las Tórtolas N64E					28	Llolleo N10E	3	Llolleo	Valparaíso	II
30	Melipilla EW	3	Melipilla	Metropolitana de Santiago	II	29	Llolleo S80E				
31	Melipilla NS					32	San Felipe N80E	3	San Felipe	Valparaíso	II
34	San Fernando EW	2	San Fernando	Libertador General Bernardo O'Higgins	II	33	San Felipe S10E				
35	San Fernando NS					36	Talca N10E	3	Talca	Maule	II
38	El Almendral N50E	3	Valparaíso	Valparaíso	III	37	Talca N80W				
39	El Almendral S40E					40	Constitución EW	3	Constitución	Maule	III
42	Llayllay N80W	3	Llayllay	Valparaíso	III	41	Constitución NS				
43	Llayllay S10W					44	Ventanas EW	3	Ventanas	Valparaíso	III
46	Viña del Mar N70W	3	Viña del mar	Valparaíso	III	45	Ventanas NS				
47	Viña del Mar S20W										

Tabla 2-2. Summary of the horizontal records obtained in the Maule earthquake [30].

	Seismic Event: Maule's Earthquake, February 27, 2010, Mw = 8.8										
	Accelerograms	Seismic zone	Location	Region	Soil's seismic classification		Accelerograms	Seismic zone	Location	Region	Soil's seismic classification
1	UTFSM L	3	Valparaíso	Valparaíso	I	3	Angol EW	3	Angol	Araucanía	II
2	UTFSM T					4	Angol NS				
5	Curicó NS	2	Curicó	Maule	II	7	Hualañe L	3	Hualañe	Maule	II
6	Curicó EW					8	Hualañe T				
9	Papudo L	3	Papudo	Valparaíso	II	11	Santiago L	2	Santiago	Metropolitana de Santiago	II
10	Papudo T					12	Santiago T				
13	La Florida NS	2	Santiago	Metropolitana de Santiago	II	15	Maipú EW	2	Santiago	Metropolitana de Santiago	II
14	La Florida EW					16	Maipú NS				
17	Puente Alto EW	2	Santiago	Metropolitana de Santiago	II	19	Talca L	3	Talca	Maule	II
18	Puente Alto NS					20	Talca T				
21	Valdivia EW	3	Valdivia	Los Ríos	II	23	Vallenar EW	3	Vallenar	Atacama	II
22	Valdivia NS					24	Vallenar NS				
25	El Almendral L	3	Valparaíso	Valparaíso	II	27	Concepción L	3	Concepción	Biobío	III
26	El Almendral T					28	Concepción T				
29	Constitución L	3	Constitución	Maule	III	31	Copiapó EW	3	Copiapó	Atacama	III
30	Constitución T					32	Copiapó NS				
33	Llolleo L	3	Llolleo	Valparaíso	III	35	Matanzas L	3	Navidad	Libertador General Bernardo O'Higgins	III
34	Llolleo T					36	Matanzas T				
37	Peñalolén EW	2	Santiago	Metropolitana de Santiago	III	39	Viña del Mar EW	3	Viña del mar	Valparaíso	III
38	Peñalolén NS					40	Viña del Mar NS				
41	El Salto NS	2	Santiago	Metropolitana de Santiago	III						
42	El Salto EW										

* SZ: Seismic zone.
** SSC: Soil seismic classification according to PEER [31] based on V_{S30} values.

Regarding the determination of the seismic hazard, the following procedure was established:

2.4.1. Selection of representative spectrum for the development of compatible accelerograms

A representative spectrum for each soil type (I, II and III) was selected to determine the seismic hazard. The research carried out by Newmark and Riddell [32] was considered, which was later suitable for the seismic classification of soils in Chile by Riddell [15]. The seismic hazard was defined, through a design spectrum normalized to a peak ground acceleration (PGA) of 1 g, without considering the different seismic hazard zones. The main characteristics of the soil for seismic classification considered in this study are shown in Table 2-3 [19]. The soil type IV defined in the current Chilean standard for the seismic design of bridges [19], is not considered in this investigation due to the lack of acceleration records.

Tabla 2-3. Definition of seismic classification of soils type I, II, III and IV according to [11] and [31].

Soil's seismic classification	Description
I	ROCK:
Natural material with in-situ shear wave propagation velocity V_{ss} equal to or greater than 800 m/s or uniaxial compression strength of intact (without cracks) specimens equal to or greater than 10[MPa] and RQD equal to or greater than 50%.	
If the thickness of the rock is less than 20m, the soil will be classified as the type of soil underlying the rock.	
II	DENSE GRAVEL – DENSE SAND – HARD COHESIVE SOIL
Soil with shear propagation velocity V_s in situ equal to or greater than 400 m/s in the top 10 m and increasing with depth, or:	
Dense gravel, with dry unit weight γ_d equal to or greater than 20 kN/m^3 or density index ID (DR) (relative density) equal to or greater than 75%, or degree of compaction greater than 95% of the value of the modified proctor test, or:	
Dense sand with ID (DR) (relative density) equal to or greater than 75%, or standard penetration index N greater than 40 (normalized to effective overload pressure of 0.10 MPa), or degree of compaction greater than 95% of the value of the modified proctor test, or:	
Hard cohesive soil with non-drained shear strength S_μ equal to or greater than 0.10 MPa (single compression strength q_μ equal to or greater than 0.20 MPa on specimens without cracks).	
In all cases, the conditions indicated must be met independently of the position of the water table and the minimum thickness of the soil layer should be 20 m.	
If the thickness on the rock is less than 20 m, the soil is classified as type I.	
If the thickness of soil type II on soil type III or IV is less than 20 m, the soil shall be classified as the underlying soil type, i.e. type III or type IV, as appropriate	
III	PERMANENTLY UNSATURATED SAND - GRAVEL OR UNSATURATED SAND - COHESIVE SOIL - SATURATED SAND
Permanently unsaturated sand, with ID (DR) (relative density) between 55% and 75%, or standard penetration index N greater than 20 (without normalizing to the effective overload pressure of 0.10 MPa), or.	
Gravel or unsaturated sand, with a degree of compaction less than 95% of the value of the modified proctor test, or,	
Cohesive soil with S_μ between 0.025 and 0.10 MPa (q_μ between 0.05 and 0.20 MPa) regardless of the water table, or,	
Saturated sand with standard penetration index N between 20 and 40 (normalized to effective overload pressure 0.10 MPa).	
Minimum thickness of layer; 10 m. If the thickness of the soil on top of the rock or type II soil is less than 10 m, then the soil will be classified as type II. If the thickness of soil III on top of soil IV is less than 25 m, the soil will be classified as type IV.	
IV	SATURATED COHESIVE SOIL
Saturated cohesive soil with S_μ equal to or less than 0.025 [MPa] (equal to or less than 0.050 [MPa]).	
Minimum layer thickness of 10 [m]. If the thickness of the layer on the saturated cohesive soil corresponding to any of the previous mentioned soil classifications is less than 10 m, the soil will be classified as type IV	

* This document does not consider studies on soils classified as type IV, due to the absence of accelerograms signals for such classification of soil

2.4.2. Modification of the representative spectrum

The displacement demand obtained from accelerograms is normally distorted by the baseline adjustment procedures applied on them, i.e., such displacements are considerably smaller than the actual ones occurred during the earthquake. Then, the representative spectrum was modified to better represent the demands observed in Chile, especially in the Maule earthquake (2010, Mw 8.8), by suppressing the zone of displacement amplification and extending the zone of velocity amplification. This establishes demands of displacement of the order of those observed in the last earthquake in Chile for periods of vibration of up to 2.5 s, range in which most of the highway bridges in the country are. The results are shown in Figs. 2-10 and 2-11.

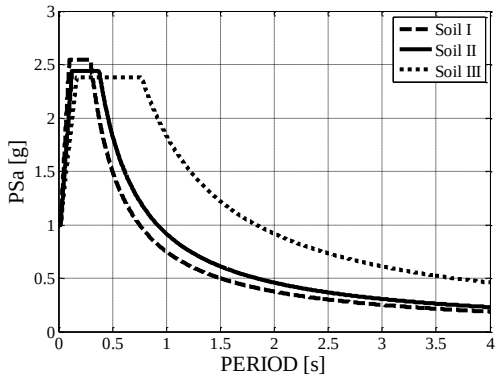

Fig. 2-10. Pseudo-acceleration response spectrum (normalized to PGA = 1 g) established by Riddell [15] and modified for use in this document, soil seismic classification I, II and III, as stipulated in INN [33].

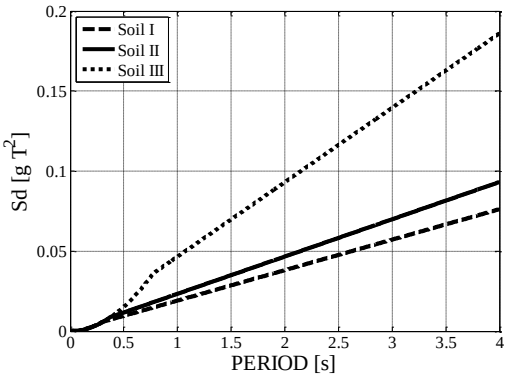

Fig. 2-11. Displacement response spectrum (normalized to PGA = 1 g) established by Riddell [15] and modified for use in this document, soil seismic classification I, II and III, as stipulated in INN [33].

2.4.3. Scaling of the reference spectra

Then the spectra were normalized to the effective peak acceleration (EPA) defined in MOP [19], according to the seismic zonation (zone 1, 2 or 3). The values of EPA are shown in Table 2-4. Although the concept of effective acceleration, originally established by ATC [34], does not exactly follow the concept of PGA, it has been used in most of the Chilean regulations so far, so it was considered to scale the demands of displacement, velocity, and acceleration in structures.

Tabla 2-4. Value of effective acceleration coefficient, according to seismic zoning [11].

Seismic zone	A_o: Effective peak acceleration (EPA)
1	0.2 [g]
2	0.3 [g]
3	0.4 [g]

[g] = Gravitational constant ($9.80[m/s^2]$)

2.4.4. Scaling compatible records

Finally, the accelerograms listed in Tables 2-1 and 2-2 are made compatible to the modified reference spectra previously scaled to the associated EPA value according to the seismic hazard zone to which it belongs, using the procedure established by Clough and Penzien [35]. The accelerograms obtained are representative of the seismic design demand on the structures. The result of this process are the compatible accelerograms, to be used for the development of fragility curves from IDA analysis.

2.5. Nonlinear response

To verify the nonlinear model proposed in this research, nonlinear time-history analyses were performed. Fig. 2-12 shows the results of the time-history analysis using the spectrum compatible record based on the Curicó EW seed. This analysis was carried out for the bridge without shear keys. The response history of the base shear is shown in Fig. 2-12(a): the maximum value of the base shear is 2520 kN (42% of the seismic weight), which occurs at 75 s. The relative displacement of the elastomeric bearings is presented in Fig. 2-12(b), where the maximum relative displacement is 330 mm, at 123 s. Finally, the load-displacement relationship of a seismic bar is presented in Fig. 2-12(c).

On the other hand, Fig. 2-13 shows the results for the same record for a bridge with shear keys. The response history of the base shear is shown in Fig. 2-13(a): the maximum value of the base shear is 2500 kN (42% of seismic weight), which also occurs at 75 s. The relative displacement of the elastomeric bearing is presented in Fig. 2-13(b), where the maximum relative displacement is 350 mm, at 123 s. Finally, the load-displacement response of a seismic bar and a shear key are presented in Fig. 2-13(c) and d, respectively. For this case, the responses of the bridges with and without shear keys area similar.

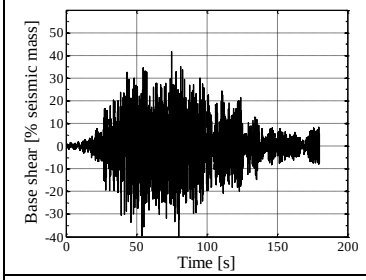

(a) Base Shear

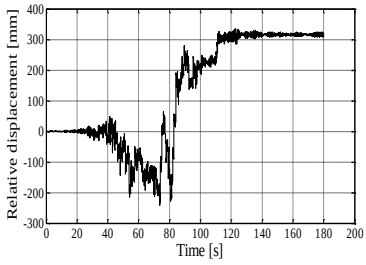

(b) Elastomeric bearings relative displacement

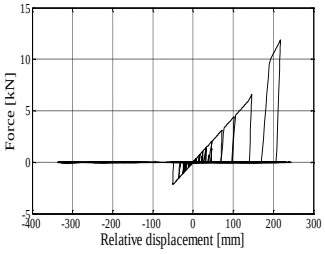

(c) Seismic bars load-displacement relationship

Fig. 2-12. Nonlinear response of the model for one spectrum compatible record. Seismic Hazard 2 (Ao = 0.30 g), soil type II. Highway Bridge without shear keys.

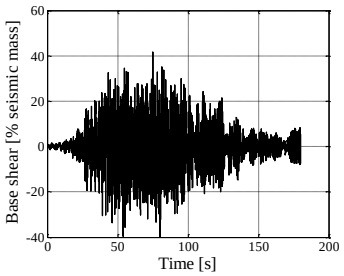

(a) Base Shear

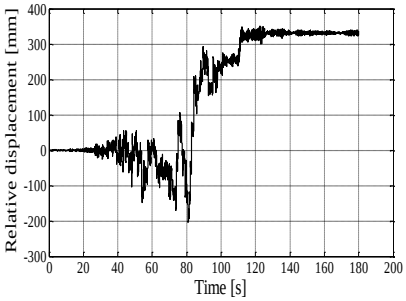

(b) Elastomeric bearings relative displacement

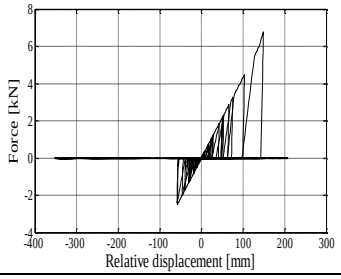

(c) Seismic bars load-displacement relationship

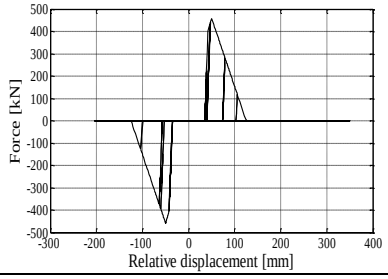

(d) Shear Keys load-displacement relationship

Fig. 2-13. Nonlinear response of the model for one spectrum compatible record. Seismic Hazard 2 (Ao = 0.30 g), soil type II. Highway Bridge with shear keys.

2.6. Analytical fragility curves

The analytical fragility curves developed in this investigation are obtained using an Incremental Dynamic Analysis [36] (IDA). The bridge under study is represented by the analytical model described in Section 3.2, which includes the inelastic behavior of the exterior shear keys, the elastomeric bearings, and the seismic bars. Compatible accelerograms were generated to the expected response spectra from real seed accelerograms considering several magnitude characteristics, seismic demands and local soil conditions (Section 4). Fig. 2-14 shows some results of the IDA, in which a large dispersion of the maximum deformation of the exterior shear keys for each seismic zone and soil type is observed. Additionally, Fig. 2-14 shows the mean response, and the mean plus/ minus a standard deviation is included.

For the construction of the fragility curves, three levels of damage are defined, corresponding to different levels of relative displacement of the superstructure. Damage level DL1 corresponds to the beginning of slip of the elastomeric bearings, which corresponds to d_{by} in Fig. 2-9(b). In the case of the analyzed bridge, this occurs at 17 mm. Damage level DL2 corresponds to a residual displacement of elastomeric bearings greater than 50 mm. This value was used by MOP [19] as the maximum residual relative lateral displacement at which no repair of the bridge was done after the 2010 Maule earthquake. Finally, damage level DL3 corresponds to the collapse of the structure, which is achieved when the maximum relative displacement of the elastomeric bearing is larger than 1000 mm. This restriction corresponds to the distance between the centerline of the externally prestressed beam and the free edge of the cap beam (Fig. 2-9(a)).

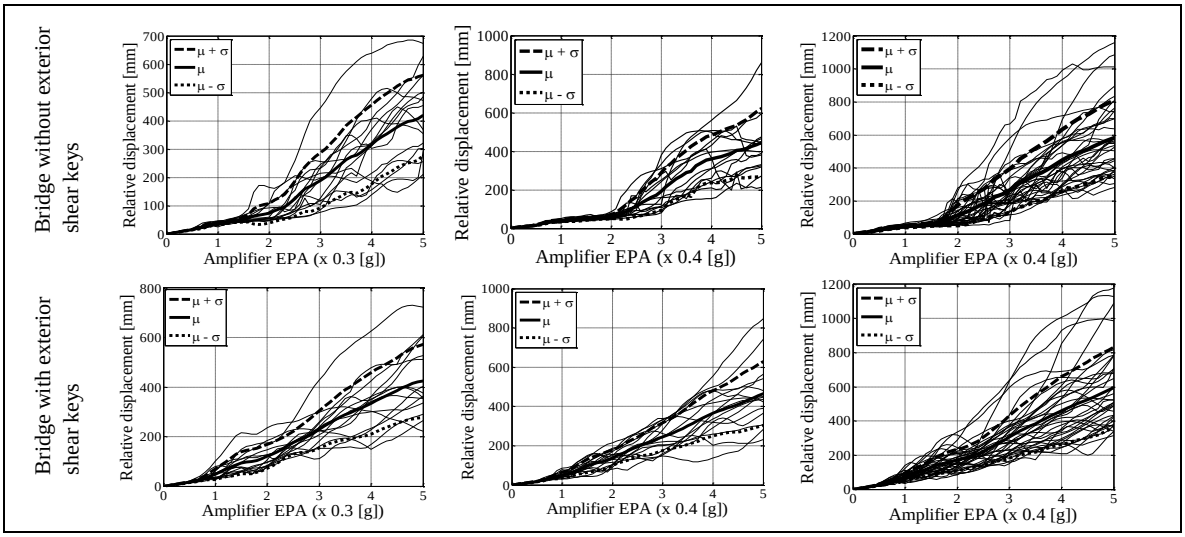

Fig. 2-14. Results of the Incremental Dynamic Analysis considering different seismic hazard zones and soil types.

It should be mentioned that the damage to columns is not considered in this study since no damage was observed in these elements during the 2010 Maule earthquake. Shear forces

transmitted from the superstructure to the bridge abutment were somehow limited by the maximum resisting force between the superstructure and substructure connection.

Fig. 2-15 shows fragility curves for the bridge with and without shear keys for the three damage levels previously defined, for different seismic zones and soil types. For each damage level, a normal logarithmic cumulative distribution function was adjusted using MATLAB software [37]. For a given damage level of a bridge, there is large variability in the calculated fragility curves. For damage levels DL1 and DL2 the fragility curves show that the bridges with shear keys have better seismic performance in terms of the probability of exceeding those damage levels. For damage level DL1, this effect is small. For example, given the same acceleration of 0.5 times the design earthquake, the probability of exceedance DL1 in seismic hazard zone 3 and soil type I slightly decreases from 44% to 40% after adding to the structure shear keys. This result was expected since the onset of slip occurs for a relative displacement of 17 mm, much less than the slip required to start the interaction between the beam and the shear key. The exception to the previous observation is the case of seismic hazard zone 3 and soil type III, in which the value of EPA at a 50% probability of exceeding DL1 increases from 0.04 for bridges without shear keys to 0.25 for bridges with shear keys. It is important to notice that the hazard zone 3 is located along most of the Chilean coast, and soil type III is very common in locations of bridges. For damage level DL2, the presence of shear keys plays an important role in improving the performance of the bridges, irrespective of the seismic hazard zone and soil type. For example, for bridges located in seismic hazard zone 3 and soil type III, at a ground acceleration of 0.5 times EPA, the external shear keys reduce the probability of exceedance of this damage level from approximately 37% to 2% (Fig. 2-15(a)). For an acceleration of 1 times EPA, there is a large reduction of the probability of exceedance of DL2 (reductions of 35% to 70%, Fig. 2-15(b)) for all cases except for seismic hazard zone 3 and soil type III, in which the reduction is smaller, about 10%.

For damage level DL3, the fragility curves show that the difference in the seismic response of bridges with and without shear keys is negligible. The probability of exceedance this damage level is not dependent on the presence of exterior shear keys. This is explained because in order to reach damage level DL3 it is necessary that a relative displacement of the superstructure of 1000 mm occurs, a value much larger than the deformation capacity of the external shear key. Therefore, after the shear key is destroyed, the responses of the two types of bridges are the same. The Incremental Dynamic Analysis was performed up to 5 times the design EPA, large values which could be thought that may never occur. However, after the Maule earthquake, some records registered values that far surpass the seismic hazard design considerations. An example of this is the longitudinal record measured in Llolleo, which has an elastic response spectrum that surpasses in more than 1.5 times the acceleration estimated by the code (Fig. 2-16). It is concluded then, that the bridges are exposed to even higher demands than the ones established by code and throughout its lifespan.

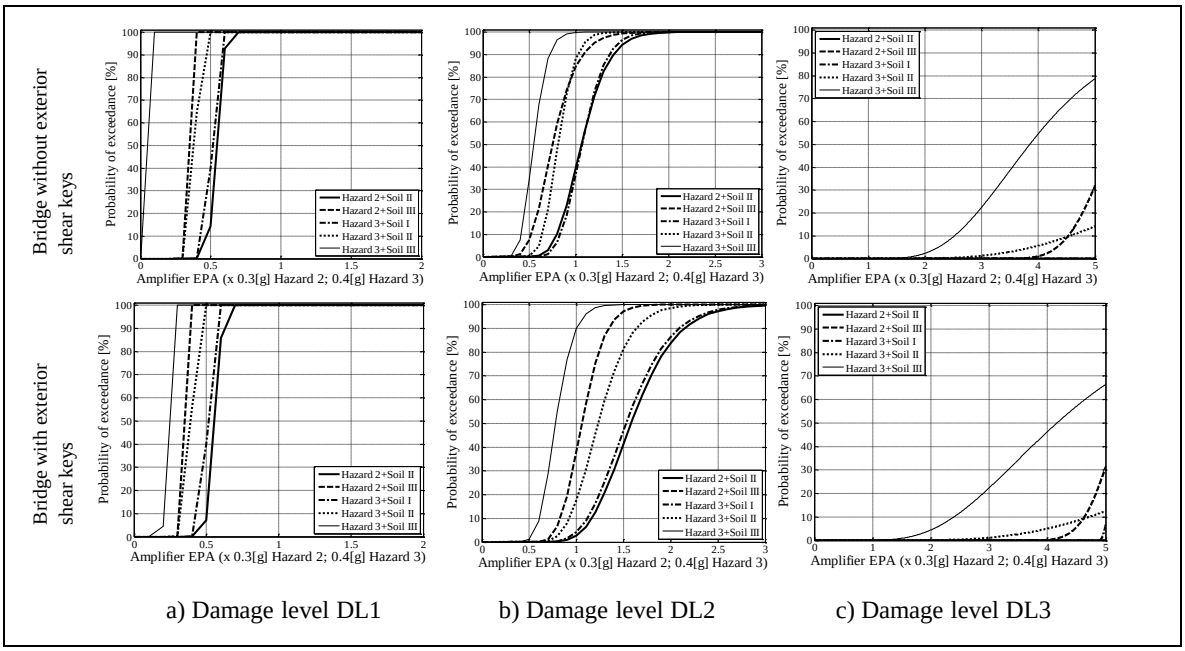

Fig. 2-15. Fragility curves for established damage levels.

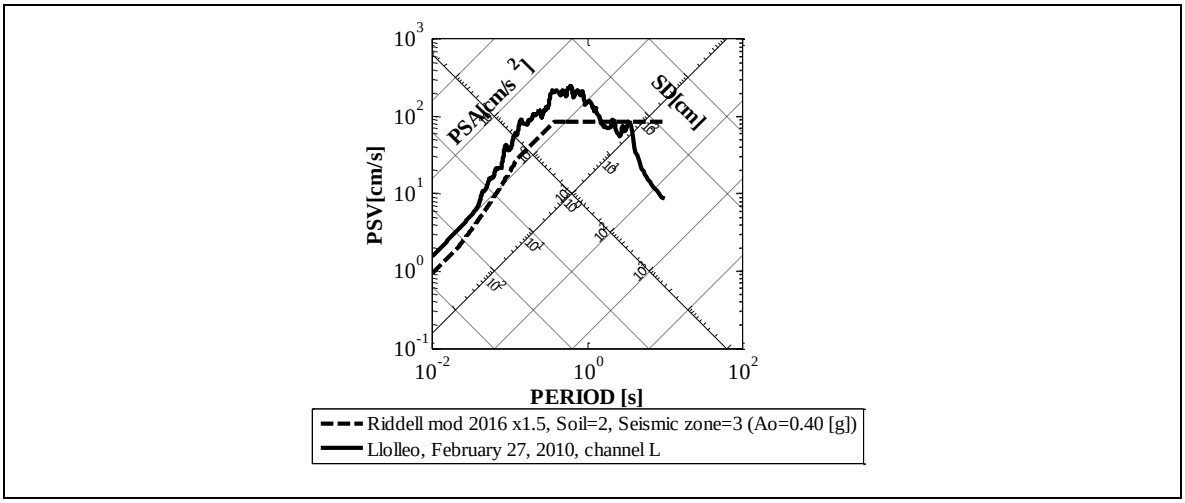

Fig. 2-16. Comparison of the elastic response spectrum of the accelerogram of Llolleo of the 2010 V/s 1.5 times the estimated response to design.

2.7. Conclusions

The role of sacrificial shear keys in the seismic response of bridges was evaluated for different seismic hazard conditions and soil types. Fragility curves were calculated using nonlinear models and a series of records compatible to Chilean response spectra. The results show that the use of external shear keys produces an improvement in the seismic performance of bridges in terms of decreasing the residual displacement. Such improvement is highly dependent on the seismic hazard level and the soil type. The following specific conclusions can be drawn regarding the response of bridges with external shear keys. These conclusions are not only restricted to the local case but are also generally valid.

1. The use of external shear keys negligibly affects the probability of occurrence of collapse, which starts to appear at values close to 1.5 times the EPA value established in the Chilean seismic resistant design standards.
2. The use of external shear keys on bridges prevents that large residual displacement of elastomeric bearings occurs prematurely. Its occurrence is transferred from values of 0.3 to 1.8 EPA design standard value to values of 0.5 to 2.5 EPA, depending on the seismic hazard zone and seismic soil type. The presence of shear keys increases the probability of continuity of use of the bridges after a severe seismic event.
3. The use of external shear keys affects only slightly the probability of occurrence of initial slip of the superstructure.
4. The role of shear keys is essential in reducing the probability of damage in bridges located in high seismic hazard zones and soft soils (type III).
5. The current Chilean design provisions of shear keys do not consider the soil classification simultaneously with the level of seismic hazard in the determination of the design forces. This is the main reason for the large variability of fragility curves of a bridge at a given damage level. These provisions should be revised and modified to establish a uniform seismic performance of bridges designed in different seismic hazard zone and seismic classification of soil.

The use of analytical fragility curves is a great tool to verify the correct calibration of design standards, regarding the performance objectives the standards pursue. This can be especially valuable for countries with a low occurrence of important seismic events, which cannot calibrate their provisions through observations of damage after earthquakes.

Acknowledgments

The research presented considered useful suggestions by the structural engineer Antonio Martínez. The authors wish to acknowledge the funding provided by CONICYT (Chilean Commission for Scientific & Technological Research) through the National Research Center for Integrated Natural Disaster Management FONDAP 15110017.

References

[1] Li JZ, Peng TB, Xu Y. Damage investigation of girder bridges under the Wenchuan earthquake and corresponding seismic design recommendations. Earthq Eng Eng Vib 2008;7:337–44.

[2] Han Q, Du X, Liu J, Li Z, Li L, Zhao J. Seismic damage of highway bridges during the 2008 Wenchuan earthquake. Earthq Eng Eng Vib 2009;8:263–73.

[3] Kawashima K, Takahashi Y, Ge H, Wu Z, Zhang J. Reconnaissance report on damage of bridges in 2008 Wenchuan, China earthquake. J Earthq Eng 2009;13:965–96.

[4] Priestley MJN, Seible F, Uang CM. The Northridge earthquake of January 17, 1994: damage analysis of selected freeway bridges, SSRP-94/06. San Diego, La Jolla, California: Department of Structural Engineering, University of California; 1994.

[5] Moehle J, Fenves G, Mayes R, Priestley MJN, Seible F, Uang CM, et al. Northridge earthquake of January 17, 1994, reconnaissance report. Earthq Spectra 1995:1.

[6] Buckle I, Hube M, Chen G, Yen W, Arias J. Structural performance of bridges in the offshore Maule earthquake of February 27, 2010. Earthq Spectra 2012;28:533–52.

[7] Buyukozturk O, Bakhoum MM, Beattie SM. Shear behaviour of joints in precast concrete segmental bridges. J Struct Eng 1990;116:3380–401.

[8] Kaneko Y, Connor JJ, Triantafillou TC, Leung CK. Fracture mechanics approach for failure of concrete shear key, I: theory. J Eng Mech 1993;119:681–700.

[9] Kaneko Y, Connor JJ, Triantafillou TC, Leung CK. Fracture mechanics approach for failure of concrete shear key, II: verification. J Eng Mech 1993;119:701–19.

[10] Megally SH, Silva PF, Seible F. Seismic response of sacrificial shear keys in bridge abutments: Structural systems research report SSRP-2001/23. San Diego, La Jolla, California: Department of Structural Engineering, University of California; 2001.

[11] Bozorgzadeh A, Megally SH, Ashford S, Restrepo JI. Capacity evaluation of exterior sacrificial shear keys of bridge abutments. J Bridge Eng 2007;11:555–65.

[12] Goel RK, Chopra AK. Role of shear keys in seismic behavior of bridges crossing fault-rupture zones. J Bridge Eng 2008;13:398–408.

[13] Nailiang X, Jianzhong L. Seismic performance of highway bridges with different transverse unseating-prevention devices. J Bridge Eng 2016;21.

[14] Mazzoni S, McKenna F, Scott MH, Fenves GL. Open system for earthquake engineering simulation user manual. Berkeley: Pacific Earthquake Engineering Research Center, University of California; 2009.

[15] Riddell R. Inelastic design spectra accounting for soil conditions. Earthq Eng Struct Dyn 1995;24:1491–510.

[16] INN. NCh433 of. 1996 Mod. 2009: Earthquake-resistant design of buildings. Chile: Instituto Nacional de Normalización; 2009 [in spanish].

[17] AASHTO. AASHTO specification for LRFD seismic bridge design, Washington, DC; 2011.

[18] CALTRANS. Seismic design criteria: Version 1.4, Sacramento, California, http:// www.dot.ca.gov; 2006.

[19] MOP. Manual de carreteras – volumen 3: Instrucciones y criterios de diseño, edición 2016 (Highway manual – volume 3: instructions and design criteria, edition 2015). Chile: Ministerio de Obras Públicas – Dirección General de Obras Públicas – Dirección de Vialidad; 2015.

[20] MOP. Comentarios y sugerencias: Criterios sísmicos para el diseño de puentes en Chile. Chile: Ministerio de Obras Públicas – Dirección General de Obras Públicas – Dirección de Vialidad; 2009. Versión G.

[21] Schlaich J, Schäfer K, Jennewein M. Strut-and-tie modelling of structural concrete. Stuttgart: IABSE Colloquium Structural Concrete; 1991. p. 62.

[22] Scott MH, Fenves GL. Plastic hinge integration methods for force-based beamcolumn elements. J Struct Eng 2006;132:244–52.

[23] Martinez A, Hube M, Rollins K. Analytical curves for highway bridges in Chile. Eng Struct 2017;141:530–42.

[24] McKenna F, Fenves G. The OpenSees command language manual: version 1.2. Berkeley: Pacific Earthquake Engineering Center, University of California; 2001. .

[25] Rubilar F. Nonlinear model to predict the sismic behavior of overpasses [Master of science thesis]. Pontificia Universidad Católica de Chile; 2015 [in spanish].

[26] Steelman J, Fahnestock L, Filipov E, LaFave J. Shear and friction response of nonseismic laminated elastomeric bridge bearings subject to seismic demands. J Bridge Eng 2013;18:612–23. [27] Li J, Xu Y. A new isolation system for small and mid-span bridges. In Seventh National seismic conference on bridges & highways. Oakland; 2013.

[28] Filipov E, Fahnestock L, Steelman J, Hajjar J, LaFave J, Foutch D. Evaluation of quasi-isolated seismic bridge behavior using nonlinear bearing models. Eng Struct 2013;49:68–181.

[29] Saragoni R, Hart G. Simulation of artificial earthquake. Earthq Eng Struct Dyn 1974;2:249–67.

[30] RENADIC. National accelerometer network Chile, http://www. terremotosuchile.cl/; 2016.

[31] PEER. PEER 2014/05 – seismic velocity site characterization of thirty-one Chilean seismometer stations by spectral analysis of surface wave dispersion. Berkeley: Pacific Earthquake Engineering Research Center, 325 Davis Hall, University of California; 2014. [32] Newmark NM, Riddell R. Inelastic spectra for seismic design. In 7th World Conference on Earthquake Engineering, Istanbul, Turkey; 1980:IV.

[33] INN. NCh433 of.1993: earthquake – resistant design of buildings. Chile: Instituto Nacional de Normalización; 1993 [in spanish].

[34] ATC. ATC 3 tentative provisions for development of seismic regulations for buildings. Redwood City, California, United States of America: Applied Technology Council; 1978.

[35] Clough R, Penzien J. Dynamics of Structures. 3rd ed. California: Computers & Structures Inc; 1995.

[36] FEMA. FEMA P695 quantification of building seismic performance factors. Redwood City, California: Applied Technology Council; 2009.

[37] MathWorks Inc. MATLAB version R2014a.

3. CHAPTER 3

EFFECTS OF CHANGES IN SEISMIC DESIGN CRITERIA IN THE TRANSVERSE AND VERTICAL RESPONSE OF CHILEAN HIGHWAY BRIDGES

Abstract: Recent earthquakes in Chile have produced extensive damage in highway bridges, such as large transverse residual displacements, yield of shear keys, and unseat of the main girders, showing that bridges are highly vulnerable structures. Many of these damages are attributed to problems in the design codes. After the 2010 Maule earthquake, new structural design criteria were incorporated for the seismic design of bridges in Chile, among which the increase of the strength of the exterior and interior shear keys and the seismic bars, and the mandatory use of diaphragms at the ends of the girders stand out. The present chapter assesses the effects of the changes in seismic design criteria in the transverse and vertical response of Chilean highway bridges. This assessment is accomplished by comparing fragility curves of a typical bridge designed using the Chilean standards before and after the 2010 Maule earthquake, taking into account the seismic soil types and the different seismic hazard zones. Firstly, the evolution of bridge seismic design codes in Chile is described. Secondly, the performance of bridges and their main failure modes during the 2010 Maule earthquake are summarized. After this, four structural configurations representative of typical bridge typologies were designed using the different design criteria and then they were modeled for the evaluation of their seismic behavior. Finally, fragility curves were generated using Incremental Dynamic Analysis (IDA), nonlinear analytical models and ground motion records from previous earthquakes. The calculated fragility curves show that bridges designed with the current design codes have a seismic performance that depends, to a large extent, on the type of soil in which the bridge is located. The changes in seismic design criteria significantly decrease the probability of collapse of bridges, while the vertical response is unaffected by those changes. Despite those changes in design criteria, the results of the models show that the shear keys behave as sacrificial elements, avoiding damage to the columns and cap beams. Design recommendations that improve the seismic performance of non-skewed bridges are provided.

3.1. Introduction

Around 300 highway bridges were damaged during the 2010 Maule earthquake (M_w 8.8) in Chile [1]. The failures ranged from minor cracking to complete collapse of the deck. The most common types of damage [2–6] observed were: (a) transverse displacement and excessive rotation of the deck, (b) collapse of segments of bridges due to the loss of vertical support in abutments or bents, (c) failure of skewed highway bridges associated with insufficient seat support length, (d) damage to the precast girders due to pounding of the girders with the exterior shear keys, and (e) diagonal tension failure of the exterior shear keys (Fig. 3-1). Only a few bridges suffered damage to the substructure. As these types of damage have also been reported in other earthquakes around the world [7–21], the vulnerability of bridges in a road system is evident.

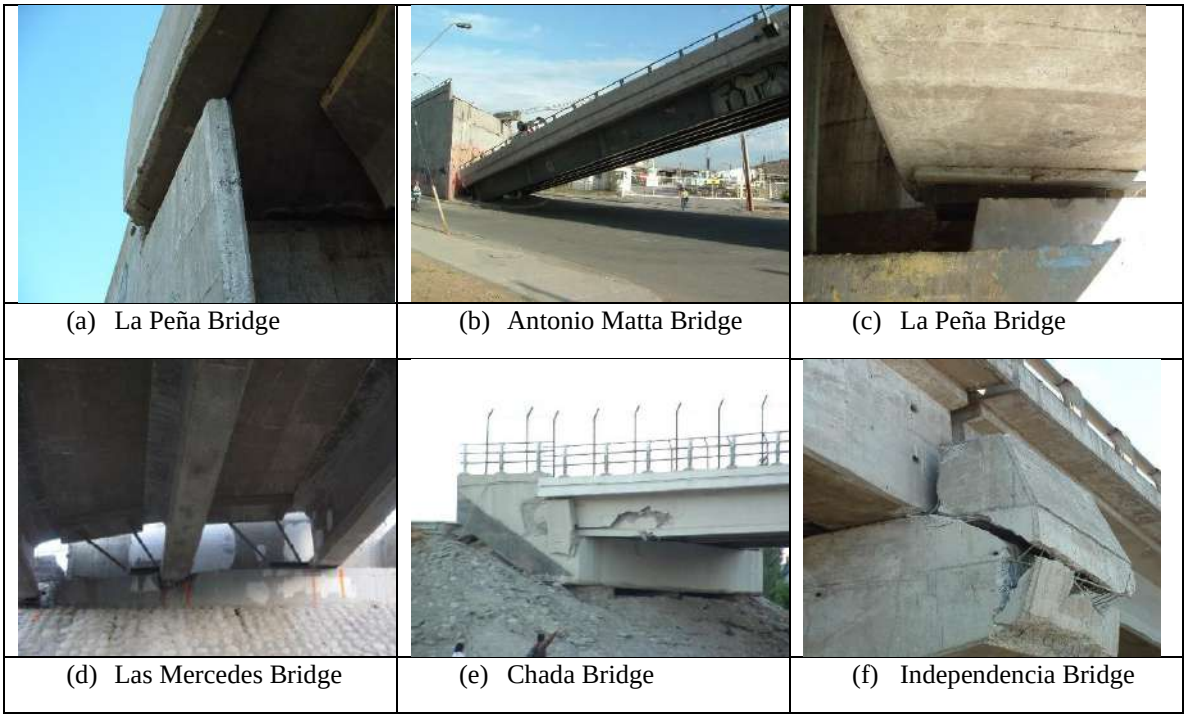

Fig. 3-1. Common types of damage observed during the 2010 Maule earthquake were: (a) transverse displacement and rotation of the deck; (b) skew bridge collapse due to insufficient seat support length; (c) sliding of elastomeric bearings; (d) damage to seismic bars; (e) damage to abutment walls and precast girders; and (f) damage to exterior shear keys in bridge bents.

To avoid the described failures in future earthquakes, new criteria were considered for the seismic design of bridges in Chile after 2010 [22–25]. The criteria included were: (a) the increase of the seat support length in abutments and bents, in order to provide a greater capacity for the longitudinal and transverse displacement of the bridges; (b) the addition of an end diaphragm connected to the deck and the girders, in order to protect the girders from the pounding against the shear keys, avoiding local damage to the girders and degradation of the lateral stiffness of the deck; (c) the increase of design forces of the vertical seismic bars, in order to avoid up-lifting of the deck; and (d) the change of the design of the exterior and

interior shear keys in abutments and bents, in order to avoid excessive in-plant rotations and collapse of the deck. An end diaphragm is an element that connects the main girders of the bridge to transmit the seismic loads to the bearings. Reinforced concrete diaphragms increase the lateral stiffness of the superstructure and protect the girders against the interaction with shear keys. Vertical seismic bars are ductile elements located in between the girders and the support bearings, embedded in the abutment or the cap beams and connected to the superstructure. The purpose of these bars is to control uplifting of the deck to limit horizontal displacement with respect to the substructure. It is important to remark that regulations such as the Japan Road Association [26], Caltrans [27], LRFD Seismic Bridge Design [28], AASHTO LRFD [29], SCT Mexico [30], have already incorporated similar criteria into their provisions.

The seismic response of sacrificial shear keys has been extensively analyzed through analytical and experimental studies (see [31–45]). The shear keys are referred to as sacrificial when they have been designed to fail before any other element in the substructure (e.g., abutment walls, piers, and cap beams). Megally et al. [35] performed an experimental campaign to study the seismic response of interior and exterior shear keys. In addition, they developed analytical models to estimate the capacity of the shear keys, as well as their post-peak performance under cyclic loads. Bozorgzadeh et al. [37] also carried out an experimental research program on exterior shear keys; however, unlike Megally et al. [35], the contribution of the walls of the abutment and the walls of the wings were included. Wilches et al. [45] evaluated the influence of sacrificial exterior shear keys in the seismic response of Chilean highway bridges for different seismic hazard conditions and soil types. The results showed that the use of exterior shear keys produces an improvement in the seismic behavior of the bridges due to the decrease in residual displacement.

Similarly, the seismic behavior of elastomeric bearings for bridges has been studied by several authors (see [46–54]). Filipov [49] developed a formulation and a model for the hysteretic response of elastomers that exhibited bidirectional friction sliding behavior. The model showed good agreement with both static and dynamic experimental results for elastomeric bearings, whose response does not have an appreciable dependence on the velocity of the load application. Steelman et al. [52] characterized the shear and friction deformation of elastomeric bearings under seismic loads. Finally, Rubilar et al. [54] proposed an elastic-perfectly-plastic force-deformation relationship based on the experimental campaign they carried out.

Finally, in spite of the extensive studies on the sacrificial shear keys and the elastomeric bearings, the vertical seismic bars have been scarcely studied. Martinez et al. [55] carried out an experimental campaign to study the effect of seismic bars on the transverse behavior of bridges with and without end diaphragm, and a nonlinear analytical model was proposed. Criado and Lüders [56] proposed an analytical model for prestressed seismic bars as an alternative to replace the conventional vertical bars stipulated in the Chilena Bridge Design Manual [23]. The proposed model showed a performance similar to classical seismic isolation but at a significantly lower cost. According to the aforementioned discussion of

literature, it can be observed that several types of damage and several structural elements of bridges have been well-documented through analytical and experimental studies. Nevertheless, to the best of the authors' knowledge, no analytical research about the effectiveness of the seismic design criteria for bridges incorporated after the 2010 Maule earthquake has been reported. Therefore, the objective of this chapter is to evaluate the effects of the changes in the seismic design criteria on the transverse and vertical response of Chilean highway bridges by comparing the Chilean design codes available before [57,58] and after the 2010 Maule earthquake [22,23,25]. To assess the effects of the new seismic design criteria, different scenarios of structural configurations and designs, seismic hazard and types of soil have been considered. There were several seismic design criteria incorporated after the Maule 2010 earthquake. However, the design criteria that were evaluated in this article are: the increase of the resistance in the design of exterior and interior shear keys, the introduction of end diaphragms, and the increase of resistance of the seismic bars. These criteria refer to the transverse and vertical seismic behavior of bridges.

To achieve the objective of this chapter, a description of the evolution of the codes and manuals of seismic design of bridges in Chile is made, then the performance of highway bridges during the 2010 Maule earthquake and its main failure modes is presented. A representative bridge was chosen as a model to design different hypothetical cases by using different seismic design codes. To select this representative bridge, a statistical analysis of Chilean highway bridges was performed considering their geometrical and material properties. To compare the seismic performance of the hypothetical cases of this bridge, a nonlinear pushover analysis was carried out using OpenSees [59], and fragility curves were generated using Incremental Dynamic Analysis (IDA). Multiple components were taken into account as concentrated nonlinearities in elements such as columns, cap beams, exterior shear keys, interior shear keys, elastomeric bearings, and seismic bars. A set of 174 strong-ground motion records obtained since 1985 was used to obtain the fragility curves.

3.2. Evolution of seismic design of bridges

This section presents a brief history of Chilean seismic design provisions of bridges and a description of the seismic design provisions and practices evaluated hereafter.

Initially, the design of highway bridges in Chile was strongly influenced by European regulations, especially from Germany (Deutsches Institut für Normung, DIN [60]). Since 1953, the design and construction of highway bridges have been revised and authorized by the Ministry of Public Works (MOP from its acronym in Spanish). Between 1970 and 1972, the preliminary version of the Volume 3 Design of the Highway Manual was developed [61]. However, since this manual did not contemplate any seismic specifications, the requirements for design and construction were based on AASHTO [62]. Only after the 1985 Algarrobo earthquake, seismic design recommendations for Chilean bridges were proposed [7,8]. Concessions for the construction and operation of transport facilities were introduced in Chile in the mid-1990s [63]. The bridges built at that time were designed following both AASHTO Standard Specifications [64] and the criteria developed by the experience acquired by the Chilean bridge engineers. Fig. 3-2(a) shows the cross-section of the support of a typical bridge. However, it was not clear in the design standards in which seismic zone this configuration was mandatory.

In 2002, and for the first time, seismic design provisions were included in the Chilean Highway Bridge Manual [57], published by MOP. The manual was based on the AASHTO Standard Specifications [64], and it officially incorporated seismic design criteria for shear keys at the ends of the abutments and bents. The 2008 version of the Chilean Bridge Design Manual (BDM2008) [58] introduced minimal changes when compared to its 2002 version [57]. The 2008 manual considers the following: (a) the longitudinal girders of the bridges located in seismic zone 3 (A0 = 0.4 g, where A0 is the effective peak acceleration and g the gravitational constant) must be connected at their ends by transverse diaphragms; (b) a vertical seismic coefficient of Kv = A0/2g must be used to design the vertical seismic anchor bars, considering that only the seismic force acts upwards and neglecting the contribution of the self-weight loads; and (c) the abutments and bents should consider shear keys to restrict the transverse displacement of the deck. For the design of each shear key, half of the total horizontal seismic force acting in the transverse direction and a gap set between the shear key and the deck, equal to the expected seismic displacement plus 50 mm, must be considered (see Fig. 3-2(b)). Both design and testing for the use of seismic isolators as support elements were regulated by AASTHO Standard Specifications [64].

Before the 2010 Maule earthquake, many bridges built under the concessions system were designed by foreign companies, which introduced modifications to the seismic design required at that time. The main change was to eliminate the exterior shear keys and the diaphragms that connected the ends of the girders (see Fig. 3-2(c)). Most of these modifications were focused on the reduction of construction periods and costs.

After the 2010 Maule earthquake, new seismic criteria were developed for the design of highway bridges in Chile [22]. Some of the new criteria were: (a) all bridges must consider

external and mid-span transverse diaphragms, with no distinction on the seismic zone nor the type of girder (e.g., steel, post-tensioned or prestressed); (b) interaction between the end diaphragm and the shear keys must be increased to an acceleration value of A0; (c) the anchor seismic bars must be designed with a larger vertical acceleration equal to A0; and (d) the abutments and bents must consider exterior and interior shear keys. Shear keys must be designed considering a horizontal acceleration equal to A0. Each shear key must be able to withstand all the transverse force of the deck divided by the number of interior shear keys. The gap between shear keys and the deck must be the maximum height (H) of the seismic isolators or elastomeric bearing plus 50 mm for interior shear keys, and H plus 70 mm for the exterior shear keys (see Fig. 3-2(d)). The latest version of the Bridge Design Manual [25] was published in 2017 (BDM2017). The most significant change compared to the BDM2015 version was that a site coefficient was included for the estimation of the seismic design forces in the shear keys, seismic bars, and diaphragms (see Fig. 3-2(e)). This site coefficient depends on the type of soil. Wilches et al. [45] had already demonstrated the need to incorporate this coefficient into the seismic design of Chilean highway bridges. Additionally, each interior shear key must be introduced into the diaphragms in a shear key shape to redirect any damage to the diaphragm itself to avoid damaging the girders (see Fig. 3-2(e)). The seismic criteria incorporated after the 2010 Maule earthquake in the Highway Bridge Manual were strongly influenced by the Japanese code [26].

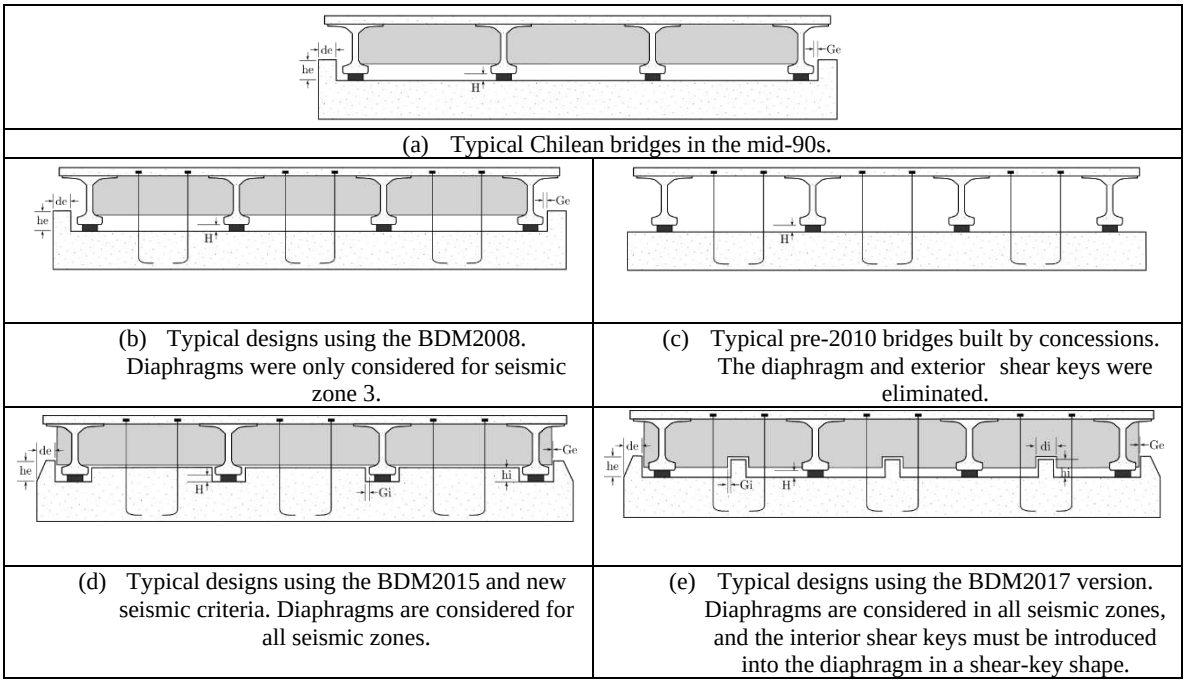

(a) Typical Chilean bridges in the mid-90s.

(b) Typical designs using the BDM2008. Diaphragms were only considered for seismic zone 3.

(c) Typical pre-2010 bridges built by concessions. The diaphragm and exterior shear keys were eliminated.

(d) Typical designs using the BDM2015 and new seismic criteria. Diaphragms are considered for all seismic zones.

(e) Typical designs using the BDM2017 version. Diaphragms are considered in all seismic zones, and the interior shear keys must be introduced into the diaphragm in a shear-key shape.

Fig. 3-2. Evolution of typical Chilean bridges: de = width of exterior shear keys, he = height of exterior shear keys, Ge = separation between the superstructure and exterior shear keys (i.e., external gap), H = height of elastomeric bearing, Gi = separation between the superstructure and interior shear keys (i.e., internal gap), di = width of interior shear keys, and hi = height of interior shear keys.

3.3. Seismic performance of highway bridges

The main area affected by the 2010 Maule earthquake was located in the south-central region of Chile, affecting the urban areas around Santiago, Valparaíso, Viña del Mar and Concepción [65]. As shown in Fig. 3-3, most of the damaged highway bridges were located along the Santiago-Temuco highway, Santiago-Los Vilos highway, Concepción, and Arauco. A total of 221 and 11 public bridges were damaged and collapsed, respectively, while 91 concession bridges were damaged or collapsed [1]. Of the damaged concession bridges, 10 were overpasses, 14 underpasses, 52 pedestrian bridges and 15 other types of bridges. These damaged bridges represent 1.6%, 2.9%, 11.8% and 2.3% of the total number of overpasses, underpasses, pedestrian bridges and other types of bridges operated by concession, respectively [66].

The types of damages that induced significant changes in Chilean regulations were: damage to exterior shear keys in bridge bents (Fig. 3-3(a)); damage to precast girders (Fig. 3-3(b)); sliding of elastomeric bearings (Fig. 3-3(c)); damage to seismic bars (Fig. 3-3(d)); collapse of the deck (Fig. 3-3(e)); drop of access embankment (Fig. 3-3(f)); damage to abutments (Fig. 3-3(g)); and damage to bents (Fig. 3-3(h)). Damages shown in Fig. 3-3(a)–(e) occurred due to transverse displacement of the deck.

Fig. 3-3. Seismic intensity, damage, and location of bridges after the 2010 Maule earthquake.

Fig. 3-4(a) summarizes the damage distribution observed in 80 bridges inspected after the 2010 earthquake. The most damaged bridges were simply supported bridges with precast girders and simply supported composite (i.e., steel girder and concrete slab) bridges, which represent 67% and 16% of all the damaged bridges, respectively. Fig. 3-4(b) shows the

different types of damage that occurred in two seismic zones, having many bridges that often presented more than one type of damage. Of the inspected bridges, 50% were located in seismic zone 2 (A_0 = 0.3 g) and 50% in seismic zone 3 (A_0 = 0.4 g). Damage in shear keys, precast girders, seismic bars, and elastomeric bearings, and excessive displacement of the deck, appeared in 88%, 83%, 37%, 26% and 49% of the bridges for the seismic hazard zone 3, respectively. Similarly, for seismic hazard zone 2 the values were 33%, 17%, 50%, 50% and 33%, respectively. This damage distribution justifies the evaluation of the effect of the hazard zone in the changes of design criteria. Also, 55% of the non-skewed bridges were damaged, showing the importance of evaluating the response of those bridges.

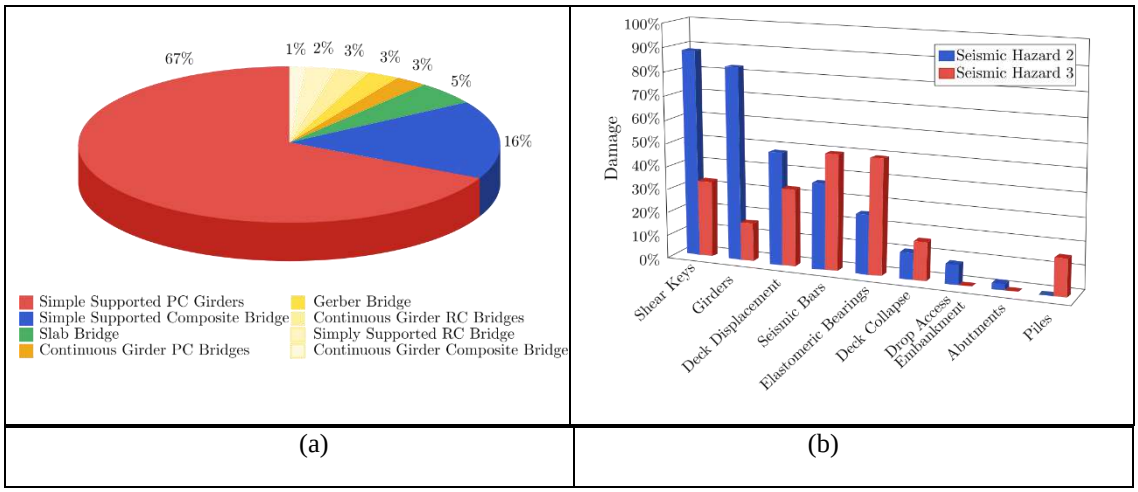

Fig. 3-4. Damage distribution of Chilean bridges after the 2010 Maule earthquake (Mw = 8.8): (a) by the type of bridge and (b) by the type of damage.

3.4. Analytical model of bridges

3.4.1. Definition of a representative bridge

To define the bridges that were analyzed, a statistical analysis of bridges in Chile was carried out using data supplied by MOP. The bridges were classified according to the material type (e.g., reinforced concrete, prestressed concrete, and steel) and the number of main girders and their support condition, classified as simply supported or continuous. As shown in Fig. 3-5, the bridges with simply supported prestressed concrete girders are the most common bridges built in Chile, comprising 38% of the total. Of this class, 23% corresponds to non-skewed bridges and 15% to skewed bridges. Other common classes include simply supported and continuous composite bridges.

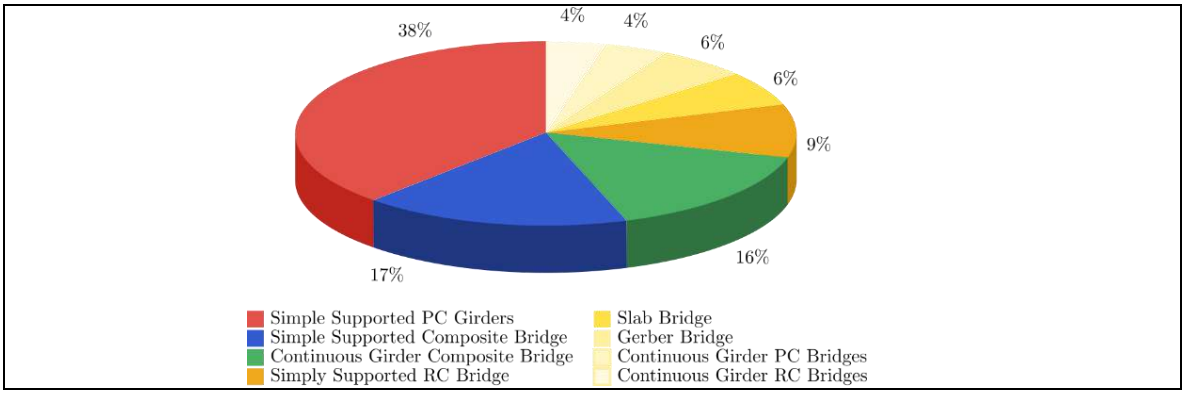

Fig. 3-5. Distribution of bridges in Chile

A representative structure of the Chilean highway bridges was selected, which can be observed repeatedly throughout the country (Fig. 3-6). The representative non-skewed bridge consists in a reinforced concrete deck, four simply-supported girders with a span of 26 m between supports. Its bents are composed of a cap beam and multiple columns. Elastomeric bearings support the girders, which are the interface between the deck and the substructure. Seismic bars are used to control the vertical uplift of the deck, while sacrificial shear keys are used in bents and abutments to control transverse displacement [28,67]. Fig. 3-6 shows the dimensions (in meters) of a typical Chilean non-skewed bridge and the structural components of a bridge bent.

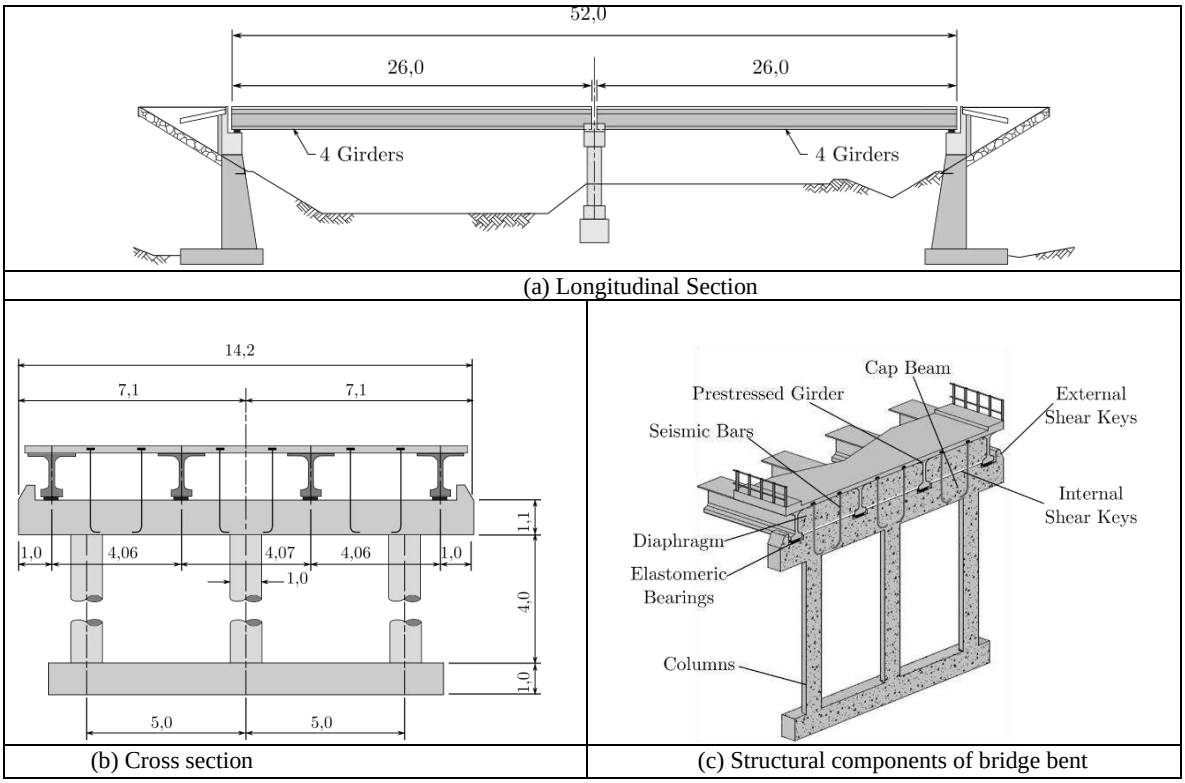

Fig. 3-6. General configuration of the representative bridge used in the study (all dimensions in meters).

Four configurations of the representative bridge bent are defined. Configuration A corresponds to the representative bridge (Fig. 3-7(a)), configuration B represents the representative bridge with end diaphragm (Fig. 3-7(b)), configuration C corresponds to configuration B with interior shear keys (Fig. 3-7(c)), and configuration D represents configuration C with exterior shear keys (Fig. 3-7(d)). Configuration D represents the structural configuration that is required by the latest version of the Bridge Design Manual [25]. To evaluate the effects of the principal changes in the seismic design criteria, each configuration was designed using three seismic bridge design manuals (i.e., BDM2008, BDM2015, and BDM2017). Three seismic hazards (A_0 = 0.2 g, A_0 = 0.3 g, and A_0 = 0.4 g) and three soil types (I, II, III) were considered, resulting in a total of 108 models of bridges. The strengths required to design the main elements of each bridge configuration were calculated using the Chilean bridge design manuals [58,23,25]. The columns, cap beams, elastomeric bearings, and shear keys were designed using AASHTO LRFD, as required by the Chilean bridge design manuals. The strength of the vertical seismic bars was calculated as the tensile yield strength of the bars (see [58,23,25]). The yield strengths of the steel reinforcement, the vertical seismic bars, and the elastomeric bearings were f_y = 420 MPa, f_y = 280 MPa, and f_y = 235 MPa, respectively; the compressive strength of the concrete of the superstructure and the substructure was f'_c = 25 MPa.

3.4.2. Nonlinear model of the bridge

Different authors have modeled the seismic response of bridges using 2D [55,68,69] and 3D [12,40,49] models. The 2D models allow to determine the transverse response of the bridges [70], but they cannot predict the rotation of the superstructure nor the longitudinal displacement. These models are best suited to evaluate the performance of the bents of non-skewed and symmetrical bridges. Considering that in this study the representative highway bridge is non-skewed and symmetrical, and that the changes in design provisions evaluated are related to the transverse response of the deck, the bridge is studied through a plane 2D model of a bridge bent.

The OpenSees software [59] was used to calculate the response of the structures with configurations A, B, C and D (Fig. 3-7). The analyses were performed using nonlinear, two-dimensional models to represent the transverse response of bridges. The nonlinearities were incorporated into the seismic bars, elastomeric bearings, exterior and interior shear keys, cap beams, and columns. All the models of the bents considered the columns fixed to the foundations, neglecting the effects of the soil-structure interaction. In Fig. 3-7, the lines in red represent nonlinear elements, the blue lines represent linear elements, and the dashed lines in blue represent rigid elements. Parameters such as the diameter of the columns, dimensions of the girders, and the ratio of longitudinal and transversal reinforcement vary according to the design of each bridge. Due to the large amount of information obtained from the analysis and design of each bridge, the design procedure was not included in this article.

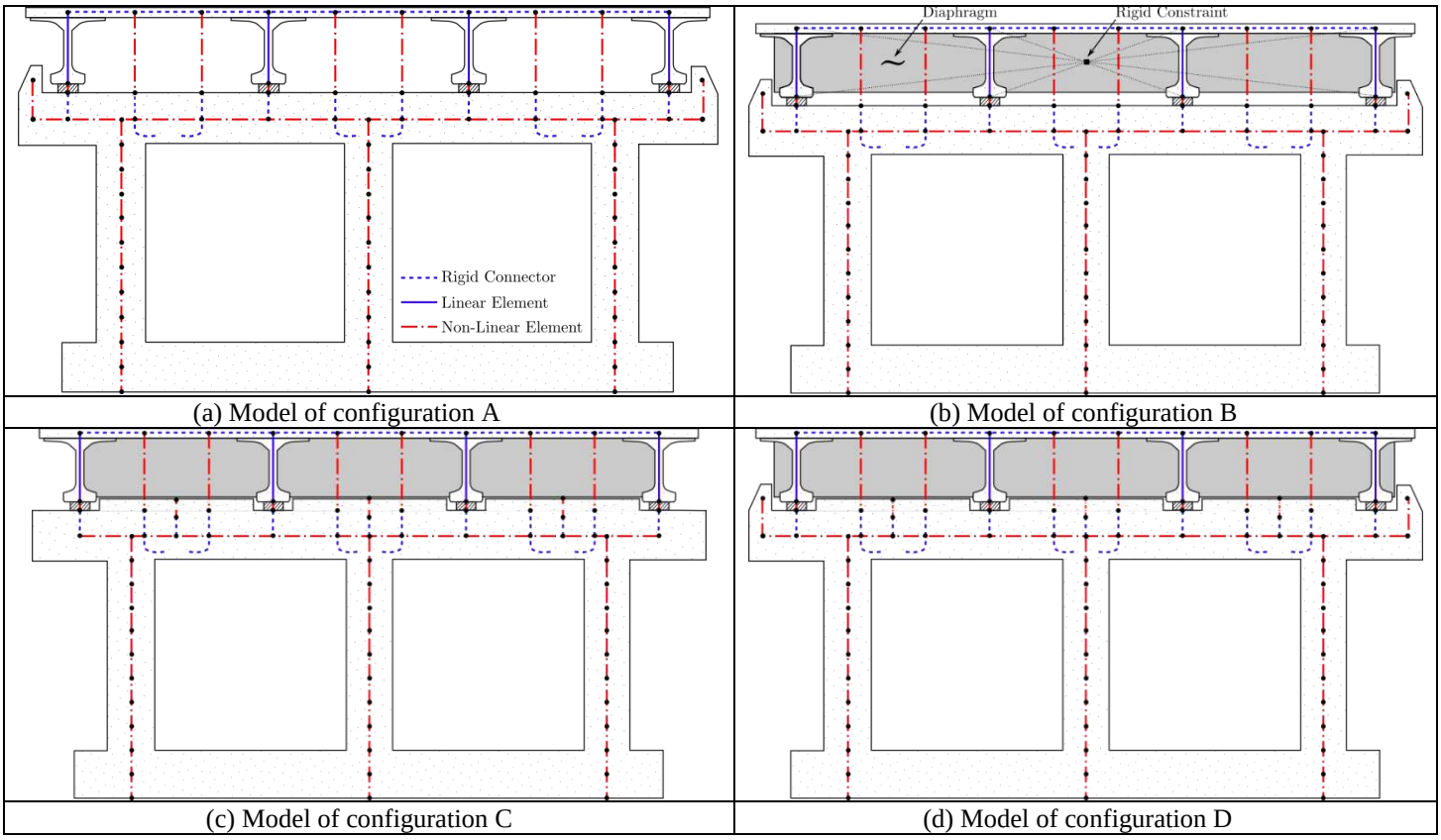

(a) Model of configuration A | (b) Model of configuration B

(c) Model of configuration C | (d) Model of configuration D

Fig. 3-7. Discretization of the finite element models of the bridge bent.

The models defined in Fig. 3-7 were used to evaluate the lateral response of the bridge. The elastomeric bearings were modeled using elastic perfectly-plastic elements, as proposed by Rubilar et al. [54] (cf. [50,52]) (see Fig. 3-8(a)). The lateral behavior of the seismic bars was modeled with the bilinear model defined by Martinez et al. [55] (see Fig. 3-8(b)), with the uniaxial material of hysteretic type by McKenna and Fenves [71]. The longitudinal girders were modeled as linear-elastic elements with the lateral stiffness calculated using a linear finite element model (*q.v.* Wilches et al. [45]). The hysteretic response of the exterior shear keys in configurations A, B and D were modeled as proposed by Megally et al. [35]. Two materials connected in series were assigned to a "twoNodeLink" element. The first material is the uniaxial material "ElasticPPGap," associated with the initial gap between the external longitudinal girder of the deck and the exterior shear keys; whereas the second material is the uniaxial material "Hysteretic," associated with the properties of reinforced concrete. The response obtained for the exterior shear keys is presented in Fig. 3-8(c). The interior shear keys in configurations C and D were modeled in the same way as the exterior shear keys, but the hysteretic response used was the same as proposed by Silva et al. [36] (see Fig. 3-8(d)). The diaphragm was defined as a rigid constraint [59].

The vertical response of the deck was analyzed using the configuration D. The effect of the elastomeric bearings and the vertical seismic bars were modeled using two parallel springs: an elastic compression-only material for the elastomeric bearing, and an elastic tension-only material for the seismic bars. Fig. 3-8(e) shows the vertical response of the deck: the first

spring represents the stiffness of the elastomeric bearings plus the stiffness of the seismic bars (K1), while the second spring represents the vertical stiffness of the seismic bars (K2). In addition, prestressed steel was considered as a different type of seismic bar, modeled as shown in Fig. 3-8(f).

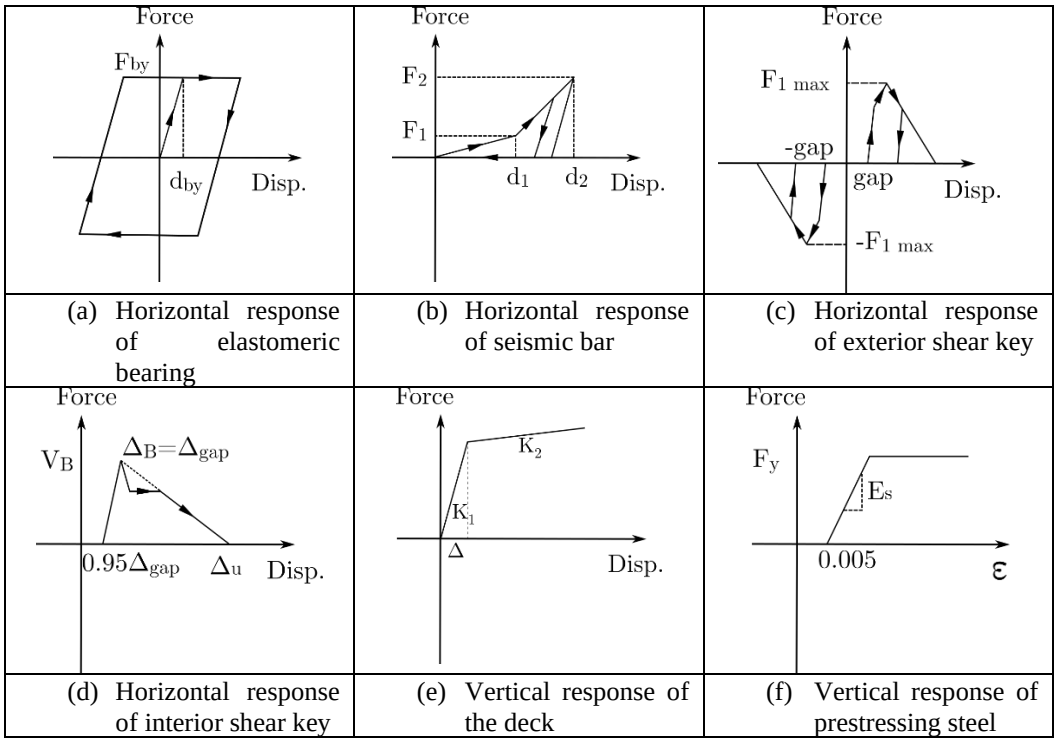

(a) Horizontal response of elastomeric bearing

(b) Horizontal response of seismic bar

(c) Horizontal response of exterior shear key

(d) Horizontal response of interior shear key

(e) Vertical response of the deck

(f) Vertical response of prestressing steel

Fig. 3-8. Force-displacement relationship of elements used in the models**.**

The columns and cap beams were modeled using the "Displacement-Based Beam-Column Element" in all models [72]. The cross-section of columns and beams were modeled using fiber elements, which help to capture the distribution of plasticity along the elements. Fig. 3-9 shows a discretized section of a column (see Fig. 3-9(a)) and a cap beam (see Fig. 3-9(b)), consisting of confined concrete and unconfined concrete fibers (see Fig. 3-9(c)), and the precise location of the longitudinal steel bars which were modeled as a bilinear (see Fig. 3-9(d)). The model proposed by Mander et al. [73] is used to simulate the confined concrete. The number of elements used in the models was calibrated by comparing the results of a pushover analysis of the columns and the bent modeled with Opensees [59] to the response obtained with a nonlinear model with SAP [74]. The columns were modeled with eight internal rings for the confined concrete and two outer rings for the unconfined concrete (see Fig. 3-9(a)). An 8x8 mesh represents the confined concrete and a 2x1 mesh represents the unconfined concrete of the cap beam (see Fig. 3-9(b)). In both cases, the steel bars are located between the last layer of confined concrete and the first layer of unconfined concrete.

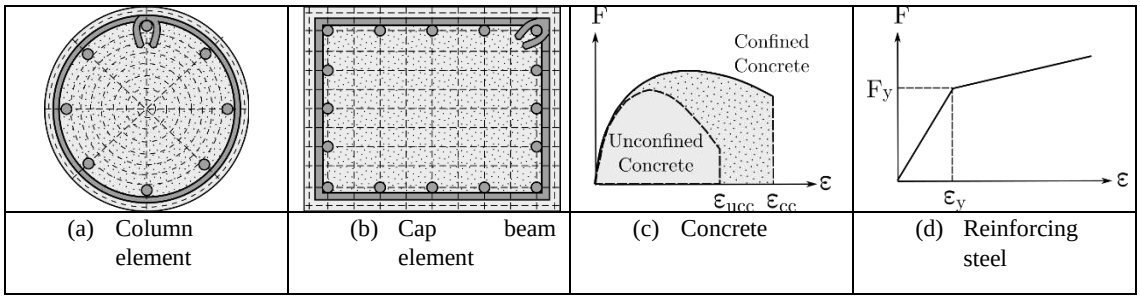

(a) Column element | (b) Cap beam element | (c) Concrete | (d) Reinforcing steel

Fig. 3-9. Fiber-based discretization of a circular reinforced concrete column and cap beam.

3.4.3. Selection of seismic records

The nonlinear response of a given structure is highly dependent on the characteristics of the excitation [75]. The characteristics of the recorded seismic events are strongly correlated with the dynamic properties of the soils and the hysteretic behavior that these soils could develop. This research analyzed the seismic performance of the highway bridges according to the seismic classification of the foundation soils and the seismic hazard zones, as defined in the bridge design standard by MOP [25]. This standard describes that soil type I corresponds to rock, soil type II corresponds to hard soils like dense gravel and sand, and soil type III corresponds to soft soils like saturated sand. The performance of the bridges was evaluated through the use of analytical fragility curves, as established by Serdar et al. [76], using the Incremental Dynamic Analysis (IDA) (Vamvatsikos et al. [77]). The seismic action considered was a linear modulation of Chilean seismic records. These records were selected using the following criteria:

1. The use of accelerograms recorded during the earthquakes of Algarrobo, Punitaqui, Tocopilla, Maule, Constitución, Iquique and Coquimbo, for which seismic soil classification exists. Table 3-1 shows the magnitude of those earthquakes and the number of records available for each one. The description of the seismic classification of the soil considered for this study is indicated in the 2017 Chilean Bridge Design Manual [25]. The seismic classification of the soil for each station of the records selected is summarized in Tables 3-2 and 3-3 as reported by [78–84].

Tabla 3-1. Number of accelerograms used in this research.

Earthquake	Date	Mw	Horizontal Channels	Vertical Channels	Source
Algarrobo	03.03.1985	8.0	47	22	[85]
Punitaqui	14.10.1997	7.1	4	2	[86]
Tocopilla	14.11.2007	7.7	2	1	[86]
Maule	27.02.2010	8.8	38	19	[86]
Constitución	25.03.2012	7.0	6	3	[87]
Iquique	03.04.2014	8.2	14	7	[87]
Coquimbo	16.09.2015	8.3	6	3	[87]
Total			**117**	**57**	

Tabla 3-2. Location and seismic soil classification of accelerometers existing before 2010.

		GPS**						GPS**			
Site of the accelerometer	**SSC***	**Latitude**	**Longitude**	**Source SSC***	**Source GPS****	**Site of the accelerometer**	**SSC***	**Latitude**	**Longitude**	**Source SSC***	**Source GPS****
Copiapó	III	-27,374	-70,322	[79]	[88]	Santiago La Florida	II	-33,514	-70,605	[79]	[88]
Vallenar	II	-28,577	-70,755	[79]	[88]	Llolleo	III	-33,616	-71,615	[78]	•
Illapel	II	-31,630	-71,170	[78]	[88]	Melipilla	II	-33,686	-71,216	[84]	•
Los Vilos	II	-31,912	-71,511	[80]	•	Rapel	I	-33,942	-71,736	[78]	•
La Ligua	II	-32,449	-71,232	[78]	•	Matanzas	III	-33,964	-71,876	[79]	•
Papudo	I	-32,520	-71,450	[80]	[88]	Pichilemu	I	-34,386	-72,004	[80]	•
Zapallar	I	-32,554	-71,458	[78]	•	San Fernando	II	-34,586	-70,991	[78]	•
Ventanas	III	-32,743	-71,489	[78]	•	Iloca	II	-34,942	-72,184	[78]	•
San Felipe	II	-32,750	-70,721	[78]	•	Hualañé	II	-34,976	-71,806	[84]	[88]
Llay-Llay	III	-32,840	-70,956	[78]	•	Curicó	II	-34,991	-71,237	[84]	[88]
Viña del Mar Centro	III	-33,025	-71,553	[79]	[88]	Constitución	III	-35,340	-72,400	[84]	[88]
Valparaíso Almendral	II	-33,030	-71,620	[79]	[88]	Talca	II	-35,430	-71,630	[84]	[88]
Valparaíso UTFSM	I	-33,030	-71,620	[79]	[88]	Cauquenes	III	-35,967	-72,322	[81]	•
Viña del Mar El Salto	III	-33,047	-71,510	[81]	[88]	Chillan Viejo	II	-36,629	-72,139	[78]	•
Las Tórtolas	II	-33,131	-70,706	[78]	•	Concepción	II	-36,828	-73,048	[79]	[88]
Quintay	I	-33,193	-71,697	[78]	•	Angol	III	-37,790	-72,710	[83]	[88]
Santiago Peñalolén	III	-33,501	-70,579	[84]	[88]	Valdivia	II	-39,831	-73,239	[79]	[88]
Santiago Maipú	II	-33,509	-70,771	[84]	[88]						

* Seismic soil classification
** Global Positioning System coordinates
• GPS coordinates estimated in this research

Tabla 3-3. Location and seismic soil classification of accelerometers installed after 2010.

			GPS**			
Name of the accelerometer	**Site of the accelerometer**	**SSC***	**Latitude**	**Longitude**	**Source SSC***	**Source GPS****
PSGCX	Pisagua	I	-19,597	-70,123	[82]	[87]
T10A	Huara	II	-19,995	-69,767	[82]	[87]
T05A	Iquique SERVIU	II	-20,210	-70,150	[82]	[87]
T07A	Pozo Almonte	III	-20,256	-69,786	[82]	[87]
T08A	Alto Hospicio	III	-20,270	-70,094	[82]	[87]
HMBCX	Humberstone	II	-20,278	-69,888	[82]	[87]
T13A	Tenencia de Pica	III	-20,496	-69,337	[82]	[87]
ROC1	Cerro El Roble	I	-32,976	-71,016	[84]	[87]
M03L	Curicó	II	-34,976	-71,231	[80]	[87]
GO05	Hualañé	II	-35,010	-71,930	[84]	[87]
M11L	Talca	II	-35,440	-71,632	[78]	[87]
CCSP	Concepción	III	-36,844	-73,109	[84]	[87]

* Seismic soil classification
** Global Positioning System coordinates

2. The accelerograms obtained by [85,86] were corrected using the methodology established by Pecknold and Riddell [89]. The correction does not apply to the signals obtained in [87] because they do not include the initial conditions of the records.
3. An assumption used in this research is that all the accelerograms are valid to be used in the analysis with the same seismic soil classification in which the signal was recorded, regardless of the corresponding seismic hazard zone. This assumption is considered because the change in the frequency content of a signal associated with the seismic hazard zone is negligible for the purposes of this study.
4. The accelerograms considered in this research are valid only for the study of the response of the structures located where seismic soil classification is the same as the one established for the soil of the accelerogram station.
5. Another assumption used in this research is that the accelerograms can be linearly modified to represent the level of seismic hazard associated with a particular value of EPA (Table 4), without changes in the frequency content that could affect the objectives of this investigation. This linear modification is done by obtaining the pseudo-acceleration response spectrum, with a 5% of critical viscous damping ratio and the subsequent reduction or increase of the signal to the value of the PGA equal to the value of EPA (see Table 3-4).

Tabla 3-4. Value of effective peak acceleration according to seismic hazard zone [25,90].

Seismic hazard zone	A_0: Effective peak acceleration
1	0.2 [g]
2	0.3 [g]
3	0.4 [g]
[g] = acceleration of gravity (9.80 m/s^2)	

6. The strong ground motion records were scaled without manipulating their frequency content, which allowed us to include the variability observed in the different Chilean records. Fig. 3-10 shows the horizontal and vertical spectra obtained for all records, which are classified by soil type.

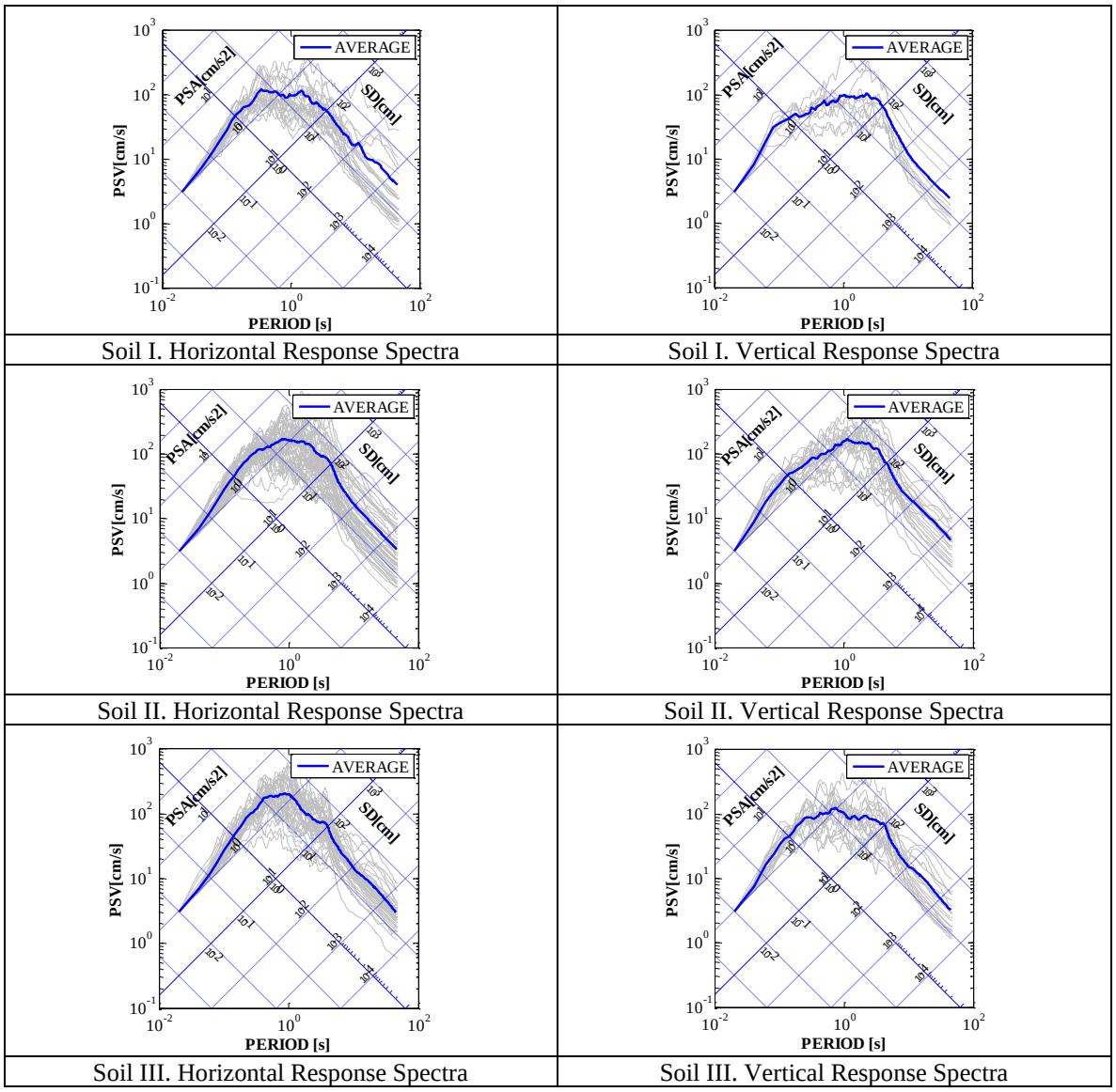

Fig. 3-10. Response spectra (normalized to PGA = 1 g and ξ = 5%) of the records belonging to seismic soil classifications I, II and III.

3.4.4. Verification of plane 2D models of a bridge

A 3D model was used to verify the results obtained using the 2D models described in section 4.2. The comparison between both models was made for a bridge designed with the 2017 Bridge Design Manual [25], see Fig. 3-7(d). The nonlinearities in the 3D model were concentrated in the columns, cap beams, exterior and interior shear keys, elastomeric bearings, and seismic bars, and were modeled similarly as the nonlinearities of the 2D model. The superstructure and the prestressed beams were modeled as beam-column elastic elements. The interaction between the superstructure and the abutments was modeled as established by Omrani et al. [91], which incorporates the effect of the passive force of the

soil behind the abutment. The impact between the superstructure and the abutment was modeled as a gap element in series with an inelastic element, with an impact material model (Muthukumar and DesRoches [92]).

Nonlinear time history analyses were performed for both models using the seismic records of the 2010 Maule earthquake from Papudo (soil type I), Concepcion (soil type II) and Constitucion (soil type III). The calculated transverse displacements of the superstructure relative to the bent are shown in Fig. 3-11. For all types of soils, maximum responses occur at different time points, which, for design purposes, is not relevant. The maximum transverse responses calculated with the 2D models differ by less than 2.3% from those calculated with the 3D models, showing no trend in which one is larger. The differences obtained are negligible for the objectives of this research. Due to the computational cost associated with developing the analytical fragility curves with 3D models, and the minimal differences in the calculated displacements shown in Fig. 3-11, the authors decided to use the 2D models to calculate the fragility curves.

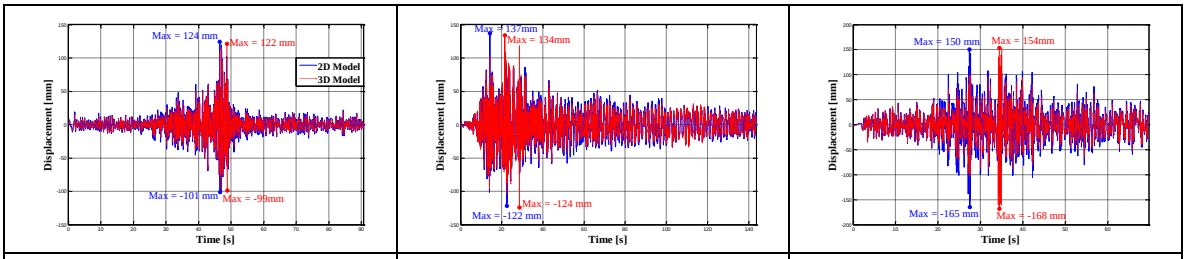

Soil I, Papudo record 2010	Soil II, Concepcion record 2010	Soil III, Constitucion record 2010

Fig. 3-11. Comparison of the nonlinear time history responses obtained with 2D and 3D models.

3.5. Analytical fragility curves

Analytical fragility curves were generated for the 108 models of bridges using the Incremental Dynamic Analysis (IDA). A two-dimensional (2D) model of the central bent of an underpass was constructed with OpenSees to predict the seismic behavior of bridges and calculate fragility curves [59]. To obtain the fragility curves, 78,300 time history nonlinear analyses were performed, using 117 horizontal and 57 vertical accelerograms. Three damage modes were defined for the construction of the fragility curves for the lateral response, corresponding to different levels of relative displacement of the superstructure and the cap beam. These three levels correspond to damage modes observed after the 2010 Maule earthquake, and these three levels of displacement they do not correspond to the increasing levels of damage of a given component of the bridge. Damage mode 1 (DM1) corresponds to a residual displacement of the elastomeric bearings greater than 50 mm. This value was used by MOP [22] as the maximum residual relative lateral displacement, which means that bridges with less than 50 mm of displacement were not repaired after the 2010 Maule earthquake. Damage mode 2 (DM2) corresponds to the displacement that produces yielding of the exterior shear keys, displacement defined as the sum of the gap and the displacement of initial yielding. Finally, damage mode 3 (DM3) corresponds to the collapse of the structure due to unseating of an external girder, achieved when the maximum relative displacement of the elastomeric bearing is greater than the distance between the centerline of the external girder and the free edge of the cap beam. The values of the relative displacements that define the damage modes are shown in Table 3-5 for each Design Manual used to design the structural configurations.

Tabla 3-5. Values of relative displacements that define the damage modes.

Year of Design Manual	Structural configuration	Damage modes*		
		DM1	DM2	DM3
2008	A, B, C, D	50	155	450
2015		50	175.5	670
2017		50	195	890

* Units in mm

A single damage mode was defined (DM1V) for the construction of the fragility curves for the vertical response (i.e., the yield displacement of the seismic bars). This value corresponds to 2.2 mm, 3.8 mm and 5 mm for the 2008, 2015 and 2017 design manuals, respectively.

3.5.1. Comparisons of fragility curves

Figs. 12–14 show the fragility curves obtained for the structural configurations A, B, C and D for the three damage modes defined, taking into account each version of the Bridge Design Manual (i.e., BDM2008, BDM2015, and BDM2017), the seismic hazard scenarios, and the

soil type. It is observed in all the figures that the fragility curves are clustered by the soil type, demonstrating that the seismic performance of the bridges in Chile depends mainly on the type of soil in which the bridges are located, regardless of the seismic hazard. Also, the fragility curves for DM1 are similar to the different structural configurations and versions of the design manual. For example, given an acceleration of 1 times the design level, the probability of exceeding the DM1 is greater than 90% in all cases, regardless of the seismic hazard and type of soil.

In terms of the effectivity of the changes of design criteria, it is observed that the probability of exceeding a given damage mode decreases for all the configurations and damage modes as the bridges are designed with a more recent bridge design manual. The preceding shows that regulations have increasingly become safer.

Analyzing the responses of configuration A (see Fig. 3-12), it is observed that the shear keys for DM2 designed with the BDM2008 yield before than those designed with the BDM2015, which also yield before than those designed with the BDM2017. However, these differences are insignificant. For example, given an acceleration of 2 times the design earthquake, the probability of exceeding DM2 for hazard level 2 and soil type II, goes from 86% using the BDM2008 to 81% using the BDM2015, and to 79% using the BDM2017. In the case of DM3, the changes in the probability of collapse depending on the bridge manual used for the design of the bridge are more significant than the variations of DM2. For example, for an acceleration of 2 times the design earthquake, the probability of exceeding DM3 for a seismic hazard 3 and a soil type III goes from 88% using the BDM2008 to 71% using the BDM2017.

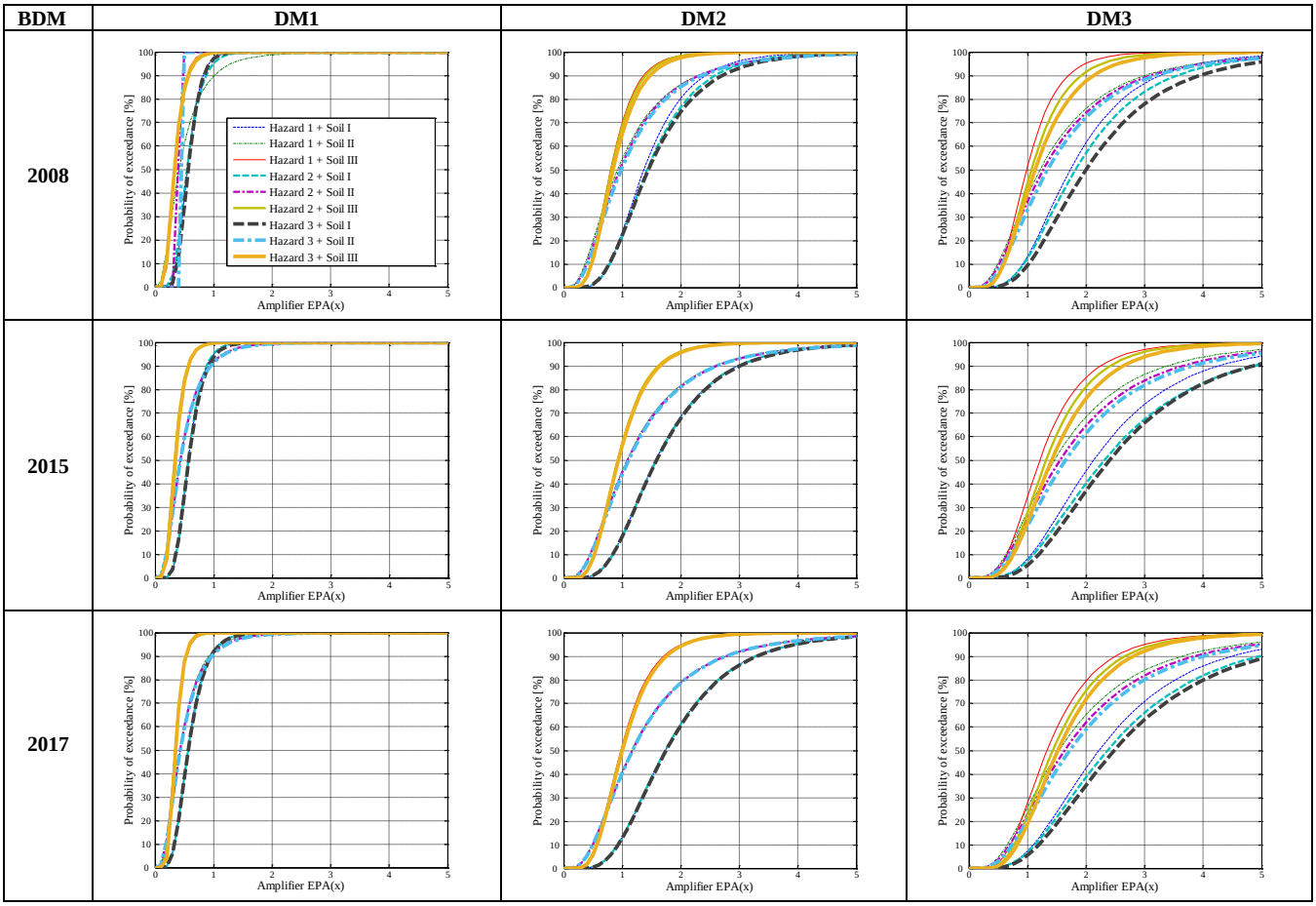

Fig. 3-12. Fragility curves for configuration A.

The observations described above also apply to the other structural configurations analyzed. For example, Fig. 3-13 shows that for configuration B, given an acceleration of 2 times the design earthquake, the probability of exceeding DM2, for seismic hazard 2 and type of soil II, fall from 86% using the BDM2008 to 83% using the BDM2015 and to 79% using the BDM2017. On the other hand, given an acceleration of 2 times the design earthquake, the probability of exceeding DM3 for seismic hazard 3 and soil type III decreases from 79% using the BDM2008 to 55% using the BDM2017.

To assess the effect of adding the diaphragm at the bents, we compared the responses of the structural configurations A, without end diaphragm (see Fig. 3-7(a)), and B, with end diaphragm (see Fig. 3-7(b)). For DM3, all the fragility curves of configuration B (see Fig. 3-13) shifted to the right of the corresponding curves of configuration A (see Fig. 3-12), regardless of the design manual used, showing that the diaphragm decreases the probability of collapse of the bridge for a given acceleration. During the 2010 Maule earthquake, many bridges suffered severe damage due to the lack of the diaphragm incorporated.

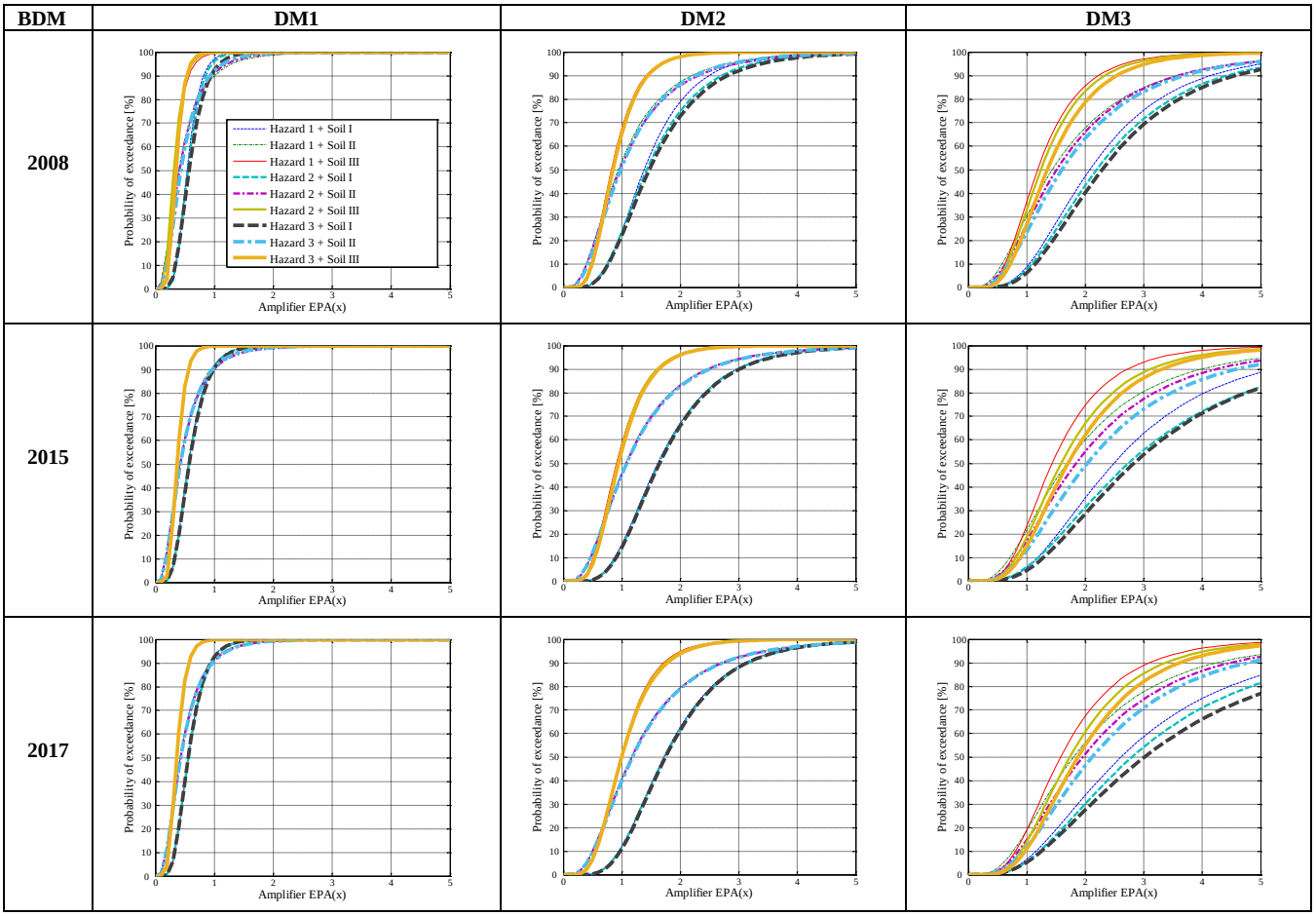

Fig. 3-13. Fragility curves for configuration B.

Increasing the design strength of the exterior shear keys according to the BDM2017 produces a significant reduction in the probability of collapse of the bridge. For example, given an acceleration of 2 times the design earthquake, seismic hazard 2 and soil type III, the probability of configuration B (see Fig. 3-13) exceeding DM3 is 84% if designed using the BDM2008 and 61% using the BDM2017. No yielding in cap beams or columns was obtained in the analysis of bridges with shear keys with larger strength.

To compare the effect of the exterior shear keys versus the effect of the interior shear keys in the transverse response of the bridge, we compare the performance of configuration B (with only exterior shear keys) to configuration C (with only interior keys) (see Figs. 3-13 and 3-14). No differences are observed between both configurations for damage modes DM1 and DM2, in any design manual. In contrast, in terms of DM3, the configuration with interior shear keys has better performance than the configuration with exterior keys. On the other hand, to evaluate the effect of adding interior shear keys to a configuration that has only exterior shear keys, the performances of configuration B (see Fig. 3-13) are compared to configuration D (see Fig. 3-15). It is observed that there are no differences for DM1 and there is a slight improvement in performance for DM2. For DM3 there is a significant change in the fragility curves, sharply decreasing the probability of collapse, regardless of the manual

used for design.

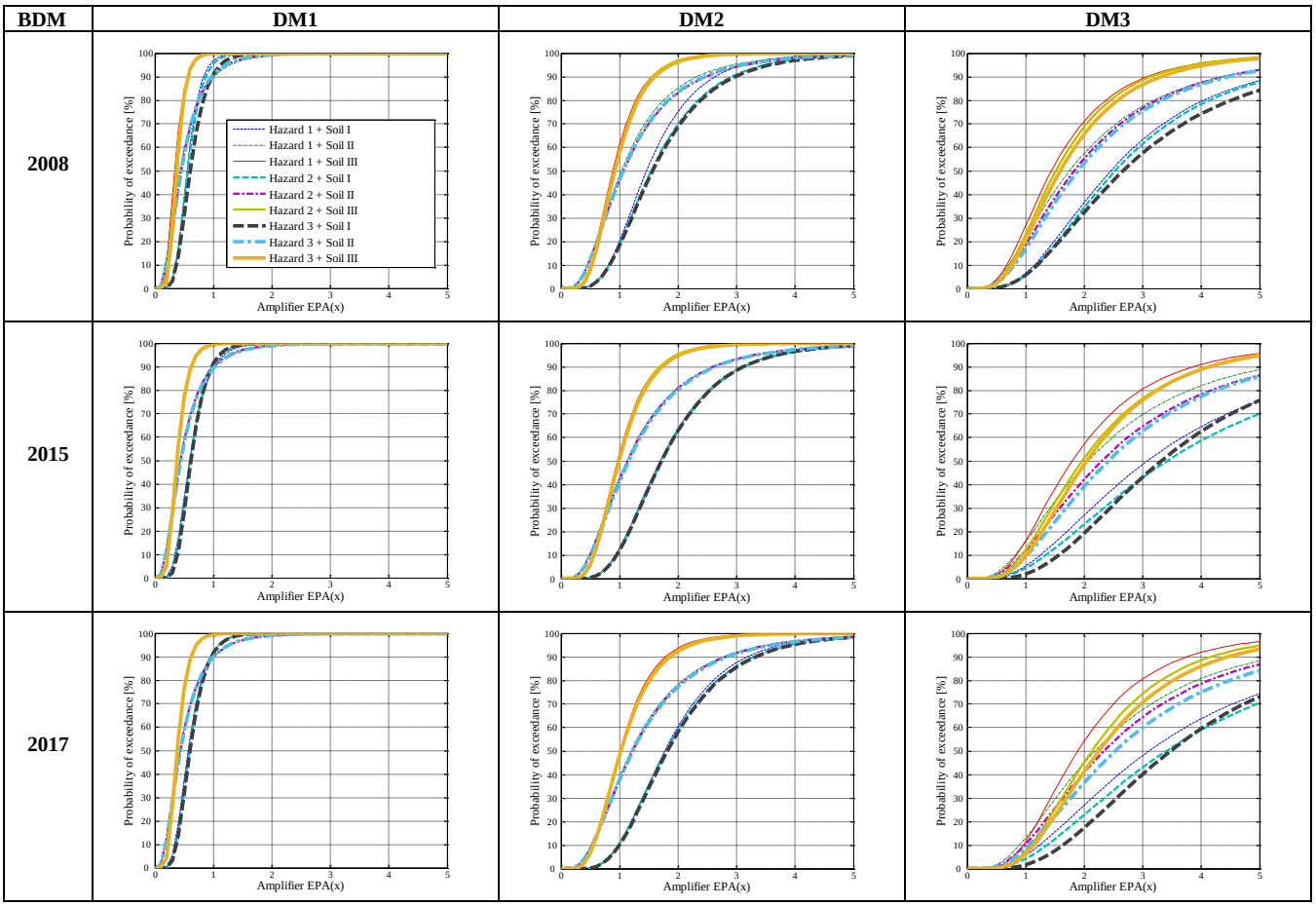

Fig. 3-14. Fragility curves for configuration C.

Finally, to evaluate the simultaneous effects of all the code changes in the design manual after the 2010 earthquake, we compare configuration A (see Fig. 3-12) designed with the BDM2008 and configuration D (see Fig. 3-15) designed with the BDM2017. The changes for DM1 are small, while the decrease in the probability of exceeding DM2 is significant. The reduction of the probability of collapse is significant. For example, for an acceleration of 2 times the design earthquake, the probability of exceeding DM3 for seismic hazard 3 and soil type III plunges from 87% using the BDM2008 to 8% using the BDM2017.

It is important to note that the exterior and interior shear keys failed before any column yielded in all the configurations analyzed, which is consistent with the design philosophy of the Chilean regulations that considers the concentration of damage in the shear keys before the columns fail.

To evaluate the effect of the changes in design criteria of the vertical seismic bars, fragility curves were constructed (see Fig. 3-16) for configuration D and damage mode DM1V, using vertical ground motions and taking into account the different seismic hazard scenarios and soil type. It is observed that for BDM2008, BDM2015, and BDM2017 the fragility curves are grouped by type of soil, irrespective of the seismic hazard. The effect of the increase of the strength of the seismic bars in the vertical response of the deck is small. For example,

given an acceleration equal to the design earthquake, seismic hazard 2 and soil type II, the probability of configuration D exceeding DM1V is 91% if designed using the BDM2008, 84% using the BDM2015, and 81% using the BDM2017.

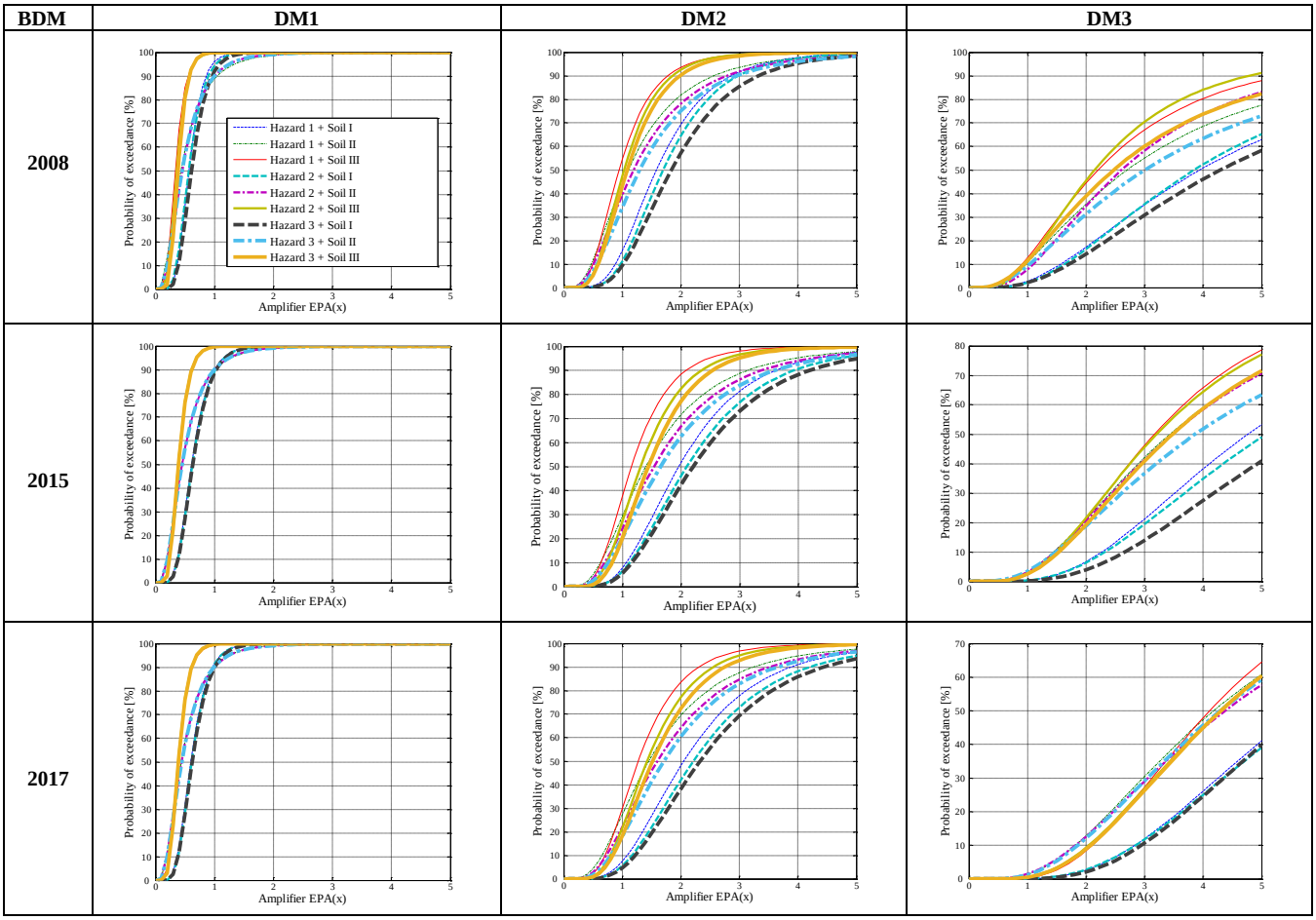

Fig. 3-15. Fragility curves for configuration D.

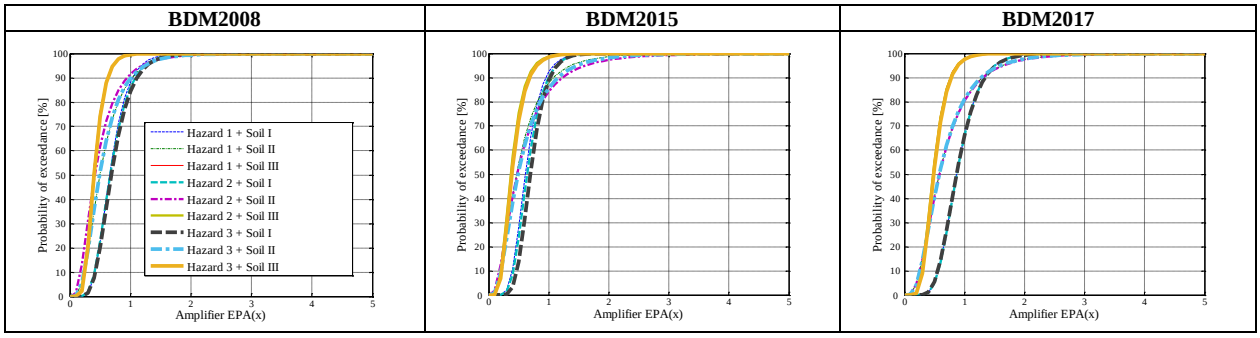

Fig. 3-16. Fragility curves of vertical seismic bars for damage mode DM1V.

Given that the code changes for the design of seismic bars produce a minimal change in the vertical response of the deck, an alternative design for the seismic bars was evaluated. Bars prestressed to 58% of the yield strength of the steel were used as seismic bars. Damage mode

DM1V was defined as a deformation of 12 mm, which corresponds to the yield of the bars. The fragility curves obtained (see Fig. 3-17) show a sharp decrease of the probability of exceeding damage mode DM1V. Also, there is a large variability among the curves. This indicates that the design parameters in the design code have not been calibrated for the vertical response of the bridges. However, Fig. 3-17 shows that including prestressed bars to reduce the uplifting of bridges is highly effective. For example, given an acceleration equal to the design earthquake, the probability of exceedance DM1V for seismic hazard 2 and soil type II for the 2008 and 2017 design manuals decreases from 91% to 81%, respectively. On the other hand, by prestressing the seismic bars, that probability drops to 12%.

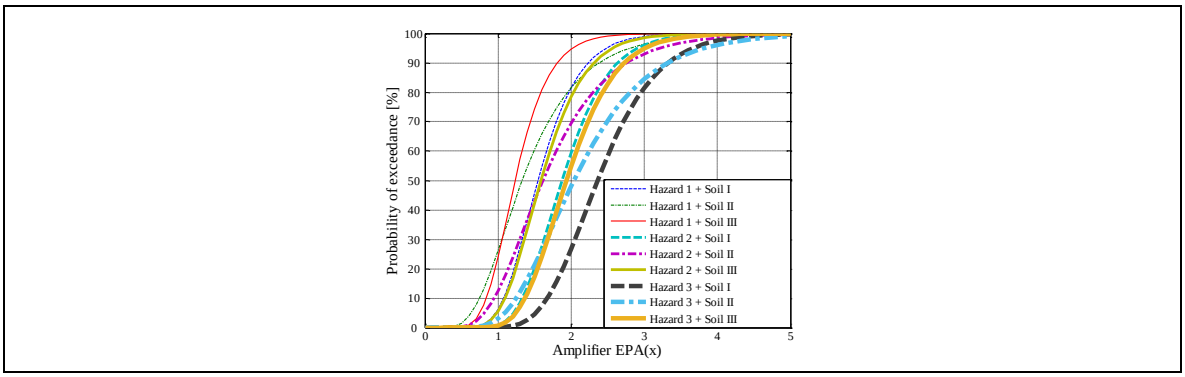

Fig. 3-17. Fragility curves for vertical analysis of configuration D, with prestressed vertical seismic bars.

3.6. Summary and conclusions.

The evolution of the bridge design codes in Chile has been influenced by the damage observed in bridges during recent earthquakes. The effects of changes in the seismic design criteria after the 2010 Maule earthquake were discussed by comparing the fragility curves obtained from bridges designed using different versions of the Bridge Design Manual. The changes in design criteria resulted in a significant decrease of probability of collapse due to transverse displacement of bridges, while the vertical response of bridges is unaffected by those changes. The reduction of probability of collapse occurred due to the addition of structural elements, such as end diaphragms and interior shear keys, as well as by the increase in the resistance of the elements existing in 2010. The fragility curves obtained show that bridges designed with the current design codes have a seismic performance that depends, to a large extent, on the soil type in which the bridge is located. The probability of exceeding a given damage mode decreases as the soil becomes stiffer.
Other specific conclusions obtained in this research are:

1. The changes in design criteria produced minimal reduction in the probability of exceeding a residual transverse displacement of 50 mm.
2. The main effect of adding an end diaphragm to a bridge is a reduction of the probability of collapse of the superstructure.
3. The main effects of the changes in design criteria of the interior shear keys are as follows:

    - The interior shear keys added by the new design criteria are more effective than the existing exterior shear keys in preventing the collapse of the bridge.
    - When adding the interior shear keys to a configuration with only exterior shear keys, the probability of yielding of the exterior shear keys decreases, same as the probability of collapse.

4. Changes in the design criteria of vertical bars produce negligible changes in the probability of uplift of the deck. The probability of uplift of the deck is significantly larger in softer soils. The use of prestressed seismic bars considerably reduces the probability of uplift of the deck.
5. The effect of all the changes in design criteria in Chile after the 2010 earthquake resulted in an important decrease in the probability of yield of the exterior shear keys, and a significant reduction in the probability of collapse of the bridges. The models show that the shear keys behave as sacrificial elements, avoiding damage to the columns and cap beams.

The following are design and detailing recommendations for concrete bridges:

a. An effective retrofit method to significantly decrease the vulnerability of bridges is to add interior shear keys between the girders of the existing bridge.
b. In areas of high seismic hazard, transverse diaphragms must be used between girders at their supports.
c. Vertical seismic bars should be prestressed to 60% of the yield strength of the bar to reduce the probability of uplifting of the deck during large earthquakes.
d. Fragility curves can be used to calibrate design regulations to the performance objectives that they pursue. This is particularly important for countries with long time intervals between large earthquakes and therefore cannot calibrate their design codes through earthquake damage observations.

Future work must include the analysis of 3D models of straight and curved skewed bridges to evaluate the collapse of bridges due to the unseating of the superstructure; experimental campaigns of the elements studied here (i.e., exterior and interior shear keys, diaphragms, and pre-stressed seismic bars) should be carried out in order to analyze their seismic response; and extreme care should be taken when designing bridges with exterior and interior shear keys, which must be included as nonlinear elements in bridge modeling. Finally, design methodologies for exterior and interior shear keys should be included in the Chilean regulations.

Acknowledgments

The authors wish to acknowledge the funding provided by CONICYT (Chilean Commission for Scientific & Technological Research) through the CONICYT Doctorate Scholarship and the National Research Center for Integrated Natural Disaster Management (CIGIDEN) FONDAP 15110017.

References

[1] Buckle I, Hube M, Chen G, Yen W-H, Arias JG. Structural performance of bridges in the offshore Maule earthquake of 27 February 2010. Earthq Spectra 2012;28:S533–52. https://doi.org/10.1193/1.4000031.

[2] Yashinsky M, Oviedo R, Ashford S, Fargier-Gabaldon L, Hube M. Performance of highway and railway structures during the February 27, 2010 Maule Chile earthquake. EERI/PEER/FHWA Bridge Team Report; 2010.

[3] Elnashai AS, Gencturk B, Kwon O-S, Al-Qadi I, Hashash YMA, Roesler J, Kim SJ, Jeong S, Dukes J, Valdivia A. The Maule (Chile) earthquake of February 27, 2010. Mid-America Earthquake Center, Report No. 10-04; 2012.

[4] Kawashima K, Unjoh S, Hoshikuma J-I, Kosa K. Damage of bridges due to the 2010 Maule, Chile, earthquake. J Earthq Eng 2011;15:1036–68. https://doi.org/10. 1080/13632469.2011.575531.

[5] Schanack F, Valdebenito G, Alvial J. Seismic damage to bridges during the 27 February 2010 magnitude 8.8 Chile earthquake. Earthq Spectra 2012;28:301–15. https://doi.org/10.1193/1.3672424.

[6] Toro F, Rubilar Moya FI, Hube M, Santa María H, Cabrera T. Statistical analysis of pedestrian bridges damaged during 2010 Chile earthquake. Seventh natl seism conf bridg highw. 2013. p. 1–12.

[7] Booth E. The Chile earthquake of March 1985. Earthq Spectra 1985;9(3):190–6. https://doi.org/10.1111/j.1467-7717.1985.tb00939.x.

[8] Willie L, Bolt B, Durhin M, Gates J, McCormick D, Smith P, et al. The Chile earthquake of March 3, 1985 – Damage to bridges and highways. Earthq Spectra 1986;2:411–27. https://doi.org/10.1193/1.1585389.

[9] Lew HS. Performance of structures during the Loma Prieta earthquake of October 17, 1989. vol. 778; 1989.

[10] Priestley MJ, Seible F, Uang C-M. The Northridge earthquake of January 17, 1994: Damage analysis of selected freeway bridges. United States of America; 1994.

[11] Moehle J, Fenves GL, Mayes R, Priestley MJ, Seible F, Uang C-M. Northridge earthquake of January 17, 1994, reconnaissance report; 1995.

[12] Fenves GL, Ellery M. Behavior and failure analysis of a multiple-frame highway bridge in the 1994 Northridge earthquake. Pacific Earthquake Engineering Research Center; 1998.

[13] Chang K-C, Chang D-W, Tsai M-H, Sung Y-C. Seismic performance of highway bridges. Earthq Eng Eng Seismol 2000;2:55–77.

[14] Kawashima K. Damage of bridges resulting from fault rupture in the 1999 Kocaeli and Duzce, Turkeu earthquake and the 1999 Chi-chi, Taiwan earthquake. Seism Fault-Induced Fail 2001:171–90. https://doi.org/10.2208/jsceseee.19.179s.

[15] Li J, Peng T, Xu Y. Damage investigation of girder bridges under the Wenchuan earthquake and corresponding seismic design recommendations. Earthq Eng Eng Vib 2008;7:337–44. https://doi.org/10.1007/s11803-008-1005-6.

[16] Han Q, Du X, Liu J, Li Z, Li L, Zhao J. Seismic damage of highway bridges during the 2008 Wenchuan earthquake. Earthq Eng Eng Vib 2009;8:263–73. https://doi.org/ 10.1007/s11803-009-8162-0.

[17] Yashinsky M. Performance of highway structures during the May 12, Wenchuan, China earthquake. Tech counc lifeline earthq eng conf. 2009. p. 1349–58https:// doi.org/10.1061/41050(357)127.

[18] Kawashima K, Takahashi Y, Ge H, Wu Z, Zhang J. Damage of bridges in 2008 Wenchuan, China, earthquake. J Earthq Eng 2009;13:965–96. https://doi.org/10. 1080/13632460902859169.

[19] Harries KA, Kasan J. Aktas C. Repair method for prestressed girder bridges. Pennsylvania Departament of Trasportation; 2009.

[20] Yashinsky M. Lessons learned from the March 11, 2011 M9.0 great Tohoku earthquake and tsunami;

2011. p. 1–15.

[21] Kawashima K. Damage of bridges due to the 2011 great east japan earthquake. Int symp eng lessons learn from 2011 Gt. East Japan Earthq. 2012. p. 82–101https:// doi.org/10.5610/jaee.12.4_319.

[22] Unión A, Guzmán M, Rivera C, Aravena L, Barrientos J, Darwiche K, et al. Nuevos criterios sísmicos para el diseño de puentes en Chile (in Spanish). Chile: Ministerio de Obras Públicas; 2010.

[23] Ministerio de Obras Públicas. Manual de carreteras – Volumen No 3 – Instrucciones y criterios de diseño (in Spanish). Chile: MOP-DGOP-Direccion de Vialidad; 2015.

[24] Unión A, Aravena L, Díaz V, Achurra S, Barrientos J, Vargas J, et al. Comentarios y sugerencias "criterios sísmicos para el diseño de puentes en Chile" (in Spanish); 2016. p. 1–45.

[25] Ministerio de Obras Públicas. Manual de carreteras – Volumen No 3 – Instrucciones y criterios de diseño (in Spanish). Chile: MOP-DGOP-Direccion de Vialidad; 2017.

[26] Japan Road Association. Design specification for highway bridges – Part V: Seismic design. Japan: Japan Road Association; 2002.

[27] California Department of Transportation. Chapter 21: Seismic design of concrete bridges. In: California Department of Transportationeditor. Bridg des pract – Febr 2015. California Department of Transportation; 2015. p. 2.

[28] American Association of State Highway and Transportation Officials. Guide specifications for LRFD seismic bridge design, 2nd ed.; 2011.

[29] American Association of State Highway and Transportation Officials. LRFD bridge design specifications, customary U.S. units; 2012.

[30] Secretaria de Comunicaciones y Transporte. Proyectos de nuevos puentes y similares (in Spanish); 2001.

[31] Buyukozturk O, Bakhoum MM, Beattie SM. Shear behavior of joints in precast concrete segmental bridges. J Struct Eng 1991;116:3380–401.

[32] Kaneko Y, Connor JJ, Triantafillou TC, Leung CK. Fracture mechanics approach for failure of concrete shear keys. I: Theory. J Eng Mech 1993;119:681–700.

[33] Kaneko Y, Connor JJ, Triantafillou TC, Leung CK. Fracture mechanics approach for failure of concrete shear keys. II: Verification. J Eng Mech 1993;119:701–19.

[34] Kaneko Y, Mihashi H. Analytical study on the cracking transition of concrete shear key. Mater. Struct. 1999;vol. 32.

[35] Megally SH, Silva PF, Seible F. Seismic response of sacrificial shear keys in bridge abutments. San Diego: University of California; 2002.

[36] Silva PF, Megally SH, Seible F. Seismic performance of sacrificial interior shear keys. ACI Struct J 2003;100:177–87.

[37] Bozorgzadeh A, Megally SH, Restrepo JI, Ashford S. Capacity evaluation of exterior sacrificial shear keys of bridge abutments. J Bridg Eng 2006;11:555–65. https://doi. org/10.1061/(ASCE)1084-0702(2006)11:5(555).

[38] Guerra A. Shear key research: Project literature review and finite element analysis. U.S. Department of the Interior Bureau of Reclamation; 2007.

[39] Aviram A, Stojadinovic B, Mackie KR. Nonlinear modeling of bridge structures in California. United States of America: Pacific Earthquake Engineering Research Center; 2008.

[40] Goel RK, Chopra AK. Role of shear keys in seismic behavior of bridges crossing fault-rupture zones. J Bridg Eng 2008;13:398–408. https://doi.org/10.1061/ (ASCE)1084-0702(2008)13:4(398).

[41] Bi K, Hao H. Modelling of shear keys in bridge structures under seismic loads. Soil Dyn Earthq Eng 2015;74:56–68. https://doi.org/10.1016/j.soildyn.2015.03.013.

[42] Raison RB, Christy CF. Review on shear slip of shear keys in bridges. Int J Sci Eng Res 2016;7:231–42.

[43] Xiang N, Li J. Seismic performance of highway bridges with different transverse unseating-prevention devices. J Bridg Eng 2016;21. https://doi.org/10.1061/ (ASCE)BE.1943-5592.0000909.

[44] Han Q, Zhou Y-L, Zhong Z-L, Du X-L. Seismic capacity evaluation of exterior shear keys of highway bridges. J Bridg Eng 2017;22:4016119. https://doi.org/10.1061/ (ASCE)BE.1943-5592.0000978.

[45] Wilches JJ, Santa María H, Riddell R, Arrate Letelier C. Influence of the use of external shear keys on the seismic behavior of Chilean highway bridges. Eng Struct 2017;147:613–24. https://doi.org/10.1016/j.engstruct.2017.06.015.

[46] Turkington DH, Carr AJ, Cooke N, Moss PJ. Seismic design of bridges on leadrubber bearings. J Struct Eng 1989;115:3000–16. https://doi.org/10.1061/(ASCE) 0733-9445(1989)115:12(3000).

[47] Mander JB, Kim D-K, Chen SS, Premus GJ. Response of steel bridge bearings to reversed cyclic loading. United States of America; 1996.

[48] Maleki S. Effect of side retainers on seismic response of bridges with elastomeric bearings. J Bridg Eng 2004;9:95–100. https://doi.org/10.1061/(ASCE)1084- 0702(2004)9:1(95).

[49] Filipov ET. Nonlinear seismic analysis of quasi-isolation systems for earthquake protection of bridges. University of Illinois at Urbana-Champaign; 2012.

[50] LaFave JM, Fahnestock LA, Foutch DA, Steelman JS, Revell JR, Filipov ET, et al. Experimental investigation of the seismic response of bridge bearings. Illinois Center for Transportation; 2013.

[51] Filipov ET, Fahnestock LA, Steelman JS, Hajjar JF, LaFave JM, Foutch DA. Evaluation of quasi-isolated seismic bridge behavior using nonlinear bearing models. Eng Struct 2013;49:168–81. https://doi.org/10.1016/j.engstruct.2012.10. 011.

[52] Steelman JS, Fahnestock LA, Filipov ET, LaFave JM, Hajjar JF, Foutch DA. Shear and friction response of nonseismic laminated elastomeric bridge bearings subject to seismic demands. J Bridg Eng 2013;18:612–23. https://doi.org/10.1061/(ASCE) BE.1943-5592.0000406.

[53] Steelman JS, Filipov ET, Fahnestock LA, Revell JR, LaFave JM, Hajjar JF, et al. Experimental behavior of steel fixed bearings and implications for seismic bridge response. J Bridg Eng 2014;19:A4014007. https://doi.org/10.1061/(ASCE)BE. 1943-5592.0000540.

[54] Rubilar Moya FI. Modelo no lineal para predecir la respuesta sísmica de pasos superiores (in Spanish). Pontificia Universidad Catolica de Chile; 2015.

[55] Martínez A, Hube M, Rollins KM. Analytical fragility curves for non-skewed highway bridges in Chile. Eng Struct 2017;141:530–42. https://doi.org/10.1016/j. engstruct.2017.03.041.

[56] Lüders C, Criado M. A new design philosophy of seismic anchor elements for bridges. 16th World Conf Earthq, Santiago, vol. 4562. 2017. p. 1–12.

[57] Ministerio de Obras Públicas. Manual de carreteras – Volumen No 3 – Instrucciones y criterios de diseño (in Spanish). Chile: Ministerio de Obras Públicas; 2002.

[58] Ministerio de Obras Públicas. Manual de carreteras – Volumen No 3 – Instrucciones y criterios de diseño (in Spanish). Chile: MOP-DGOP-Direccion de Vialidad; 2008.

[59] Mazzoni S, McKenna F, Scott MH, Fenves GL. OpenSees command language manual. Pacific Earthquake Engineering Research Center; 2006.

[60] Deutsches Institut für Normung. DIN Regulations. Germany; 1940.

[61] Ministerio de Obras Públicas, Consultores E y FI. Manual de carreteras (in Spanish). Chile; 1972.

[62] American Association of State Highway and Transportation Officials. Standard specifications for highway bridges. 11th ed. United States of America: American Association of State Highway and Transportation Officials; 1973.

[63] Cruz Lorenzen C, Barrientos ME, Babbar S. Toll road concessions – The Chilean experience. PFG Discuss Pap Ser 2001:1–36.

[64] American Association of State Highway and Transportation Officials. Standard specifications for highway bridges. 16th ed. United States of America: American Association of State Highway and Transportation Officials; 1996.

[65] Moehle J, Riddell R, Boroschek R. The Mw 8.8 Chile earthquake of February 27, 2010. Earthquake Engineering Research Institute; 2010.

[66] Ministerio de Obras Públicas. Cuenta pública 2010, cuenta sectorial. Chile: Ministerio de Obras Públicas; 2010. (in Spanish).

[67] California Department of Transportation. Standard specifications. United States of America: California Department of Transportation; 2006.

[68] Hwang JS, Sheng LH. Equivalent elastic seismic analysis of base-isolated bridges with lead-rubber bearings. Eng Struct 1994;16:201–9. https://doi.org/10.1016/ 0141-0296(94)90078-7.

[69] Jangid RS. Seismic response of isolated bridges. J Bridg Eng 2004;9:156–66. https://doi.org/10.1061/(ASCE)1084-0702(2004)9:2(156).

[70] Kannan AE, Powell GH. General purpose computer program for inelastic dynamic response of plane structures. Berkeley: University of California; 1973.

[71] McKenna F, Fenves GL. The OpenSees command language manual; 2001.

[72] Scott MH, Franchin P, Fenves GL, Filippou FC. Response sensitivity for nonlinear beam–column elements. J Struct Eng 2004;130:1281–8. https://doi.org/10.1061/ (ASCE)0733-9445(2004)130:9(1281).

[73] Mander JB, Priestley MJ, Park R. Fellow. Theoretrical stress - strain modelo for confined concrete. J Struct Eng 1989;114:1804–26.

[74] Computers and structures I. SAP2000; 2018.

[75] Saragoni R, Hart G. Simulation of artificial earthquakes. Earthq Eng Struct Dyn 1973;2:249–67. https://doi.org/10.1002/eqe.4290020305.

[76] Serdar Kirçil M, Polat Z. Fragility analysis of mid-rise R/C frame buildings. Eng Struct 2006;28:1335–45. https://doi.org/10.1016/j.engstruct.2006.01.004.

[77] Vamvatsikos D, Cornell CA. Incremental dynamic analysis and its application to performance-based earthquake engineering. 12th Eur conf earthq eng, London. 2002. p. 10.

[78] Riddell R. Inelastic design spectra accounting for soil conditions. Earthq Eng Struct Dyn 1995;24:1491–510. https://doi.org/10.1002/eqe.4290241106.

[79] Kayen R, Carkim BD, Cobert S, Pinilla C, Ng A, Gorbis E, et al. Seismic velocity site characterization of thirty-one Chilean seismometer stations by spectral analysis of surface wave dispersion. Berkeley: Pacific Earthquake Engineering Research Center; 2014.

[80] Universidad Diego Portales, Leyton Flórez F. FUCHIGE – Mediciones de microvibraciones en 6 estaciones sismicas (in Spanish); 2014.

[81] DICTUC S.A, Sáez Robert E. FUCHIGE – Report of project: study of seismographic stations (in Spanish); 2014.

[82] Universidad de Concepción, Montalva Alvarado G, Bastías N, Troncoso P. FUCHIGE – Mediciones geofísicas: estaciones acelerográficas norte de Chile (in Spanish); 2014.

[83] Universidad de Concepción, Montalva Alvarado G. FUCHIGE – Mediciones geofísicas: Estaciones acelerográficas centro-sur de Chile (in Spanish); 2014.

[84] Boroschek R, Yañez UF, Bejarano BI, Molnar S, Torres GA. Caracterización geotécnica estaciones de acelerógrafos de la Universidad de Chile (in Spanish); 2012.

[85] United States Geological Survey, Universidad de Chile, Geotecnica Ltda. Records of 1985 Algarrobo earthquake in Chile (database); 1990.

[86] Centro Sismológico Nacional. Earthquakes of Chile – Records between 1992 and 2010 (database) 2010.

http://terremotos.ing.uchile.cl/ [accessed April 20, 2017].

[87] Centro Sismológico Nacional. Records of significant seismic events – Records between 2012 to present (database); 2015. http://evtdb.csn.uchile.cl/ [accessed April 20, 2017].

[88] Red Nacional de Acelerógrafos, Oficina Nacional de Emergencia del Ministerio del Interior y Seguridad Pública. Ubicacion de estaciones de registro (rev agosto 2012) (in Spanish); 2012.

[89] Pecknold DA, Riddell R. Effect of initial base motion on response spectra. J Eng Mech Div 1978;104:485–91.

[90] Instituto Nacional de Normalización. NCh2369.Of2003 – Diseño sísmico de estructuras e instalaciones industriales (in Spanish). Chile; 2003.

[91] Omrani R, Mobasher B, Liang X, Gunay S, Mosalam KM, Zareian F, et al. Guidelines for nonlinear seismic analysis of ordinary bridges: Version 2.0. Caltrans; 2015.

[92] Muthukumar S, DesRoches R. A Hertz contact model with non-linear damping for pounding simulation. Earthq Eng Struct Dyn 2006;35:811–28. https://doi.org/10. 1002/eqe.557.

4. CHAPTER 4

A NEW TECHNIQUE FOR SELF-CENTERING SHEAR KEYS IN HIGHWAY BRIDGES

Abstract: Shear keys are elements in bridges designed to prevent or limit transverse unseating, rotation, and/or collapse of the superstructure responding to strong-intensity earthquake input ground motion, as well as to absorb breaking and various self equilibrating forces. During the 2010 Maule earthquake, Chile's highway infrastructure was seriously impacted. Shear key failures were endemic and did not function as intended. As a result, some bridges experienced partial or complete collapse. Even when the shear keys appeared to have worked, the superstructure exhibited large offsets, which required expensive repairs. An expensive retrofit of undamaged bridges was also carried out as a result of the inadequate response of the bridge infrastructure. This paper addresses the behavioral issues of bridges designed incorporating conventional shear keys and proposes an innovative self-centering concept that eliminates residual displacements in the superstructure. The self-centering shear key concept, as it will be termed here, makes use of the bridge self-weight as a restoring force to ensure self-centering. This concept proposal takes advantage of the kinematics of the bridge. The self-centering shear key concept was validated for a typical Chilean bridge via an extensive study that made use of nonlinear time history analyses. The results indicate that the increase in seismic demand on the substructure is small enough to maintain the bridge base structure in the elastic range while eliminating any residual displacements in the superstructure.

4.1 Introduction

As a highly seismic country, Chile has to implement advanced protective technologies in highway bridges' seismic design and construction. Chile has traditionally been the leader in developing seismic design provisions in South America, and its provisions are typically modified and adopted in other high seismicity countries like Peru, Ecuador, and Colombia. The cost of implementing such technologies is high and not a priority for many governments facing large economic and social constraints; consequently, the political urgency to fully support seismic design and modernization efforts is not as strong as in North America, Japan, China, and New Zealand. Despite these challenges, Chile has invested significant resources in improving seismic design, retrofitting techniques, and construction methods for transportation infrastructure. Many of these improvements in recent decades have been on the implementation of seismic protection systems for highway bridges [1–4].

Before the 2010 Maule earthquake, the Ministry of Public Works (MOP) [5] had been modernizing the seismic requirements for the design of highway bridges. After the 2010 Maule earthquake, this work intensified, resulting in several new editions of the Highway Manual [6–8], henceforth the MOP Manual. This work included the direct participation of the Japan Road Association [9] and extensive reviews of the USA [10] and New Zealand [11] seismic design provisions for highway bridges. One of the most important revisions in these new versions of the MOP Manual was the design of shear keys, for which a specific geometry was defined based on assumed failure mechanisms. However, the most relevant overall change was the incorporation of the soil class in the calculation of the seismic response of the shear keys [12]. While the new design shear key provisions will decrease the potential for unseating in future seismic events, many existing bridges may be susceptible to collapse due to lack of seismic detailing or the potential for stronger ground shaking than those considered in the original design [13].

Ordinary highway bridges in Chile are often designed with sacrificial shear keys at the bents and abutments. These shear keys are intended to prevent the collapse of the superstructure and prevent additional damage to the infrastructure but are assumed to be highly damaged in the process and thus are classified as sacrificial elements. As observed during the 2010 Maule earthquake, endemic diagonal tension failure of shear keys that left the superstructure with an offset and in precarious conditions was observed [14] (Fig. 4-1). Furthermore, some bridges collapsed because the shear keys did not meet their design objective. These failures can be attributed to: (i) poor detailing and construction practices and (ii) structural deficiencies that originated in the conceptual design phase. Assuming that the arrangement of the shear keys is adequate, i.e., that no failures of type (i) occur, it is possible to associate all the remaining failures with the stresses and deformations in the shear keys. Thus, a robust model for determining values for those stresses and deformations in the design phase is essential. Currently, such a model is not present in the MOP Manual.

Fig. 4-1. Typical shear key failure in shear keys during the 2010 Maule earthquake: diagonal tension. Independencia Highway Bridge (Photo: M. Hube).

The shear keys are designed to exhibit high-initial stiffness followed by the unidirectional plastic deformations in compliance with the imposed superstructure deformations. The required design strength of the shear keys in the MOP Manual is defined by Equation 1 [8]. However, the typical aspect ratio for these shear keys in Chile means that the superstructure can be left with appreciable residual displacements that make repairs mandatory after a major earthquake. Based on the current design concept of shear keys and investigations of damage during the 2010 Maule earthquake [14], a self-centering shear key concept is proposed and validated via extensive nonlinear time-history analysis.

$$F = \frac{m * A_0 * S}{\#_{int}+1} \qquad (4\text{-}1)$$

where:

F = Required design strength.
m = Seismic mass, considering the tributary length of the longitudinal elements with respect to the bent, plus the corresponding mass of the upper half of the bent height.
A_0 = Maximum effective ground acceleration as defined in Table 3.1004.302.A [8].
S = Soil coefficient. For soil type I, II, III, and IV the soil coefficients are 0.9, 1.0, 1.2, and 1.3, respectively [8].
$\#_{int+1}$ = Number of internal shear keys. The value "+1" refers to the exterior shear key that will oppose the direction of the deck movement

Given the imperative need to avoid superstructure unseating, numerous analytical and experimental studies have been carried out on devices that modify its response or prevent its collapse [15–25]. Saiidi et al. [15] carried out a parametric study of restrainer devices as an alternative to seismic retrofitting of bridges. A cable connecting the longitudinal beams was used as a retrofitting device. Although the results showed that the cables reduce the longitudinal displacement between beams during an earthquake, they recommend carrying out more detailed studies to implement these devices. Megally et al. [16], Silva et al. [19], Bozorgzadeh et al. [21], and Han et al. [17] carried out experimental programs to evaluate the seismic behavior of shear keys as transverse support for bridge superstructures. They

developed formulations and hysteresis models to model the seismic behavior of external and internal shear keys on highway bridges. DesRoches et al. [18] carried out full-scale experimental tests of cable retainer assemblies on simply supported steel girder bridges. The results showed that cable retainers increase the strength and rigidity, reducing the deformation of the connection elements. Padgett et al. [24] developed experimental and analytical tests of an SMA (shape memory alloy) cable device to determine its effectiveness in the seismic response of bridges of various spans. The cables substantially improve the seismic response of the bridges, and reduce the displacement of the hinges and the deviations of the column. Guo et al. [23] studied the reduction of structural pounding through the use of magnetorheological (MR) dampers with a passive and semi-active control system, carrying out an experimental and analytical study. Although passive MR dampers decrease but do not prevent pounding between adjacent bridge elements, MR dampers with a semi-active system significantly reduce displacement and pounding between adjacent bridge elements.

Among studies related to transverse displacements, Xiang and Li [25] analytically and experimentally evaluated the seismic behavior of concrete shear keys, flexible steel dampers, and friction dampers as transverse displacement prevention devices. Although these devices reduce the seismic demand, the results showed that the seismic demands are lower for the friction damper and the flexible steel damper as compared to the shear keys. Additionally, the shear keys and the friction damper lead to larger residual displacements than the flexible steel damper. Goel and Chopra [26] analytically investigated the role of sacrificial shear keys in the earthquake-resistant behavior of highway bridges arranged on geological faults, or zones of seismic activity, for which they used a simplified force-deformation model characterizing the behavior of the shear keys, based on the experimental results obtained by Megally et al. [16]. They concluded that the seismic demands of a bridge with nonlinear shear keys over geological faults are limited by the demands of a bridge with elastic shear keys. Wilches et al. [12,13] evaluated the influence of shear keys on the seismic behavior of Chilean highway bridges considering the seismic hazard and the type of soil. They developed analytical models in 2D and 3D, and, just as Goel and Chopra [26], considered a simplified trilinear constitutive model. Wilches et al. [12,13] determined that the main reason for the great variability in the seismic response of typical Chilean bridges with shear keys is because Chilean bridge design codes did not simultaneously consider the soil variability in determining the design forces. Peralta and Hube [27] evaluated the seismic behavior of Chilean highway bridges, especially the rotation of the superstructure considering the incorporation of transverse diaphragms in the superstructure, which were not mandatory for all Chilean highway bridges before the 2010 Maule earthquake [28]. To do so, they developed a 3D analytical model of a bridge, where they incorporated the shear keys through a multilinear constitutive model developed by Megally et al. [16]. The incorporation of transverse diaphragms reduces approximately 90% of the superstructure's rotation and ultimate displacements. Therefore, considering these elements in the design and construction of highway bridges improves the seismic performance of the bridges.

In all the investigations reviewed, the superstructure is left with a residual displacement after strong earthquakes, which implies that the bridge's immediate and potentially expensive repair will probably be needed. Other devices used to control the transverse displacement demand in bridges are seismic isolators: laminated rubber lead of high-damping rubber bearings [29] and friction sliding devices (pendulum friction isolators) [30]. Generally

speaking, these devices reduce the seismic demand by two mechanisms: (1) increasing the bridge's fundamental period and (2) providing energy dissipation to the structure, thus lowering the seismic demand immediately, reducing the spectral displacements due to hysteretic damping [31].

The amount of dissipated energy by isolators depends on the properties of the rubber, that is, whether high-damped or low-damped rubber is used [32]. Also, considering that they are connected both to the superstructure and substructure, they are susceptible to producing residual displacements of the superstructure after its failure. Lead-core elastomers dissipate energy mainly through the lead core but are susceptible to residual displacements. On the other hand, isolators with friction pendulum devices dissipate energy by friction between the Teflon surfaces and the steel and are also self-centering systems [33–35]. Other self-centering systems used for bridge seismic protection are buckling-restrained-braces [36,37]. With these type of devices, optimization of the design is achieved due to the decrease in seismic demand.

With this background, the objective of this research is to propose a new self-centering geometry of shear keys to modify the seismic response of bridges to eliminate residual displacements of the superstructure. A new geometry of the shear keys is developed by modifying the conventional aspect ratios for shear keys used in Chile. In this new proposal, the shear key will not act as a sacrificial element but as a self-centering element through the kinematics between the substructure and superstructure and henceforth will be referred to as the self-centering shear key (SCSK). Finally, a case study is investigated to validate the effectiveness of the proposed shear key compared to current shear keys. Since a concept is described in this paper, the paper does not extend knowledge to many possible bridge typologies and configurations such as curved and skewed bridges, which may require careful consideration of the bridge kinematics.

4.2 Modeling Aspects

4.2.1 Bridge case study

The selection of a case study bridge was based on a statistical analysis of many highway bridges currently operating in Chile [12,13]. The most common bridge in Chile is two-span, symmetrical, with four traffic lanes, not skewed, and with about 26 m between supports (Fig. 4-2). These characteristics will be used to build a dynamic model to simulate the transverse response of a typical bridge due to ground motions. There are three essential concepts that define this model: substructure, substructure-superstructure interface, and superstructure. The substructure consists of abutments at the ends and a central bent. The abutment structure consists of a reinforced concrete stem wall, behind which there is an access slab above compacted fills. The intermediate bent structure consists of three 1.0 m diameter columns, spaced at 5.0 m and 6.05 m of free height. On top of this bent sits a reinforced concrete cap beam 1.0 m high, 1.2 m wide, and 14.2 m long, adequately reinforced so this cap beam does not fail under the imposed displacements. The cap beam has external shear keys; when the relative displacement between the superstructure and the substructure exceeds some design level, both structures make contact, and the increase in relative displacement will temporarily stop. The connection between the superstructure and the cap beam is made by elastomeric bearings, whose dimensions are 300 mm wide, 450 mm long, and 30 mm high. The superstructure of the bridge is formed by two discontinuous spans, simply supported, whose structure consists of a 0.2 m thick and 11.75 m wide reinforced concrete slab, supported on four 1.35 m prestressed concrete girders high (Fig. 4-2). The cross-section in Fig. 4-2 shows the seismic bars used in Chile to prevent lateral unseating of the bridge, without end diaphragms and internal shear keys as is common elsewhere. The seismic bars performed very poorly, and many bridges have been retrofitted as a result.

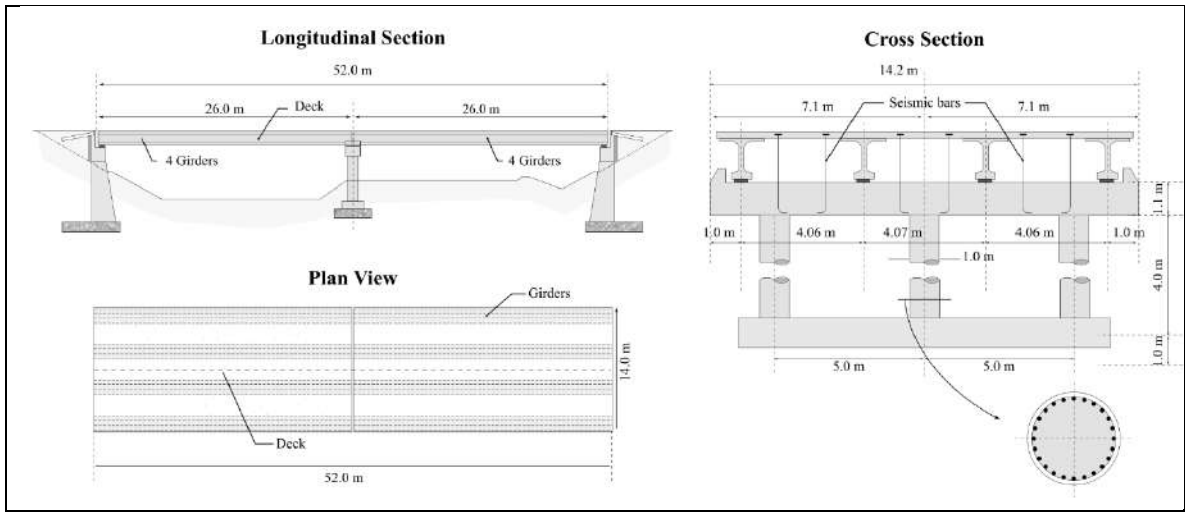

Fig. 4-2. Layout of a typical highway bridge in Chile.

4.2.2 General description of the proposed self-centering shear key

Figure 4-3a shows the typical bridge defined by the Chilean highway manual [8], while Figure 4-3b shows the model of the proposed shear key. It should be noted that, unlike the rectangular geometries of conventional shear keys (Fig. 4-3a), this new proposal presents a trapezoidal geometry in order to allow a self-centering movement with an angle (α) that defines the inclination of the shear key. These values can vary according to the characteristics of each model. Elastomeric bearings are placed on the inclined sides of the model, fixed to the substructure (i.e., they cannot slide at this interface). It is important to consider that in the SCSK concept, the superstructure, including the diaphragm, must work as a rigid body for the system to be efficient. In this investigation, the structural configuration for $\alpha = 0°$ corresponds to the prototype bridge before the 2010 Maule earthquake, that is, only with external shear keys (Fig. 4-2). All structural configurations with $\alpha > 0°$ refer to Figure 3b, which is the model proposed in this investigation.

Considering that in this paper, the representative highway bridge is symmetrical and not skewed, the transversal behavior of the bridge is studied through a 2D model of the central axis of the bridge. This approach, which has been used in this type of studies [38–41], cannot predict superstructure rotation nor longitudinal displacement. Next, a detailed description of the variables in the proposed shear key is presented.

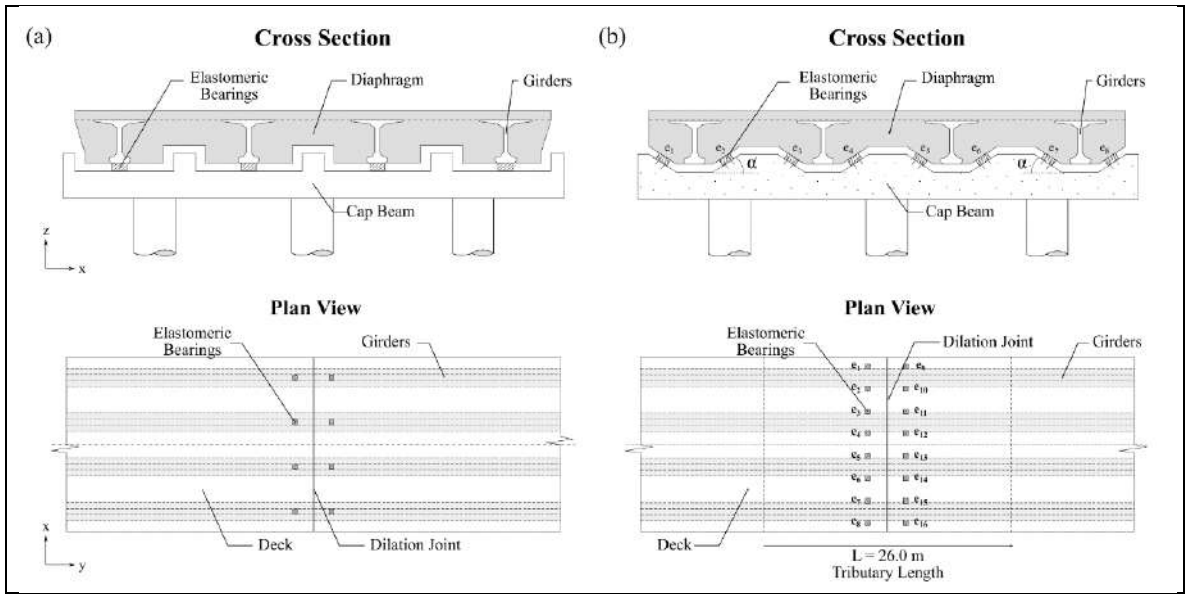

Fig. 4-3. Cross-section and plan of a typical Chilean Bridge (a) Defined by the MOP [8] and (b) proposed model.

4.2.3 Elastomeric elements: static force-deformation properties

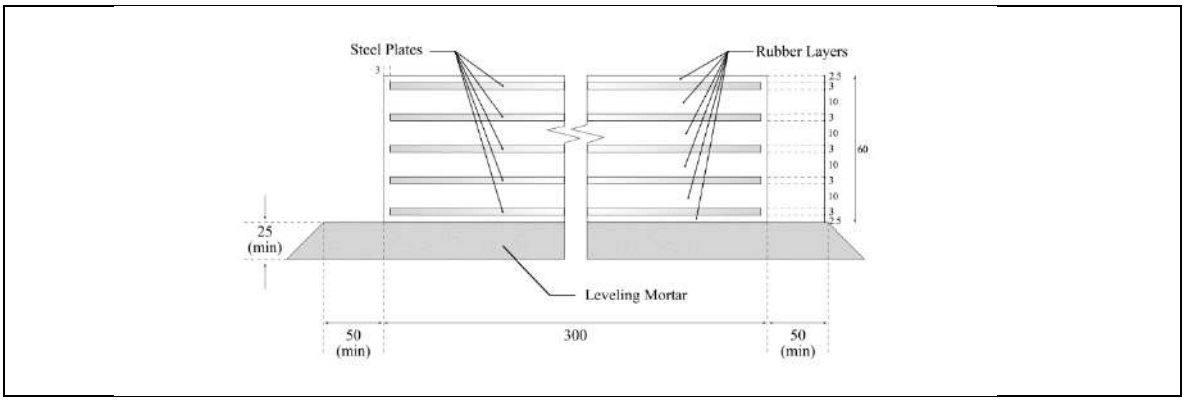

Fig. 4-4. Detail of elastomeric bearings (dimensions in millimeters).

The geometry of the elastomeric bearings at the interface between substructure and superstructure in the central section of the bridge is shown in Figure 4-4. Each elastomeric bearing has a 450 mm x 300 mm rectangular section, with 60 mm height. Inside each elastomeric bearing, five steel plates 3 mm thick constrain the lateral deformation for the whole element. Then, the effective height of the elastomer is computed as H_r=60–5·3=45 mm and the typical height of one layer of elastomer is taken as t_r=10 mm, as is shown in Figure 4-4. Using a shear modulus of elastomer G_r=130 MPa [42], the lateral stiffness of the element is computed as [29]:

$$k_s = \frac{G_r A_r}{H_r}, \qquad (4-2)$$

where A_r is the cross-section area of the element. Thus, based on an area of 135000 mm2, the elastomeric bearings have a lateral stiffness of k_s=390 kN/mm. Moreover, the axial stiffness of the element is computed as [29]:

$$k_n = \frac{A_r E_n}{H_r} \qquad (4-3)$$

In Equation (4-3), E_n corresponds to the axial modulus of elasticity, which can be approximately computed as [29]:

$$E_n = 6.75 G_r S^2 \qquad (4-4)$$

In Equation (4-4), S is the shape factor, defined as the ratio between the loaded area of the elastomeric element and the free deformation area. For rectangular shape elements with transversal dimensions B_r and L_r, and thickness t_r, shape factor can be computed as [29]:

$$S = \frac{0.5 B_r L_r}{(B_r + L_r) t_r} \qquad (4-5)$$

Using the geometry of the elastomeric bearings located on the interface between substructure

and superstructure, a shape factor of S=9 is obtained. Using Equation (4-4), an axial modulus of elasticity E_n=71 GPa results, and from Equation (4-3) an axial stiffness of k_n=213x103 kN/mm is computed. Comparing the computed shear stiffness k_s and the computed axial stiffness k_n, the last one is three orders of magnitude larger than the former one. For this reason, and with the aim of developing a model as simple as possible, the elastomeric bearings are considered axially rigid, and only shear deformations are considered. This assumption imposes an important kinematic constraint: when a lateral displacement of the superstructure relative to the substructure is imposed, contact between them will occur only through half of the elastomeric bearings. For the bridge examined herein, eight elastomeric bearings lose contact, and loads are transmitted only through the other eight where contact exists. When the lateral displacement between the superstructure relative to the substructure is reversed, contact is interchanged between elastomeric bearings supports. This phenomenon is schematically shown in Figure 4-5.

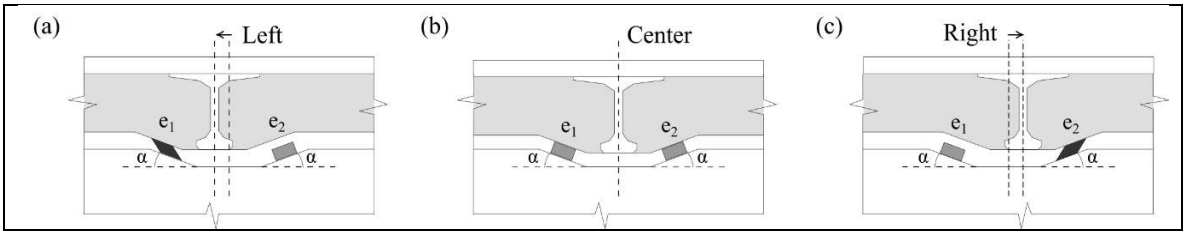

Fig. 4-5. Kinematic constraints of relative displacement of the superstructure with respect to substructure for (a) a lateral relative displacement to the left, (b) zero relative displacement and (c) a lateral relative displacement to the right.

To ease constructability, elastomeric bearings are fixed to the substructure and contact the superstructure via a steel plate with no connection of any kind. Hence, these bearings can roll and can eventually slip relative to the superstructure. Considering a friction force acting between the bearings and the steel plate, a simple model can assume linear behavior of the bearing the friction force is overcome. This simplification obviously ignores the non-linear elastic response of the bearing while rolling [43]. After friction is overcome, constant shear force is assumed to develop at the bearing-superstructure interface. The dynamic friction coefficient is computed using the Equation (4-6) [44]:

$$\mu = 0.18 + \frac{0.38}{\sigma} \qquad (4-6)$$

where σ is the normal stress between surfaces, in MPa. It is important to note that more complex viscoelastic theories of rubber friction have been developed when its upper or lower surface slides on a hard and rough surface [45]. However, to maintain the simplicity of the model, Coulomb friction is used in the present study.

Due to the kinematic constraint shown in Figure 4-5, contact between substructure and superstructure of the case study bridge will always be through eight elastomeric bearings Then, if W_u is the weight of the superstructure defined by the tributary length shown in Figure 4-3b, and if we assume that normal stresses are distributed evenly over the eight elastomeric bearings in contact, σ can be computed approximately as:

$$\sigma = \frac{W_u cos\alpha}{8A_r} \qquad (4-7)$$

In Equation (4-7) the angle α measures the slope of the contact surface between the upper face of the elastomeric bearing element and the steel surface from the superstructure. Finally, the maximum friction force is computed assuming the same normal stress σ from Equation (4-7) on the eight elastomeric bearings in contact with superstructure and using the dynamic friction coefficient given by Equation (4-6):

$$F_y = \mu\sigma A_r \qquad (4-8)$$

Since linear-elastic behavior is expected until the shear force exceeds the maximum friction given by Equation (4-8) and the elastomeric bearings are fixed to the substructure at the lower surface and simply supported at the upper surface, an elasto-plastic model for shear force-deformation is used in each elastomeric bearing. Then, the following force–deformation relationship for the elastomeric bearings is expected from a push-over sense: (1) initially, the elastomer responds with a linear-elastic behavior; and (2) when the contact force between the upper surface of the bearing and the superstructure exceeds the maximum friction force, both surfaces slide with respect to one another. This sliding action dissipates energy by friction, reducing the seismic demand of the bridge. No dissipation is expected from damping in the bearings. However, friction is not responsible for the elimination of residual displacements. The self-centering condition, which will be explained in the following section, is responsible of this. It is important to consider that given the kinematic constraint mentioned before, the forces will be zero in all elements that are not in contact with the superstructure.

It is important to note that the dynamic properties of the elastomeric bearings described above, such as stiffness, can be affected by long-term deformations due to constant load [46]. However, these variations do not significantly alter the behavior of the proposed model whose objective is self-centering.

4.2.4. Equation of motion

4.2.4.1 Degrees of freedom

A simple two degree-of-freedom model can simply simulate the dynamic lateral response of the bridge due to input ground excitation. Since the high axial stiffness in the elastomeric bearings does not allow rotations in the superstructure, only the lateral displacement of the superstructure relative to the substructure needs to be modeled. In the same way, the high value of the axial stiffness in the concrete columns relative to its lateral stiffness constrains the vertical displacement of the substructure, and only one lateral displacement relative to the ground is needed. To summarize, one horizontal displacement u_d relative to the ground is used to define the position of the substructure, and one horizontal displacement u_u relative to substructure is used to define the position of the superstructure. Absolute horizontal and vertical displacements of the ground are termed x_g and z_g, respectively. This definition of

coordinates is shown in Figure 4-6.

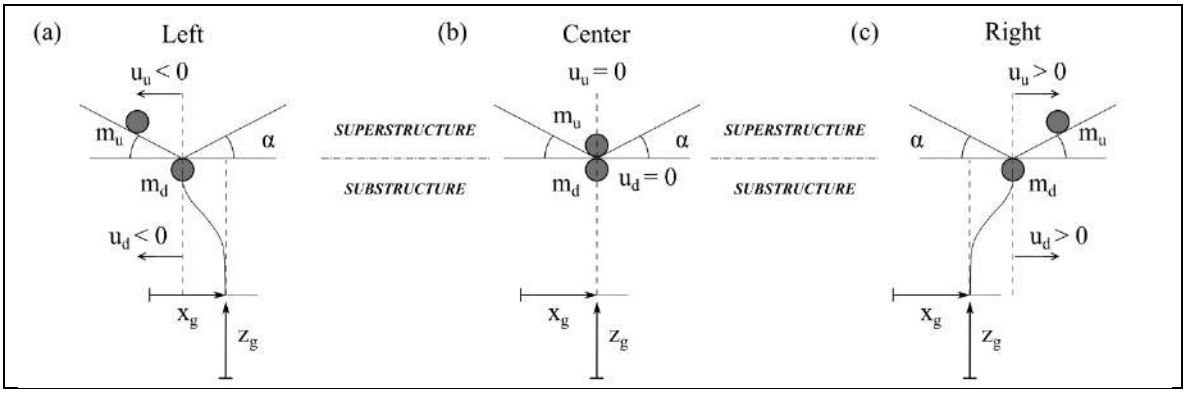

Fig. 4-6. Scheme to define the degrees of freedom of the structure. (a) Substructure deformed to the left and superstructure with relative displacement to the left with respect to the substructure, (b) zero displacements for both substructure and superstructure, and (c) substructure deformed to the right and superstructure with relative displacement to the right with respect to the substructure.

4.2.4.2 Mass and stiffness

Lumped masses m_d and m_u for the substructure and superstructure respectively are used, as is schematically shown in Figure 4-6. The value of m_d includes half of the mass from the three columns at the center of the bridge length, and m_u includes the mass of the diaphragms, eight prestressed concrete girders, the concrete slab, and the asphalt layer considering the tributary length (Fig. 3). Mass values are computed using specific weights of 25 kN/m^3 for concrete [8] and 20 kN/m^3 for asphalt [8], resulting in a m_d=80 tons and m_u=390 tons.
The value for the lateral stiffness of the three columns is also needed. In this model, the rotation of both the lower and the upper nodes of each column is not allowed. Thus, the lateral stiffness of the three columns bending in a fixed-fixed mode is estimated as $k_c = 3 \cdot 12E_cI_c/h_c^3$ where E_c is a representative value of the modulus of elasticity of the reinforced concrete, I_c is the moment of inertia of the cross-section of one column, and h_c is the clear height of each column. Taking values of E_c=25GPa [8], I_c=0.049 m^4 and h_c=6050 mm, the lateral stiffness of the three columns is estimated as k_c=200 kN/mm.

4.2.4.3 Kinematic relationships

Following the definition of coordinates shown in Figure 4-6, kinematic velocity relationships can be written to compute the absolute velocities of the substructure and the superstructure as follows,

$$\dot{x}_d^t = \dot{x}_g + \dot{u}_d \qquad (4-9)$$

$$\dot{z}_d^t = \dot{z}_g \qquad (4-10)$$

$$\dot{x}_u^t = \dot{x}_g + \dot{u}_d + \dot{u}_u \qquad (4-11)$$

$$\dot{z}_u^t = \dot{z}_g + \dot{u}_u \tan\alpha \,\text{sign} u_u \qquad (4-12)$$

where $\dot{x}_d^t$ and $\dot{z}_d^t$ are respectively the absolute horizontal and vertical velocities of the substructure, and $\dot{x}_u^t$ and $\dot{z}_u^t$ are the absolute horizontal and vertical velocities of the superstructure. Note that the sign function in Equation (4-12) manages the change of the slope when u_u changes its sign. In other words, if the relative velocity $\dot{u}_u$ is positive, the second term at the right hand of Equation (4-12) should be positive when u_u>0 and negative when u_u<0.

The lateral deformations of the elastomeric bearing elements can be expressed in terms of the lateral displacement u_u of the superstructure relative to the substructure. A linear relationship between shear deformations v_i of each elastomeric bearing element e_i ($i = 1, \dots, 16$) (Fig. 4-3) and relative displacement u_u can be written. However, since the elastomeric bearing elements are considered axially rigid, a kinematic constraint should be imposed. For positive values of u_u, the shear deformation in odd elements e_1, e_3, e_5, …, e_{15} must be zero, and for negative values of u_u, the shear deformation in even elements e_2, e_4, e_6, …, e_{16} must be zero. Thus, a contact function is defined as follow to enforce these conditions,

$$\phi = \frac{1}{2} + \frac{1}{2}\text{sign}(u_u) = \begin{cases} 1 & u_u > 0 \\ 0 & u_u < 0 \end{cases} \qquad (4-13)$$

Using Equation (4-13), the forces and deformation values in the elastomeric bearings can be managed in terms of which elements are in contact with the superstructure. However, the function $\text{sign}(x)$ is highly nonlinear since it is non-differentiable at x=0. For convergence purposes in the integration process of the dynamic equation of motion, a continuously differentiable function is used instead of the sign function defined in Equation (4-13) [47],

$$\tilde{\phi} = \frac{1}{2} + \frac{1}{2}\tanh(u_u/u_o), \qquad (4-14)$$

where u_o is a small enough value to approximate the sign function with the hyperbolic tangent function [47]. In this research, a value of $u_o = 10^{-3}$ mm is used.

Using the approximated contact function defined in Equation (4-14), kinematic relationships can be written for shear deformations v_i in terms of the relative lateral displacement u_u of the superstructure,

$$v_i = (1 - \tilde{\phi})\boldsymbol{L}_{ri} u_u \quad i = 1, 3, 5, \dots, 15 \qquad (4-15)$$

$$v_i = \tilde{\phi}\boldsymbol{L}_{ri} u_u \quad i = 2, 4, 6, \dots, 16, \qquad (4-16)$$

where $\boldsymbol{L}_{ri}$ is a constant matrix that stablishes a linear kinematic relationship between the shear deformation v_i in elastomeric bearings and the relative lateral displacement of the superstructure u_u when the element is in contact with the superstructure, for each elastomeric bearing e_i. Since u_u and v_i are both scalar values, these matrices also become scalar values. Assuming that all elastomeric bearings have an inclination α with respect to the horizontal,

the kinematic term can be written as $\boldsymbol{L}_{ri} = 1/\cos\alpha$ for i=1, …, 16. Then, Equations (4-15) and (4-16) can be written in matrix form,

$$\boldsymbol{v} = \boldsymbol{\Phi}\boldsymbol{L}_r u_u \,, \qquad (4-17)$$

where $\boldsymbol{v} = [v_1 \quad \cdots \quad v_{16}]^T$ is the deformation vector of elastomeric bearings, $\boldsymbol{L}_r = [\boldsymbol{L}_{r1}^T \quad \ldots \quad \boldsymbol{L}_{r16}^T]^T$ is the kinematic transformation matrix and $\boldsymbol{\Phi}$ is a 16x16 diagonal matrix containing contact functions as follows,

$$\boldsymbol{\Phi} = \begin{bmatrix} 1-\tilde{\phi} & 0 & 0 \\ 0 & \tilde{\phi} & 0 \\ 0 & 0 & \ddots \end{bmatrix} \qquad (4-18)$$

4.2.4.4 Dynamic force – deformation modeling

Elastomeric bearings located in the interface area between substructure and superstructure can be modeled as elasto-plastic elements, since they have a Coulomb friction force-deformation relationship. A Bouc-Wen model is used for it, using an internal state variable for each element. Then, a state equation and a force-displacement relationship can be written as follows for each elastomeric bearing e_i [48],

$$\dot{z}_i = \frac{1}{v_y}(A\dot{v}_i - \beta|v_i||z_i|^{n-1}z_i - \gamma\dot{v}_i|z_i|^n) \qquad (4-19)$$

$$f_{ri} = (1-\tilde{\phi})z_i F_y \quad i = 1,3,5,\ldots,15 \qquad (4-20)$$

$$f_{ri} = \tilde{\phi} z_i F_y \quad i = 2,4,6,\ldots,16 \qquad (4-21)$$

In Equations (4-19), (4-20) and (4-21), term v_y is the deformation of the elastomeric bearings at the onset of slip. This value can be computed using the maximum friction force given by Equation (8) and the shear stiffness in elastomeric bearings given by Equation (4-2). Then, the sliding deformation can be computed as $v_y = F_y/k_s$ and it depends on the inclination α of the elastomeric bearings relative to the horizontal. Also, v_i stands for the relative local displacement between superstructure and substructure at each element position, z_i is an internal state variable for each element that controls the elastic and plastic deformations, and f_{ri} in (4-20) and (4-21) is the shear force in elastomeric bearings. The other parameters for the Bouc-Wen model in Equation (4-19) are $A = 1$, $\beta = \gamma = 0.5$ and $n = 6$ [48]. In Equations (4-20) and (4-21), forces in elastomeric bearings can be represented by a single force vector as:

$$\boldsymbol{f}_r = [f_{r1} \quad \cdots \quad f_{r16}]^T. \qquad (4-22)$$

The columns located below the superstructure apply a shear force to the substructure, which is proportional to its lateral deformation. Moreover, if damping is present in the dynamic behavior of the substructure, a damping force should be included in the shear force as,

$$f_c = k_c u_d + c_c \dot{u}_d, \qquad (4-23)$$

where k_c is the stiffness of the columns system and c_c is a coefficient associated to the viscous damping of the columns. This coefficient can be computed as:

$$c_c = 2\xi_c \sqrt{k_c m_d} \qquad (4-24)$$

where ξ_c is the damping ratio associated to the substructure. In this research, $\xi_c = 0.05$ is used [49].

4.2.4.5 Euler-Lagrange approach

The equations of motion for the substructure and the superstructure can be obtained using the well-known equations of Euler-Lagrange. All forces acting on each structure are treated as external forces, i.e., potential energy is not included in this problem. Using expressions in Equations (4-9) to (4-12) for the absolute velocities of the substructure and the superstructure, the kinetic energy of the system can be written as:

$$T = \frac{1}{2} m_d \left[\left(\dot{x}_g + \dot{u}_d \right)^2 + \dot{z}_g^2 \right] + \frac{1}{2} m_u \left[\left(\dot{x}_g + \dot{u}_d + \dot{u}_u \right)^2 + \left(\dot{z}_g + \dot{u}_u \tan\alpha \, \mathrm{sign} u_u \right)^2 \right] \qquad (4-25)$$

If a virtual displacement field is applied to the system, the virtual work from external forces can be computed and the generalized forces associated with each coordinate can be found.

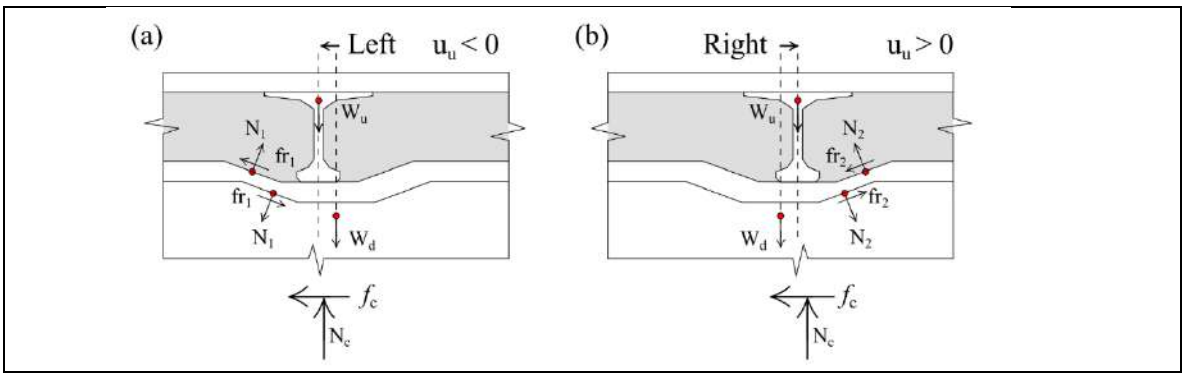

Fig. 4-7. A portion of the free-body diagrams for the structural system when (a) the relative displacement of the superstructure with respect to the substructure is to the left and elastomeric bearings e_1, e_3, e_5, e_7, e_9, e_{11}, e_{13} and e_{15} are developing internal forces, and (b) the relative displacement of the superstructure with respect to the substructure is to the right and elastomeric bearings e_2, e_4, e_6, e_8, e_{10}, e_{12}, e_{14} and e_{16} are developing internal forces.

Considering the free body diagrams for the substructure and the superstructure shown in

Figure 4-7 and the kinematic relationships defined in Equations (4-9) to (4-12), it can be shown that the total virtual work done by the external forces can be written as (see Appendix 1),

$$\delta\widetilde{W} = -f_c\delta x_g + (-W_d + N_c - W_u)\delta z_g - f_c\delta u_d + (-\boldsymbol{L}_r^T\boldsymbol{f}_r - W_u\tan\alpha\ \mathrm{sign}u_u)\delta u_u \quad (4-26)$$

where δx_g, δz_g, δu_d and δu_u are virtual displacements. The terms that multiply the virtual displacements are the generalized forces associated to each coordinate. In particular, for the degrees of freedom u_d and u_u, the associated generalized forces are:

$$F_d = -f_c \quad (4-27)$$

$$F_u = -\boldsymbol{L}_r^T\boldsymbol{f}_r - W_u\tan\alpha\ \mathrm{sign}u_u \quad (4-28)$$

The two equations of motion are obtained from the following Euler-Lagrange equations:

$$\frac{d}{dt}\left(\frac{\partial T}{\partial \dot{u}_d}\right) - \frac{\partial T}{\partial u_d} = F_d \quad (4-29)$$

$$\frac{d}{dt}\left(\frac{\partial T}{\partial \dot{u}_u}\right) - \frac{\partial T}{\partial u_u} = F_u \quad (4-30)$$

Introducing the kinetic energy from Equation (4-25) and the generalized forces from Equations (4-27) and (4-28), the equations of motion for the substructure and the superstructure result:

$$(m_d + m_u)\ddot{u}_d + m_u\ddot{u}_u + k_c u_d + c_c\dot{u}_d = -(m_d + m_u)\ddot{x}_g \quad (4-31)$$

$$m_u\ddot{u}_d + m_u(1+\tan^2\alpha)\ddot{u}_u + \boldsymbol{L}_r^T\boldsymbol{f}_r = -m_u\ddot{x}_g - m_u\tan\alpha\ \mathrm{sign}u_u\ddot{z}_g - W_u\tan\alpha\ \mathrm{sign}u_u \quad (4-32)$$

Moreover, Equations (4-31) and (4-32) can be resumed in one matrix equation as follows:

$$\begin{bmatrix} m_d + m_u & m_u \\ m_u & m_u(1+\tan^2\alpha) \end{bmatrix}\begin{bmatrix}\ddot{u}_d \\ \ddot{u}_u\end{bmatrix} + \begin{bmatrix} c_c & 0 \\ 0 & 0\end{bmatrix}\begin{bmatrix}\dot{u}_d \\ \dot{u}_u\end{bmatrix} + \begin{bmatrix} k_c & 0 \\ 0 & 0\end{bmatrix}\begin{bmatrix}u_d \\ u_u\end{bmatrix} + \begin{bmatrix} 0 \\ \boldsymbol{L}^T\boldsymbol{f}\end{bmatrix} = -\begin{bmatrix} m_d + m_u \\ m_u\end{bmatrix}\ddot{x}_g - \begin{bmatrix} 0 \\ m_u\tan\alpha\ \mathrm{sign}u_u\end{bmatrix}\ddot{z}_g - \begin{bmatrix} 0 \\ W_u\tan\alpha\ \mathrm{sign}u_u\end{bmatrix} \quad (4-33)$$

Please note that in Equation (4-33), the term $W_u\tan\alpha\ \mathrm{sign}u_u$ is responsible for the self-centering behavior of the proposed model. Equation (4-33) is solved using a variable-step integration method for a set of earthquakes, using ten different values of inclination α, from 0 to 45º.

4.2.4.6 Self-centering conditions

The self-centering behavior of the superstructure is mainly controlled by the inclination angle α of the elastomeric bearings defined in Figure 4-5. For $\alpha = 0°$, which is the case in Chilean bridges depicted in Figure 4-2, no self-centering behavior is expected, and residual displacements will be generated after large earthquakes. However, the self-centering behavior is not automatically attained by satisfying $\alpha > 0°$. For small values of α, the component of the weight of the superstructure over the shear direction of the elastomeric bearings could not be large enough to overcome the maximum static friction developed by bearings. In other words, the superstructure could stay in static equilibrium with $u_u \neq 0$ for small values of α. Consider a general case of $2n$ elastomeric bearings, where the n elements with a positive slope are numbered with even numbers, and the n elements with a negative slope are numbered with odd numbers. Figure 4-8b shows the particular case of the bridge analyzed in this research with n=8. Considering this, Equation (4-7) can be written in a more general form as:

$$\sigma = \frac{W_u cos\alpha}{nA_r} \qquad (4-34)$$

Following [44], the dynamic friction coefficient is computed using Equation (4-6), and the maximum friction force in each elastomeric bearing is given by Equation (8). Then, the static self-centering condition can be written as:

$$W_u \sin\alpha > nF_y \qquad (4-35)$$

which indicates that the static self-centering condition needs the component of the weight of the superstructure over the shear direction of the elastomeric bearings to be greater than the maximum friction developed on the elastomeric bearings. Equation (4-35) guarantees that, for example, under an initial condition of displacement of the superstructure with respect to the superstructure and zero velocity, the self-centering behavior occurs. Considering Equations (4-34), (4-6) and (4-8), the Equation (4-35) can be written as:

$$nA_r < (\sin\alpha - 0.18\cos\alpha)\frac{W_u}{0.38} \qquad (4-36)$$

Equation (4-36) constraints the design parameters α, n and A_r given the weight of the superstructure W_u. In this research, values of W_u=3822 kN, A_r =135000 mm^2 and n=8 give a theoretical condition of α > 15º that satisfies Equation (4-3). However, it is important to note that this limit value of α is based on static conditions. Considering the dynamic behavior of the bridge due to ground motions, Equation (4-36) is not restrictive for choosing the design value α.

4.2.5. Ground motion characteristics

The sensitivity of the structural response of the proposed shear key will be tested using a ground motion ensemble representative for Chile and classified by soil class as established in the Highway Manual [8]. These records are from different Chilean earthquakes (Table 4-1 [50,51]). The seismic soil classification for each station of the selected records is summarized in Table 2 as reported by [52–57].

Table 4-1. Number of accelerograms used in this research.

Earthquake	**M_w**	**Horizontal Channels**	**Vertical Channels**
Algarrobo, 1985	8.0	46	24
Punitaqui, 1997	7.1	4	2
Tocopilla, 2007	7.7	2	1
Maule, 2010	8.8	38	19
Constitución, 2012	7.0	6	3
Iquique, 2014	8.2	14	7
Coquimbo, 2015	8.3	6	3
Total		118	59

Table 4-2. Location and seismic soil classification of accelerometers.

Site of the accelerometer	**SSC***	**Site of the accelerometer**	**SSC***
Copiapó	III	Santiago La Florida	II
Vallenar	II	Llolleo	III
Illapel	II	Melipilla	II
Los Vilos	II	Rapel	I
La Ligua	II	Matanzas	III
Papudo	I	Pichilemu	I
Zapallar	I	San Fernando	II
Ventanas	III	Iloca	II
San Felipe	II	Hualañé	II
Llay-Llay	III	Curicó	II
Viña del Mar Centro	III	Constitución	III

Valparaíso Almendral	II	Talca	II
Valparaíso TFSM	I	Cauquenes	III
Viña del Mar El Salto	III	Chillan Viejo	II
Las Tórtolas	II	Concepción	II
Quintay	I	Angol	III
Santiago Peñalolén	III	Valdivia	II
Santiago Maipú	II	Tenencia de Pica	III
Pisagua	I	Cerro El Roble	I
Huara	II	Curicó	II
Iquique SERVIU	II	Hualañé	II
Pozo Almonte	III	Talca	II
Alto Hospicio	III	Concepción	III
Humberstone	II		

* Soil seismic classification

Figure 4-8 shows the horizontal and vertical pseudo acceleration spectrum computed using a damping ratio of 5% obtained for all Chilean ground motions, as classified by soil class. These ground motions were selected using the criteria described by Wilches et al. [13]. All the ground motions were used without altering their frequency content, which allowed us to include the variability observed in the different earthquakes.

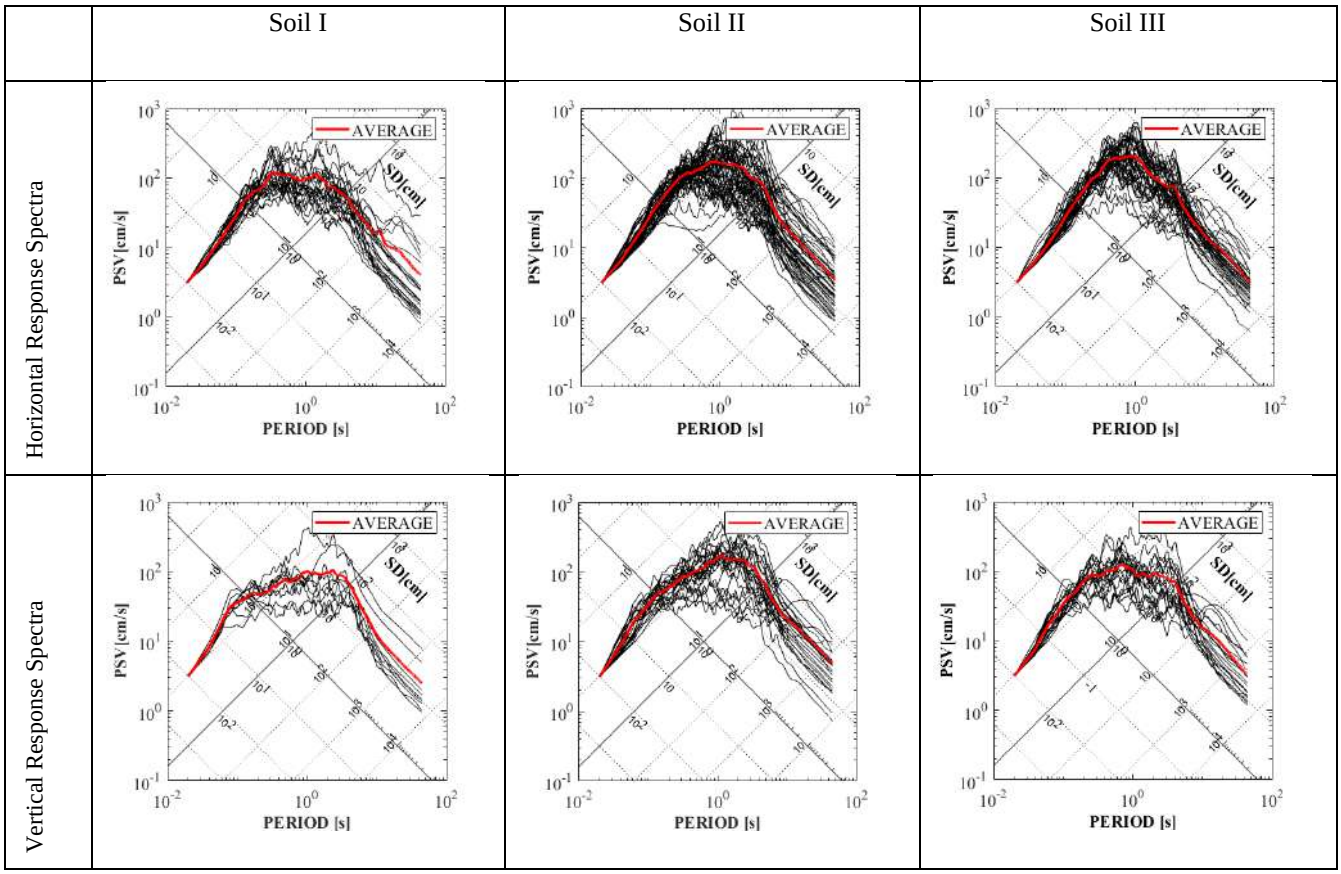

Fig. 4-8. Response spectra (normalized to PGA=1 g and ξ=5%) of the records belonging to seismic soil classifications I, II and III.

4.3 Key results

The displacements of the bridge and the shear forces in the columns will be used as the main performance indices and are computed using two different approaches. The first approach is a time-history response using the ground motions described in the former section, while the second approach involves an estimation of the maximum values of the response using a design spectrum. The results will be discussed both as comparisons of the two approaches as well as functions of some of the input parameters used in the time-history analyses.

4.3.1 Lateral displacement demands

Equation (4-33) was solved for the three components of each earthquake listed in Table 4-1. Furthermore, bridges incorporating the SCSK concept were also studied. In these bridges, angle α was varied from 5° to 45° every 5° for each ground motion. Parallels runs were carried out also for the prototype bridge (α = 0°). For each of these cases, the displacement u_d of the substructure relative to the ground, the displacement u_u of the superstructure relative to the substructure, and the shear force computed from Equation (4-23) were calculated. Figure 4-9 shows time-history series for displacements u_d and u_u for α = 0° and 15°, for three soil classes and three specific records. The maximum displacements {u_u , u_d, soil class} for the prototype bridge are {80 mm, 10 mm, I}, {111 mm, 12 mm, II}, {355 mm, 14 mm, III}, whereas for α = 15° are {19 mm, 17 mm, I}, {27 mm, 19 mm, II}, and {66 mm, 22 mm, III}, respectively. Angles α > 0° result in a large decrease in relative displacement between the superstructure and the substructure. As a consequence, the displacement of the substructure increases, which results in a significant increase in the seismic demand on the columns, see Table 4-3. For the case of the prototype bridge, which represents the conventional configuration of typical Chilean bridges, the superstructure had residual displacements of 76 mm, 76 mm, and 279 mm for soil class I, II, and III, respectively. In contrast, for a α = 15° the residual displacements are zero regardless of the earthquake and soil class. This is because with this inclination the system establishes a kinematic restriction that eliminates the residual displacements of the superstructure.

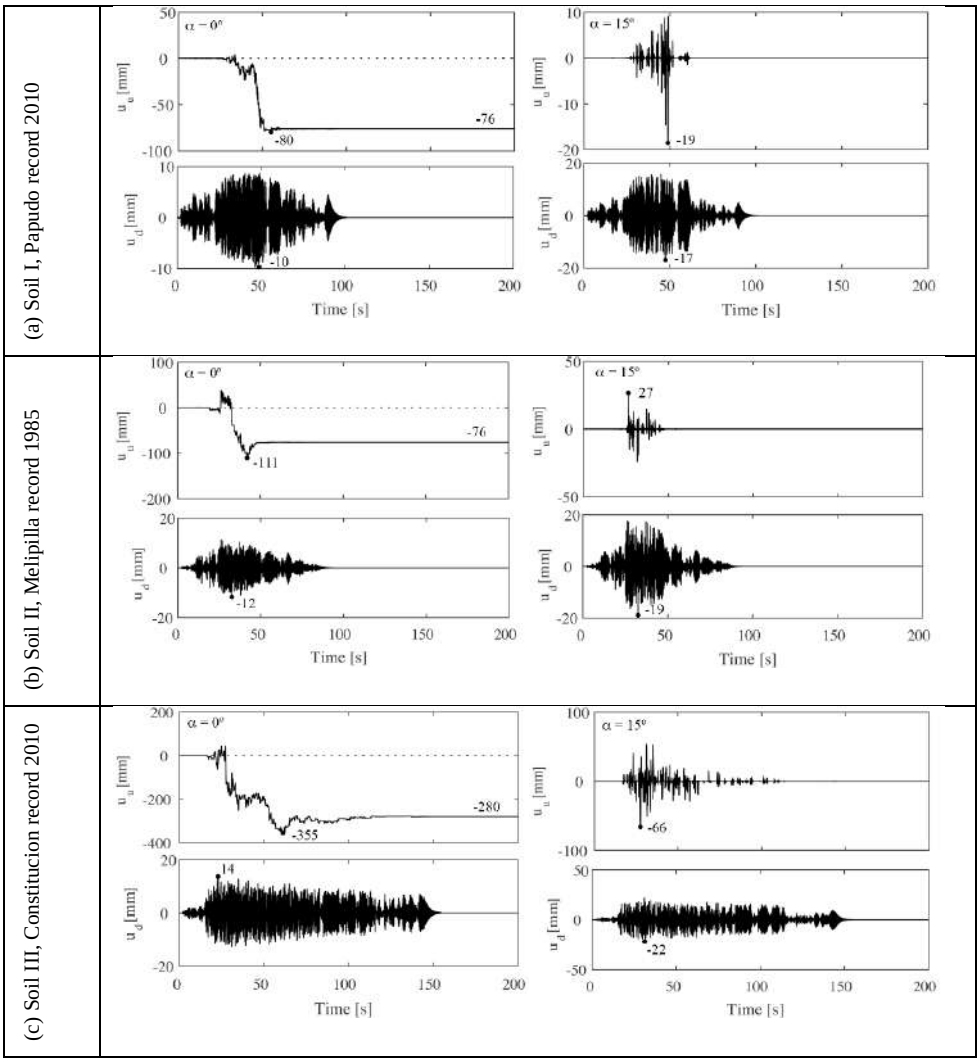

Fig. 4-9. Relative displacement demands u_u and u_d for α = 0° (prototype bridge) and α = 15° (bridge with SCSK concept).

Table 4-3. Maximum ratios of seismic shear demand on the columns of SCSK bridges to the demand for the prototype bridge considering all records. The first row shows the absolute value for the prototype bridge and the following rows the ratio relative to it.

α [°]	Soil I	Soil II	Soil III
0	733 kN	940 kN	927 kN
5	1.06	1.04	1.13
10	1.35	1.25	1.38
15	1.55	1.41	1.65
20	1.87	1.70	1.85
25	2.25	2.05	2.17
30	2.63	2.29	2.45
35	3.22	2.57	2.80

Now, if we consider all the values of α, the earthquakes with different magnitudes (Table 4-1), and the records classified by types of soils (Table 4-2), we can construct Figure 10, which shows time-history envelopes for the displacements u_u and u_d.

The seismic demand on the columns increases as angle α increases (see Table 4-3) because the kinematic restriction between the superstructure and substructure becomes more restrictive. For α = 5° the maximum displacements u_u are 19 mm (I), 53 mm (II), and 106 mm (III), the residual displacement is eliminated, and the seismic demand on the columns increases between 4 and 13% with respect to the case of the prototype bridge (Table 4-3). Although, for α = 5° the residual displacement is eliminated, it must be considered that the aspect ratio that this angle generates in the shear key is very small if we consider the construction process of this element; with these dimensions we cannot meet the construction requirements specified by MOP [8], such as cover of the reinforcement, amount of reinforcement, etc. However, different α values were evaluated to propose an optimal value for the typical Chilean bridge. The selected α value may be different in other regions depending on the technical specifications and ground motion types.

Another relevant aspect shown in Figure 4-10 is the relationship of the magnitude of the maximum displacements of the superstructure (u_u) and substructure (u_d) with the type of soil. For α values between 5° and 45°, the maximum displacements u_u and u_d for soil class I and II remain in a small range. For soil class I, u_u ranges between 19 mm and 32 mm while u_d ranges between 11 mm and 47 mm, respectively. For soil class II, u_u varies between 20 mm and 53 mm, while u_d varies between 14 mm and 39 mm. For soil class III, u_u varies between 46 mm and 107 mm, while u_d varies between 14 mm and 51 mm. This shows that whereas the maximum displacement u_u for soil class III presents great variability, the maximum value of u_d is almost the same regardless of the soil class.

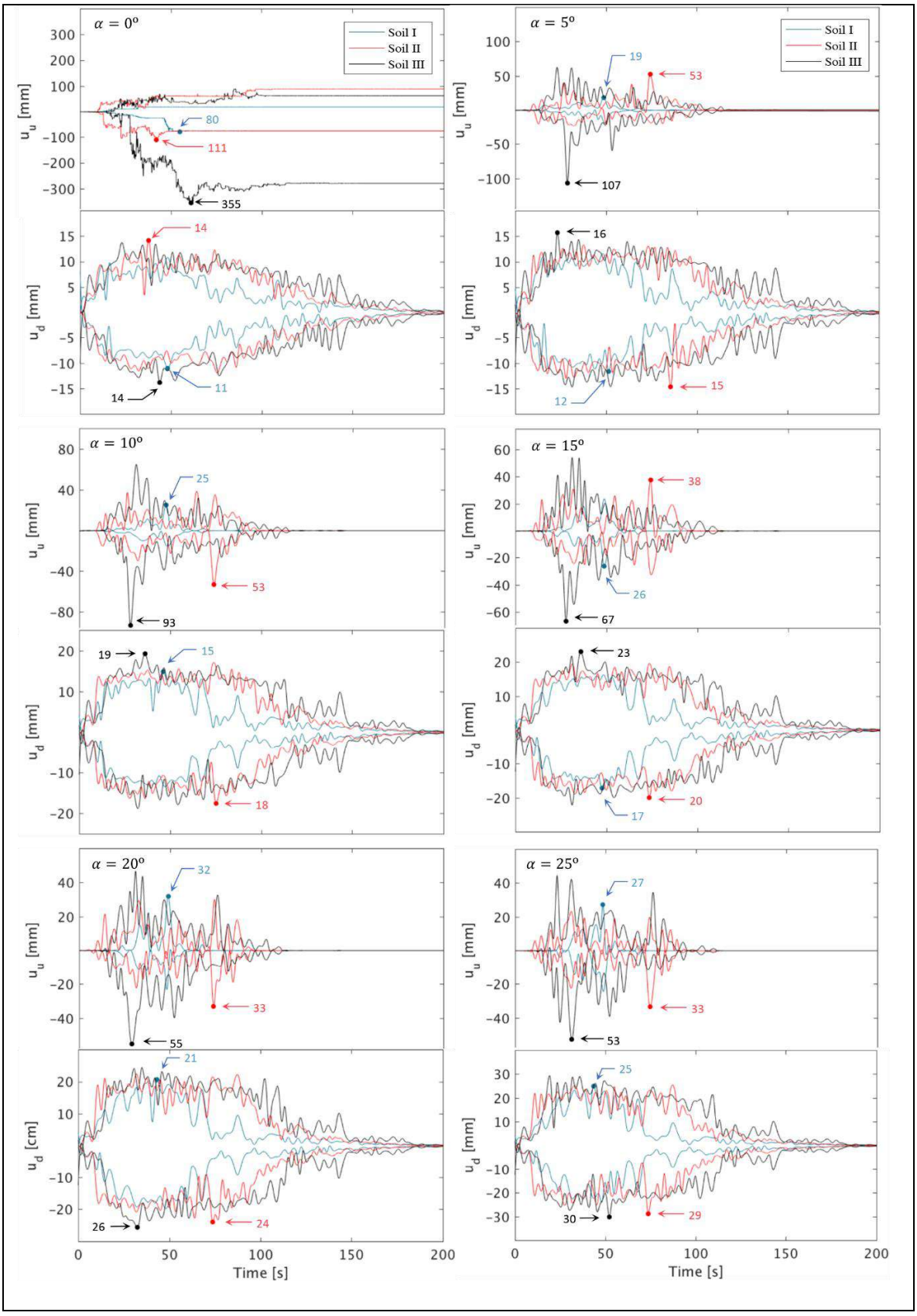

Fig. 4-10. Envelope of the displacements of the superstructure (u_u) and substructure (u_d).

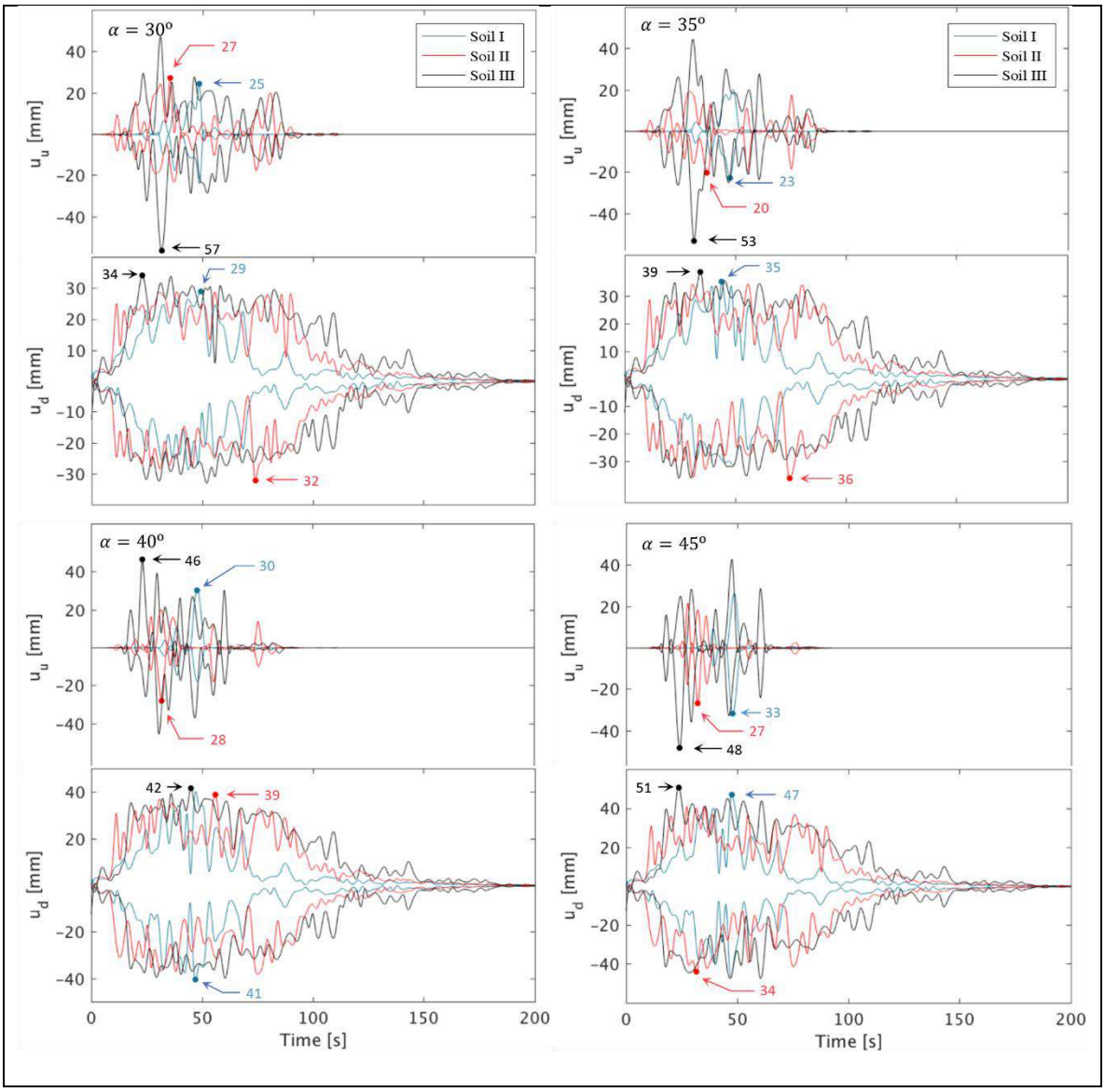

(Continued) **Fig. 4-10.** Envelope of the displacements of the superstructure (u_u) and substructure (u_d).

4.3.2 Estimation of the displacements using a design spectrum

The seismic response of the bridge using the proposed self-centering shear keys is estimated using the Chilean seismic design code NCh3411 [58], which defines a Newmark – Hall design spectrum to design structures including passive energy dissipation devices. The cut-off periods to define the acceleration, velocity, and displacement zones of the spectrum depend on the soil classification defined in MOP [8], as well as its amplitude. Moreover, the amplitude of the spectrum is affected by a zone classification which defines three different hazard levels [58]. Figure 4-11 shows the base design spectra for the highest hazard zone and the three soil classifications. The response of the bridge due to a ground motion characterized by the design spectra is computed and compared with the maximum values obtained from time-history analyses.

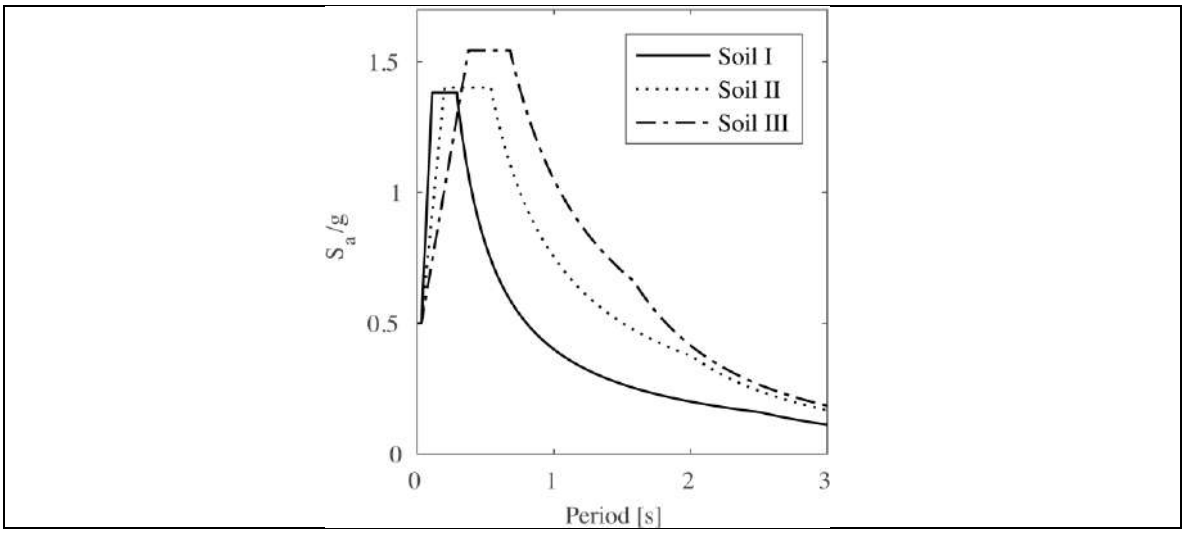

Fig. 4-11. Base design spectra from NCh3411 for each type of soil (PGA=0.5g, 5% damping).

To estimate the response of the structure, the bridge is simplified as an equivalent nonlinear single degree-of-freedom oscillator obtained from a pushover curve expressed in the spectral coordinates space. This is called the *capacity curve*. The intersection point between the capacity curve and the design spectrum modified considering the energy dissipation due to friction, is the *performance point*, which is an estimation for the maximum response of the bridge for a ground motion represented by the design spectrum [59]. Using this procedure, the maximum displacements u_u and u_d are computed for three soil classifications and three seismic zones with different hazard levels. Considering the results from time-history analysis discussed in the previous section, four α values are used: prototype bridge, 5º, 10º and 15º.

Figure 4-12 shows the performance points for each case, including the equivalent damping ratio developed by the inelastic system. The results are summarized and compared with the time-history results in Table 4-4. These show two important results,

i. The NCh3411 [58] standard establishes a factor of 1.2 that is applied to design displacements to determine maximum displacement values equivalent to those experienced by the structure with a probability of occurrence of 10% in 100 years (maximum expected earthquake). The displacements obtained for the bridge from the design spectrum defined in Fig. 4-11 multiplied by 1.2 are smaller than those determined from the time-history analyses. This is due to the fact that the latter were carried out with earthquakes of magnitudes even greater than 8.
ii. As the angle α increases, a decrease in displacement u_u and an increase in displacement u_d are generally observed. The latter explains the increase in the seismic demand of the columns This occurs both in the case of the response calculated with the design spectrum and in the time-history analysis. Finally, if we compare the u_d for the prototype bridge and α = 10° we notice that there is no significant increase in the seismic demand of the columns. But if we compare the prototype bridge and α = 15° we notice a significant increase in the seismic demand of the columns. However, it is important to note that these maximum values are higher than those caused by the maximum possible earthquake defined in the standard [58], which

translates into a low probability of occurrence. Therefore, it is recommended that an angle range for the proposed system be between 10° and 15°.

It is important to note that Wilches et al. [12,13] analyzed the influence of shear keys on the seismic behavior of Chilean bridges using most of the same earthquakes from this study and showed that for different structural configurations, especially where there was a pounding between the superstructure and shear keys, the columns did not suffer any damage, but the superstructure was left with a residual displacement.

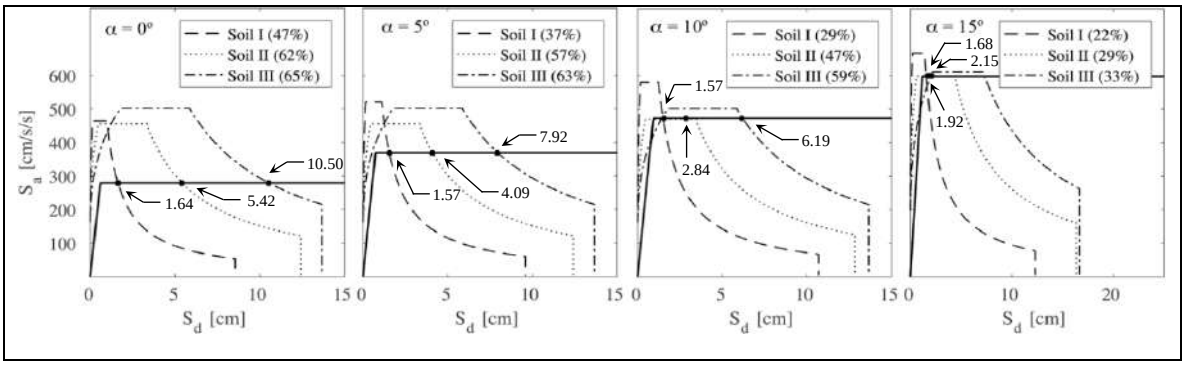

Fig. 4-12. Capacity curves (solid thick line), design spectra (dashed and dotted lines), and performance points for each case, including the equivalent damping ratio (%) developed by the inelastic system.

Table 4-4. Comparison of results.

α [°]	Demand-capacity [mm]						Time-history [mm]					
	Soil Class I		Soil Class II		Soil Class III		Soil Class I		Soil Class II		Soil Class III	
	u_u	u_d	u_u	u_d	u_u	u_d	u_u	u_d	u_u	u_d	u_u	u_d
Prototype bridge	16.4	5.6	54.2	5.6	105.0	5.6	79.7	11.0	110.5	14.1	354.8	13.9
5	15.6	7.3	40.6	7.3	78.6	7.3	18.6	11.7	52.8	14.7	106.5	15.7
10	15.2	9.1	27.6	9.1	60.1	9.1	25.2	14.8	53.2	17.6	93.2	19.2
15	15.6	11.1	17.9	11.1	20.1	11.1	26.3	17.1	37.5	19.9	66.6	23.0

4.4 Conclusions

This paper proposes a self-centering shear key concept for bridges that, through kinematics, uses the superstructure's weight as a restoring force. The shear key relies on steel-laminated elastomeric bearings to validate the proposed concept, a large number of nonlinear time-history analyses were performed. The main variables studied were the angle of inclination of the elastomeric bearings, α, and the input ground motions. The ground motions were chosen from the Chilean ground motion database for different soil classes. The main findings of this study are,

1. The self-centering shear key concept described in the paper makes it possible to eliminate the residual lateral displacements of the superstructure.
2. The increase in seismic demand on the bridge columns due to the self-centering mechanism is proportional to the inclination angle α. Under certain circumstances, the inertia forces are reduced, and the substructure can remain elastic.
3. Self-centering shear keys are a simple solution, as they do not require the incorporation of new materials or additional steps than normal for the analysis, design, and construction stages.
4. The proposed shear key concept does not need additional devices such seismic isolators or energy dissipation devices. With a simple change of the geometry, the elimination of the residual displacements ensures the superstructure’s self-centering behavior.
5. In the proposed system there is the possibility that after a large earthquake the elastomeric bearings will be left with shear stress and residual deformation, but the bridge will still re-centerd, which is the objective pursued by this research. A number of practical details will need to be addressed in the construction process to minimize spurious sources of strains in the elastomeric bearings.

The technique proposed herein represents a step towards resilience-based design, any road bridge after a major event must have a high probability of maintaining immediate functionality. The proposed solution is adaptable to other structural morphologies of bridges where there is an interface between substructure and superstructure that allows the incorporation of the new self-centering geometry, independent of the seismic hazard and the seismic classification of the soil class.

Acknowledgements

The authors wish to acknowledge the funding provided by ANID (Chilean National Agency for Research and Development) through the ANID Doctorate Scholarship and the Research Center for Integrated Disaster Risk Management (CIGIDEN) ANID/FONDAP 15110017. ANID has funded the double doctoral studies of the first author at both the Pontificia Universidad Catolica de Chile and Virginia Tech.

References

[1] Sarrazin M, Moroni O, Roesset JM. Evaluation of dynamic response characteristics of seismically isolated bridges in Chile. Earthq Eng Struct Dyn 2005;34:425–48. https://doi.org/10.1002/eqe.443.

[2] Moroni MO, Boroschek R, Sarrazin M. Dynamic Characteristics of Chilean Bridges with Seismic Protection. J Bridg Eng 2005;10:124–32. https://doi.org/10.1061/(asce)1084-0702(2005)10:2(124).

[3] Dai W, Moroni MO, Roesset JM, Sarrazin M. Effect of isolation pads and their stiffness on the dynamic characteristics of bridges. Eng Struct 2006;28:1298–306. https://doi.org/10.1016/j.engstruct.2005.12.012.

[4] Sarrazin M, Moroni O, Neira C, Venegas B. Performance of bridges with seismic isolation bearings during the Maule earthquake, Chile. Soil Dyn Earthq Eng 2013;47:117–31. https://doi.org/10.1016/j.soildyn.2012.06.019.

[5] Ministerio de Obras Públicas. Manual de carreteras – Volumen No3 – Instrucciones y criterios de diseño (in Spanish). Chile: Ministerio de Obras Públicas; 2002.

[6] Ministerio de Obras Públicas. Cuenta pública 2010, cuenta sectorial, Ministerio de Obras Públicas, Chile (in spanish) 2010.

[7] Ministerio de Obras Públicas. Manual de carreteras - Volumen nº3 - Instrucciones y criterios de diseño (in spanish). Chile: Ministerio de Obras Públicas; 2015.

[8] Ministerio de Obras Públicas. Manual de carreteras - Volumen nº3 - Instrucciones y criterios de diseño (in spanish). Chile: Ministerio de Obras Públicas; 2017.

[9] Japan Road Association. Design Specifications for Highway Bridges. Japan: Japan Road Association; 2012.

[10] American Association of State Highway and Transportation Officials. AASTHO Guide Specifications for LRFD Seismic Bridge Design. 2011.

[11] New Zealand Transport Agency. New Zealand bridge manual, 3rd edition. New Zeland: 2014.

[12] Wilches Están J de J, Santa María H, Riddell R, Arrate Letelier C. Influence of the use of external shear keys on the seismic behavior of Chilean highway bridges. Eng Struct 2017;147:613–24. https://doi.org/10.1016/j.engstruct.2017.06.015.

[13] Wilches Están J de J, Santa María H, Riddell R, Arrate Letelier C. Effects of changes in seismic design criteria in the transverse and vertical response of Chilean highway bridges. Eng Struct 2019;191:370–85. https://doi.org/10.1016/j.engstruct.2019.04.064.

[14] Buckle IG, Hube M, Chen G, Yen W-H, Arias JG. Structural performance of bridges in the offshore Maule earthquake of 27 february 2010. Earthq Spectra 2012;28:S533–52. https://doi.org/10.1193/1.4000031.

[15] Saiidi M, Maragakis E, Feng S. Parameters in Bridge Restrainer Design for Seismic Retrofit. J Struct Eng 1996;122:61–8. https://doi.org/10.1061/(asce)0733-9445(1996)122:1(61).

[16] Megally SH, Silva PF, Seible F. Seismic response of sacrificial shear keys in bridge abutments. University of California, San Diego; 2002.

[17] Han Q, Zhou Y-L, Zhong Z-L, Du X-L. Seismic capacity evaluation of exterior shear keys of highway bridges. J Bridg Eng 2017;22:04016119. https://doi.org/10.1061/(ASCE)BE.1943-5592.0000978.

[18] DesRoches R, Pfeifer T, Leon RT, Lam T. Full-Scale Tests of Seismic Cable Restrainer Retrofits for Simply Supported Bridges. J Bridg Eng 2003;8:191–8. https://doi.org/10.1061/(asce)1084-0702(2003)8:4(191).

[19] Silva PF, Megally SH, Seible F. Seismic performance of sacrificial interior shear keys. ACI Struct J 2003;100:177–87.

[20] Roberts JE. Caltrans structural control for bridges in high-seismic zones. Earthq Eng Struct Dyn 2005;34:449–70. https://doi.org/10.1002/eqe.439.

[21] Bozorgzadeh A, Megally SH, Restrepo JI, Ashford S. Capacity evaluation of exterior sacrificial shear keys of bridge abutments. J Bridg Eng 2006;11:555–65. https://doi.org/10.1061/(ASCE)1084-0702(2006)11:5(555).

[22] Tobias DH, Anderson RE, Hodel CE, Kramer WM, Wahab RM, Chaput RJ. Overview of Earthquake Resisting System Design and Retrofit Strategy for Bridges in Illinois. Pract Period Struct Des Constr 2008;13:147–58. https://doi.org/10.1061/(asce)1084-0680(2008)13:3(147).

[23] Guo A, Li Z, Li H, Ou J. Experimental and analytical study on pounding reduction of base-isolated highway bridges using MR dampers. Earthq Eng Struct Dyn 2009:1307–33. https://doi.org/10.1002/eqe.

[24] Padgett JE, DesRoches R, Ehlinger BF. IExperimental response modification of a four-span bridge retrofit with shape memory alloys. Struct Control Heal Monit 2009;17:694–708. https://doi.org/10.1002/stc.

[25] Xiang N, Li J. Seismic performance of highway bridges with different transverse unseating-prevention devices. J Bridg Eng 2016;21. https://doi.org/10.1061/(ASCE)BE.1943-5592.0000909.

[26] Goel RK, Chopra AK. Role of shear keys in seismic behavior of bridges crossing fault-rupture zones. J Bridg Eng 2008;13:398–408. https://doi.org/10.1061/(ASCE)1084-0702(2008)13:4(398).

[27] Peralta L, Hube MA. Deck rotation of straight bridges induced by asymmetric characteristics and effect of transverse diaphragms. Eng Struct 2018;173:729–43. https://doi.org/10.1016/j.engstruct.2018.06.107.

[28] Wilches J, Santa Maria H, Leon R, Riddell R, Hube M, Arrate C. Evolution of seismic design codes of highway bridges in Chile. Earthq Spectra 2020:1–61.

[29] Kelly JM, Konstantinidis DA. Mechanics of Rubber Bearings for Seismic and Vibration Isolation. 2011. https://doi.org/10.1002/9781119971870.

[30] Almazán JL, De La Llera JC, Inaudi JA. Modelling aspects of structures isolated with the frictional pendulum system. Earthq Eng Struct Dyn 1998;27:845–67. https://doi.org/10.1002/(SICI)1096-9845(199808)27:8<845::AID-EQE760>3.0.CO;2-T.

[31] Skinner,R.I., Robinson WH, McVerry GH. An Introduction to Seismic Isolation. John Wiley. New York: 1999.

[32] Chen MC, Restrepo JI, Benzoni G. Response of a high damping rubber bearing to multiaxial excitation. J Test Eval 2019;49. https://doi.org/10.1520/JTE20180558.

[33] Filiatrault A, Restrepo J, Christopoulos C. Development of Self-Centering Earthquake Resisting Systems. 13th World Conf. Earthq. Eng. (13 WCEE), August 1-6, 2004, p. Paper No. 3393.

[34] Pantelides C. Self-Centering Bridge Bent for Accelerated Bridge Construction in Seismic Regions. 2017.

[35] Xia X, Zhang X, Shi J, Tang J. Seismic isolation of railway bridges using a self-centering pier. Smart Struct Syst 2021;27:447–55. https://doi.org/10.12989/sss.2021.27.3.447.

[36] Upadhyay A, Pantelides CP, Ibarra L. Residual drift mitigation for bridges retrofitted with buckling restrained braces or self centering energy dissipation devices. Eng Struct 2019;199:109663. https://doi.org/10.1016/j.engstruct.2019.109663.

[37] Xue D, Bi K, Dong H, Qin H, Han Q, Du X. Development of a novel self-centering slip friction brace for enhancing the cyclic behaviors of RC double-column bridge bents. Eng Struct 2021;232:111838. https://doi.org/10.1016/j.engstruct.2020.111838.

[38] Martínez A, Hube M, Rollins KM. Analytical fragility curves for non-skewed highway bridges in Chile. Eng Struct 2017;141:530–42. https://doi.org/10.1016/j.engstruct.2017.03.041.

[39] Jangid RS. Seismic response of isolated bridges. J Bridg Eng 2004;9:156–66. https://doi.org/10.1061/(ASCE)1084-0702(2004)9:2(156).

[40] Hwang JS, Sheng LH. Equivalent elastic seismic analysis of base-isolated bridges with lead-rubber bearings. Eng Struct 1994;16:201–9. https://doi.org/10.1016/0141-0296(94)90078-7.

[41] Kannan AE, Powell GH. General purpose computer program for inelastic dynamic response of plane structures. University of California, Berkeley, 1973.

[42] Naeim F, Kelly JM. Design of seismic isolated structures. 1999.

[43] Konstantinidis D, Kelly JM, Makris N. Experimental investigation on the seismic response of bridge bearings. vol. EERC 2008-. 2008.

[44] Steelman JS, Fahnestock LA, Filipov ET, LaFave JM, Hajjar JF, Foutch DA. Shear and friction response of nonseismic laminated elastomeric bridge bearings subject to seismic demands. J Bridg Eng 2013;18:612–23. https://doi.org/10.1061/(ASCE)BE.1943-5592.0000406.

[45] Persson BNJ. Theory of rubber friction and contact mechanics. J Chem Phys 2001;115:3840–61. https://doi.org/10.1063/1.1388626.

[46] Schaefer R. Mechanical properties of rubber. Shock Vib. Handb. McGraw–Hil, New York: 2002
.

[47] Reyes SI, Almazán JL. A novel device for a vertical rocking isolation system with uplift allowed for industrial equipment and structures. Eng Struct 2020;214:110595. https://doi.org/10.1016/j.engstruct.2020.110595.

[48] Charalampakis AE. Parameters of Bouc-Wen hysteretic model revisited. Proc 9h HSTAM Int Congr Mech 2010:12–4.

[49] Chopra AK. DYNAMICS OF STRUCTURES Theory and Applications to Earthquake Engineering. Fourth Edi. 2012.

[50] Centro Sismológico Nacional. Earthquakes of Chile - Records between 1992 and 2010 (database) 2010. http://terremotos.ing.uchile.cl/ (accessed April 20, 2017).

[51] Centro Sismológico Nacional. Records of significant seismic events - Records between 2012 to present (database) 2015. http://evtdb.csn.uchile.cl/ (accessed April 20, 2017).

[52] Riddell R. Inelastic design spectra accounting for soil conditions. Earthq Eng Struct Dyn 1995;24:1491–510. https://doi.org/10.1002/eqe.4290241106.

[53] Kayen R, Carkim BD, Cobert S, Pinilla C, Ng A, Gorbis E, et al. Seismic velocity site characterization of thirty-one chilean seismometer stations by spectral analysis of surface wave dispersion. Berkeley: 2014.

[54] Universidad Diego Portales, Leyton Flórez F. FUCHIGE - Mediciones de microvibraciones en 6 estaciones sismicas (in spanish). 2014.

[55] DICTUC, Sáez Robert E. FUCHIGE - Report of project: study of seismographic stations (in spanish). 2014.

[56] Universidad de Concepción, Montalva Alvarado G, Bastías N, Troncoso P. FUCHIGE - Mediciones geofísicas: estaciones acelerográficas norte de Chile (in spanish). 2014.

[57] Boroschek R, Yañez U F, Bejarano B I, Molnar S, Torres G A. Caracterización geotécnica estaciones de acelerógrafos de la Universidad de Chile (in spanish). 2012.

[58] Instituto Nacional de Normalización. NCh3411:2017 - Diseño sísmico de edificios con sistemas pasivos de disipación de energía - Requisitos y métodos de ensayo (in spanish). Chile: Instituto Nacional de Normalización; 2017.

[59] Porter K. Cracking an open safe: HAZUS vulnerability functions in terms of structure-independent spectral acceleration. Earthq Spectra 2009;25:361–78. https://doi.org/10.1193/1.3106680.

5. CHAPTER 5

CONCLUSIONS

This research presents an analytical investigation on the influence of shear keys on the seismic behavior of typical Chilean highway bridges through three specific objectives that correspond to the different chapters of this thesis:

(i) to evaluate numerically the influence of sacrificial external shear keys on the seismic response of typical Chilean highway bridges;
(ii) to assess the effects of changes in seismic design criteria on the transverse and vertical response of Chilean highway bridges; and,
(iii) to propose a new technique for self-centering shear keys in highway bridges.

Although the analytical models considered throughout this investigation are very different from each other and still sensitive to the assumptions of the model, the results show that the geometry and type of damage observed during earthquakes, as well as the maximum and residual transverse displacement of the superstructure, can be represented by analytical models under certain conditions. The results show a ductile behavior of the shear keys, represented by a diagonal tension failure, as the governing mechanism. The resulting damage requires that the bridges be repaired/retrofitted after major seismic events. To address that issue, this dissertation proposes an economical and efficient self-centering shear key configuration that minimizes or eliminates damage and residual displacements of the superstructure.

The first objective of this dissertation (Chapter 2) is an evaluation of the role of sacrificial shear keys in the seismic response of bridges for different seismic hazard conditions and soil types. The results of a statistical analysis of Chilean highway bridges were used to identify a representative typology of bridges. Two models were used for the evaluation of the seismic behavior of the selected typology, given different soil conditions and seismic hazard zones, as follows: (1) one without sacrificial shear keys, which has no transverse displacement restriction and (2) other with non-linear shear keys, which offers transverse constraint to displacement up to a maximum deformation of the sacrificial shear key. Fragility curves were generated using non-linear analytical models and a series of records compatible with Chilean response spectra. The results show that the use of external shear keys produces an improvement in the seismic performance of bridges in terms of decreasing the residual displacement. However, such improvement is highly dependent on the seismic hazard level and the soil type.

The use of external shear keys on bridges prevents premature occurrence of large residual displacement in the elastomeric bearings. This occurrence is transferred from values of 0.3g to 1.8g EPA design standard value to values of 0.5g to 2.5g EPA, depending on the seismic

hazard zone and seismic soil type. The presence of shear keys increases the probability of continuity of use of the bridges after a severe seismic event. It is important to note that the role of the shear keys is essential in reducing the probability of damage to bridges located in high seismic hazard areas and soft soils (type III).

Finally, the current Chilean design provisions for shear keys do not consider the soil classification simultaneously with the level of seismic hazard in the determination of the design forces. This is the main reason for the large variability of fragility curves of a bridge at a given damage level. These provisions should be revised and modified to establish a uniform seismic performance of bridges designed in different seismic hazard zone and seismic classification of soil.

The second objective of this dissertation (Chapter 3) was to asses the effects of changes in seismic design criteria on the transverse and vertical response of Chilean highway bridges. This assessment is accomplished by comparing fragility curves of a typical bridge designed using the Chilean standards before and after the 2010 Maule earthquake, considering the seismic soil types and the different seismic hazard zones. Chapter 3 first describes the evolution of bridge seismic design codes in Chile. Chapter 3 then summarizes the performance of bridges and their main failure modes during the 2010 Maule earthquake. After this, four structural configurations representative of typical bridge typologies are designed using different design criteria and then are modeled to evaluate their seismic behavior. Finally, fragility curves were generated using Incremental Dynamic Analysis (IDA), nonlinear analytical models and ground motion records from previous earthquakes. The analytical models considered external and internal shear keys. The external shear keys had a ductile behavior, while the internal shear keys had a fragile behavior, both behaviors were consistent with what was observed in the 2010 Maule earthquake.

The fragility curves obtained show that bridges designed with the current design codes have a seismic performance that depends, to a large extent, on the soil type in which the bridge is located. The probability of exceeding a given damage mode decreases as the soil becomes stiffer. The changes in the Bridge Design Manual implemented since 2010 result in a significant decrease of the probability of collapse due to transverse displacements. The vertical response of the bridges is largely unaffected by those design changes. The reduction of probability of collapse results from the addition of structural elements, such as end diaphragms and interior shear keys, as well as by the required increase in the resistance of the elements as compared to those existing in 2010. The effect of all the changes in design criteria in Chile after the 2010 earthquake is a statistically significant decrease in the probability of yielding of the exterior shear keys, and, consequently, a significant reduction in the probability of collapse of the bridges. The models show that the shear keys behave as sacrificial elements, preventing damage to the columns and cap beams. It is important to note that the changes in the design criteria of vertical bars produce negligible changes in the

probability of uplift of the deck. The probability of uplift of the deck is significantly larger in softer soils but the use of prestressed seismic bars considerably reduces this effect.

Finally, considering the seismic behavior of the different structural configurations for the bridges studied in this chapter, it can be inferred that an effective retrofit method to significantly decrease the vulnerability of bridges is to add interior shear keys between the girders of the existing bridge. Moreover, in areas of high seismic hazard, transverse diaphragms must be used between girders at their supports.

Finally, the third objective of this dissertation (Chapter 4) proposes a new self-centering shear key technique that eliminates residual displacements in the superstructure. The proposed shear key uses the bridge self-weight as a restoring force to ensure self-centering. Unlike conventional solutions that incorporate vibration reduction devices, this proposal takes advantage of the kinematics of the bridge. The proposed shear key was validated for a typical Chilean bridge using a set of records classified by type soil that considered horizontal and vertical input ground motion components. A variety of α angles were analyzed for the shear keys to investigate the transverse displacement of the superstructure and the seismic demand in the columns considering a set of records classified by type soil and magnitudes between Mw 7.0 and Mw 8.8. To validate the proposal of the central shear key, a time-history analysis was performed for all the records and for 10 ten values of the alpha angle.

The proposed self-centering shear keys makes it possible to eliminate 100% of the residual displacements of the superstructure of the type of bridge analyzed against ground movements caused by earthquakes, even those of great magnitude. However, the increase in seismic demand on the bridge columns due to the self-centering mechanism is directly proportional to the inclination angle α. Thus, the choice of the latter makes it possible to maintain said increase at levels that can be accommodated in the design.

The proposed solution is a simple change in the kinematics of the bridge, allowing self-centering and the dissipation of energy by friction. Thus, it does not incorporate new devices into the structure, such as seismic isolators or energy dissipators. Additionally, self-centering shear keys are a simple and economical solution, as they do not require the incorporation of new materials or skilled labor greater than normal for both the analysis and design and construction stages. Finally, the conventional bridge design philosophy utilizes shear keys as sacrificial elements, which requires expensive repairs after a large seismic event, while with the proposal of the self-centering shear key this repair is eliminated.

In summary, it is considered that different analytical models can capture the damage observed in the shear keys during the 2010 Maule earthquake. The different structural configurations are evaluated through time-history analysis considering different magnitudes of earthquakes, seismic hazard, and the seismic classification of soils. For the analytical models developed

in Chapters 2 and 3, it was assumed that shear keys function as sacrificial elements, that is, they fail before any other element of the bridge. For the proposed self-centering shear key model, this assumption is not considered as the shear keys are not damaged. Although the analytical models are very different and still sensitive to the modeling assumptions, the results consistently show that the ductile behavior of shear keys is characterized by a diagonal failure. Furthermore, analytical models were able to predict the expected lateral displacement demand on the bridge superstructure. However, with these analytical models, it is not possible to capture the rotation of the bridge superstructure.

5.1. Impact and contributions

The present research project is distinct in several ways. Some points that make this project unique include:

- The seismic performance of Chilean highway bridges is evaluated considering the influence of classification of the soil and seismic hazard. This has resulted in changes that account for these factors in the Bridge Design Manual.
- A database of records classified by soil type and seismic hazard is provided. This database can be used in the future to assess the performance of other bridge design provisions.
- The work indicates that the design forces for shear keys requires that the combination of soil classification and level of seismic hazard must be considered simultaneously to properly determine the demand.
- The work indicates that vertical seismic bars should be prestressed to 60% of the yield strength of the bar to reduce the probability of uplifting of the deck during large earthquakes. This is the first time that a limit of this type is proposed.
- The proposal of self-centering shear keys makes it possible to eliminate 100% of the residual displacements of the superstructure of the "type" bridge analyzed against ground movements caused by earthquakes, even of great magnitude.

The author expects that, based on the results presented in this research project, shear keys will be incorporated into the design of Chilean highway bridges, whether in the construction of new bridges or in retrofitting existing bridges.

5.2. Suggested topics for future research studies

The present research study intended to include many of the main parameters that influence the seismic behavior of bridges with shear keys, considering different seismic hazards and the seismic classification of the soil type, as well as to propose a new structural configuration of self-centering shear keys. However, there are still some uncertainties and unexplored issues that were not included and studied in this project. The following list summarizes some of the topics that may be explored in future research studies:

- Detailed numerical or experimental studies are needed to realistically simulate the response and damage of a bridge structure to given earthquake ground motions, considering different geometric configurations to those evaluated in this research.
- Experimentally evaluate and calibrate the proposed self-centering shear keys model. These studies should be accompanied by finite element models that reflect the experimental behavior.
- Experimental and analytical determination of the influence of pounding between the surfaces of shear key and superstructures.
- Evaluation of the influence of the skew and seat length in the abutments and bents in highway bridges with external and internal shear keys.
- Analysis of 3D models of straight and curved skewed bridges to evaluate the collapse of bridges due to the unseating of the superstructure.
- Experimental campaigns on the elements studied here (i.e., exterior and interior shear keys, diaphragms, and pre-stressed seismic bars) should be carried out in order to analyze their seismic response.

APPENDIX A

Records used in this investigation classified by soil type

Total vertical signals	169
Total horizontal signals	341
Total	510

Horizontal signs with soil classification NCh2369	117
Vertical signs with soil classification NCh2369	57
Total	174

Horizontal signs with soil classification D.S.61	91
Vertical signs with soil classification D.S.61	45
Total	136

	Soil						
	I	II	III	A	B	C	D
Hazard 1	-	-	-	-	-	-	-
Hazard 2	-	14	4	-	8	6	
Hazard 3	23	42	34	17	20	40	-
	Horizontal signs		117				91

	Soil						
	I	II	III	A	B	C	D
Hazard 1	-	-	-	-	-	-	-
Hazard 2	-	7	2	-	4	3	
Hazard 3	12	19	17	9	10	19	-
	Vertical signs		57				45

Earthquake	Year	M_w
Algarrobo	1985	8
Antofagasta	1995	8
Punitaqui	1997	7,1
South of Perú	2001	8,4
Tarapacá	2005	7,8
Tocopilla	2007	7,7
Maule	2010	8,8
Constitución	2012	7
Iquique	2014	7,7
Coquimbo	2015	8,3
Chiloé	2016	7,6

Code	Earthquake	Station	Locality	Direction	Soil 1	Soil 2	Earthquake Year	Magnitude (M_w)	Seismic Hazard Zone	V_{s30}	T_{nak}	Latitude	Longitude	Earthquake	Station	Locality
1	Algarrobo	Valparaíso Almendral	Valparaíso Almendral	H	C	II	1985	8,0	3	454		-33,030	-71,620	Algarrobo	Valparaíso Almendral	Valparaíso Almendral
2	Algarrobo	Valparaíso Almendral	Valparaíso Almendral	H	C	II	1985	8,0	3	454		-33,030	-71,620	Algarrobo	Valparaíso Almendral	Valparaíso Almendral
3	Algarrobo	Cauquenes	Cauquenes	H	C	III	1985	8,0	3	328	0,333	-35,967	-72,322	Algarrobo	Cauquenes	Cauquenes
4	Algarrobo	Cauquenes	Cauquenes	H	C	III	1985	8,0	3	328	0,333	-35,967	-72,322	Algarrobo	Cauquenes	Cauquenes
5	Algarrobo	Cauquenes	Cauquenes	V	C	III	1985	8,0	3	328	0,333	-35,967	-72,322	Algarrobo	Cauquenes	Cauquenes
6	Algarrobo	Chillan Viejo	Chillan Viejo	H		II	1985	8,0	3			-36,629	-72,139	Algarrobo	Chillan Viejo	Chillan Viejo
7	Algarrobo	Chillan Viejo	Chillan Viejo	H		II	1985	8,0	3			-36,629	-72,139	Algarrobo	Chillan Viejo	Chillan Viejo
8	Algarrobo	Chillan Viejo	Chillan Viejo	V		II	1985	8,0	3			-36,629	-72,139	Algarrobo	Chillan Viejo	Chillan Viejo
9	Algarrobo	Constitución	Constitución	H	C	III	1985	8,0	3	339	0,431	-35,340	-72,400	Algarrobo	Constitución	Constitución
10	Algarrobo	Constitución	Constitución	H	C	III	1985	8,0	3	339	0,431	-35,340	-72,400	Algarrobo	Constitución	Constitución
11	Algarrobo	Constitución	Constitución	V	C	III	1985	8,0	3	339	0,431	-35,340	-72,400	Algarrobo	Constitución	Constitución
12	Algarrobo	Hualañé	Hualañé	H	B	II	1985	8,0	3	541	0,408	-34,976	-71,806	Algarrobo	Hualañé	Hualañé
13	Algarrobo	Hualañé	Hualañé	H	B	II	1985	8,0	3	541	0,408	-34,976	-71,806	Algarrobo	Hualañé	Hualañé
14	Algarrobo	Hualañé	Hualañé	V	B	II	1985	8,0	3	541	0,408	-34,976	-71,806	Algarrobo	Hualañé	Hualañé
15	Algarrobo	Illapel	Illapel	H		II	1985	8,0	3			-31,630	-71,170	Algarrobo	Illapel	Illapel
16	Algarrobo	Illapel	Illapel	H		II	1985	8,0	3			-31,630	-71,170	Algarrobo	Illapel	Illapel
17	Algarrobo	Illapel	Illapel	V		II	1985	8,0	3			-31,630	-71,170	Algarrobo	Illapel	Illapel
18	Algarrobo	Iloca	Iloca	H		II	1985	8,0	3			-34,942	-72,184	Algarrobo	Iloca	Iloca
19	Algarrobo	Iloca	Iloca	H		II	1985	8,0	3			-34,942	-72,184	Algarrobo	Iloca	Iloca
20	Algarrobo	Iloca	Iloca	V		II	1985	8,0	3			-34,942	-72,184	Algarrobo	Iloca	Iloca
21	Algarrobo	La Ligua	La Ligua	H		II	1985	8,0	3			-32,449	-71,232	Algarrobo	La Ligua	La Ligua
22	Algarrobo	La Ligua	La Ligua	H		II	1985	8,0	3			-32,449	-71,232	Algarrobo	La Ligua	La Ligua
23	Algarrobo	Las Tórtolas	Las Tórtolas	H		II	1985	8,0	2			-33,131	-70,706	Algarrobo	Las Tórtolas	Las Tórtolas
24	Algarrobo	Las Tórtolas	Las Tórtolas	H		II	1985	8,0	2			-33,131	-70,706	Algarrobo	Las Tórtolas	Las Tórtolas
25	Algarrobo	Las Tórtolas	Las Tórtolas	V		II	1985	8,0	2			-33,131	-70,706	Algarrobo	Las Tórtolas	Las Tórtolas
26	Algarrobo	Llay-Llay	Llay-Llay	H		III	1985	8,0	3			-32,840	-70,956	Algarrobo	Llay-Llay	Llay-Llay
27	Algarrobo	Llay-Llay	Llay-Llay	H		III	1985	8,0	3			-32,840	-70,956	Algarrobo	Llay-Llay	Llay-Llay
28	Algarrobo	Llay-Llay	Llay-Llay	V		III	1985	8,0	3			-32,840	-70,956	Algarrobo	Llay-Llay	Llay-Llay
29	Algarrobo	Llolleo	Llolleo	H	C	III	1985	8,0	3	360		-33,616	-71,615	Algarrobo	Llolleo	Llolleo
30	Algarrobo	Llolleo	Llolleo	H	C	III	1985	8,0	3	360		-33,616	-71,615	Algarrobo	Llolleo	Llolleo
31	Algarrobo	Llolleo	Llolleo	V	C	III	1985	8,0	3	360		-33,616	-71,615	Algarrobo	Llolleo	Llolleo
32	Algarrobo	Los Vilos	Los Vilos	H	B	II	1985	8,0	3	592	0,250	-31,912	-71,511	Algarrobo	Los Vilos	Los Vilos
33	Algarrobo	Los Vilos	Los Vilos	H	B	II	1985	8,0	3	592	0,250	-31,912	-71,511	Algarrobo	Los Vilos	Los Vilos
34	Algarrobo	Los Vilos	Los Vilos	V	B	II	1985	8,0	3	592	0,250	-31,912	-71,511	Algarrobo	Los Vilos	Los Vilos
35	Algarrobo	Melipilla	Melipilla	H	B	II	1985	8,0	3	700	0,441	-33,686	-71,216	Algarrobo	Melipilla	Melipilla
36	Algarrobo	Melipilla	Melipilla	H	B	II	1985	8,0	3	700	0,441	-33,686	-71,216	Algarrobo	Melipilla	Melipilla
37	Algarrobo	Melipilla	Melipilla	V	B	II	1985	8,0	3	700	0,441	-33,686	-71,216	Algarrobo	Melipilla	Melipilla
38	Algarrobo	Papudo	Papudo	H	A	I	1985	8,0	3	982	0,126	-32,520	-71,450	Algarrobo	Papudo	Papudo
39	Algarrobo	Papudo	Papudo	V	A	I	1985	8,0	3	982	0,126	-32,520	-71,450	Algarrobo	Papudo	Papudo

40	Algarrobo	Pichilemu	Pichilemu	H	A	I	1985	8,0	3	1242	0,146	-34,386	-72,004	Algarrobo	Pichilemu	Pichilemu
41	Algarrobo	Pichilemu	Pichilemu	H	A	I	1985	8,0	3	1242	0,146	-34,386	-72,004	Algarrobo	Pichilemu	Pichilemu
42	Algarrobo	Pichilemu	Pichilemu	V	A	I	1985	8,0	3	1242	0,146	-34,386	-72,004	Algarrobo	Pichilemu	Pichilemu
43	Algarrobo	Quintay	Quintay	H		I	1985	8,0	3			-33,193	-71,697	Algarrobo	Quintay	Quintay
44	Algarrobo	Quintay	Quintay	H		I	1985	8,0	3			-33,193	-71,697	Algarrobo	Quintay	Quintay
45	Algarrobo	Quintay	Quintay	V		I	1985	8,0	3			-33,193	-71,697	Algarrobo	Quintay	Quintay
46	Algarrobo	Rapel	Rapel	H		I	1985	8,0	3			-33,942	-71,736	Algarrobo	Rapel	Rapel
47	Algarrobo	Rapel	Rapel	H		I	1985	8,0	3			-33,942	-71,736	Algarrobo	Rapel	Rapel
48	Algarrobo	Rapel	Rapel	V		I	1985	8,0	3			-33,942	-71,736	Algarrobo	Rapel	Rapel
49	Algarrobo	San Felipe	San Felipe	H		II	1985	8,0	3			-32,750	-70,721	Algarrobo	San Felipe	San Felipe
50	Algarrobo	San Felipe	San Felipe	H		II	1985	8,0	3			-32,750	-70,721	Algarrobo	San Felipe	San Felipe
51	Algarrobo	San Felipe	San Felipe	V		II	1985	8,0	3			-32,750	-70,721	Algarrobo	San Felipe	San Felipe
52	Algarrobo	San Fernando	San Fernando	H		II	1985	8,0	2			-34,586	-70,991	Algarrobo	San Fernando	San Fernando
53	Algarrobo	San Fernando	San Fernando	H		II	1985	8,0	2			-34,586	-70,991	Algarrobo	San Fernando	San Fernando
54	Algarrobo	San Fernando	San Fernando	V		II	1985	8,0	2			-34,586	-70,991	Algarrobo	San Fernando	San Fernando
55	Algarrobo	Talca	Talca	H	B	II	1985	8,0	3	648		-35,430	-71,630	Algarrobo	Talca	Talca
56	Algarrobo	Talca	Talca	H	B	II	1985	8,0	3	648		-35,430	-71,630	Algarrobo	Talca	Talca
57	Algarrobo	Talca	Talca	V	B	II	1985	8,0	3	648		-35,430	-71,630	Algarrobo	Talca	Talca
58	Algarrobo	Valparaíso (U.T.F.S.M.)	Valparaíso (U.T.F.S.M.)	H	A	I	1985	8,0	3	926		-33,030	-71,620	Algarrobo	Valparaíso (U.T.F.S.M.)	Valparaíso (U.T.F.S.M.)
59	Algarrobo	Valparaíso (U.T.F.S.M.)	Valparaíso (U.T.F.S.M.)	H	A	I	1985	8,0	3	926		-33,030	-71,620	Algarrobo	Valparaíso (U.T.F.S.M.)	Valparaíso (U.T.F.S.M.)
60	Algarrobo	Valparaíso (U.T.F.S.M.)	Valparaíso (U.T.F.S.M.)	V	A	I	1985	8,0	3	926		-33,030	-71,620	Algarrobo	Valparaíso (U.T.F.S.M.)	Valparaíso (U.T.F.S.M.)
61	Algarrobo	Ventanas	Ventanas	H		III	1985	8,0	3			-32,743	-71,489	Algarrobo	Ventanas	Ventanas
62	Algarrobo	Ventanas	Ventanas	H		III	1985	8,0	3			-32,743	-71,489	Algarrobo	Ventanas	Ventanas
63	Algarrobo	Ventanas	Ventanas	V		III	1985	8,0	3			-32,743	-71,489	Algarrobo	Ventanas	Ventanas
64	Algarrobo	Viña del Mar Centro	Viña del Mar Centro	H	C	III	1985	8,0	3	289		-33,025	-71,553	Algarrobo	Viña del Mar Centro	Viña del Mar Centro
65	Algarrobo	Viña del Mar Centro	Viña del Mar Centro	H	C	III	1985	8,0	3	289		-33,025	-71,553	Algarrobo	Viña del Mar Centro	Viña del Mar Centro
66	Algarrobo	Viña del Mar Centro	Viña del Mar Centro	V	C	III	1985	8,0	3	289		-33,025	-71,553	Algarrobo	Viña del Mar Centro	Viña del Mar Centro
67	Algarrobo	Zapallar	Zapallar	H		I	1985	8,0	3			-32,554	-71,458	Algarrobo	Zapallar	Zapallar
68	Algarrobo	Zapallar	Zapallar	H		I	1985	8,0	3			-32,554	-71,458	Algarrobo	Zapallar	Zapallar
69	Algarrobo	Zapallar	Zapallar	V		I	1985	8,0	3			-32,554	-71,458	Algarrobo	Zapallar	Zapallar
70	Antofagasta	Tocopilla	Tocopilla	H			1995	8,0	3			-22,090	-70,201	Antofagasta	Tocopilla	Tocopilla
71	Antofagasta	Tocopilla	Tocopilla	H			1995	8,0	3			-22,090	-70,201	Antofagasta	Tocopilla	Tocopilla
72	Antofagasta	Tocopilla	Tocopilla	V			1995	8,0	3			-22,090	-70,201	Antofagasta	Tocopilla	Tocopilla
73	Punitaqui	Illapel	Illapel	H		II	1997	7,1	3			-31,630	-71,170	Punitaqui	Illapel	Illapel
74	Punitaqui	Illapel	Illapel	H		II	1997	7,1	3			-31,630	-71,170	Punitaqui	Illapel	Illapel
75	Punitaqui	Illapel	Illapel	V		II	1997	7,1	3			-31,630	-71,170	Punitaqui	Illapel	Illapel
76	Punitaqui	Papudo	Papudo	H	A	I	1997	7,1	3	982	0,126	-32,520	-71,450	Punitaqui	Papudo	Papudo
77	Punitaqui	Papudo	Papudo	H	A	I	1997	7,1	3	982	0,126	-32,520	-71,450	Punitaqui	Papudo	Papudo
78	Punitaqui	Papudo	Papudo	V	A	I	1997	7,1	3	982	0,126	-32,520	-71,450	Punitaqui	Papudo	Papudo

79	Punitaqui	Santiago Centro	Santiago Centro	H			1997	7,1	2			-33,620	-71,600	Punitaqui	Santiago Centro	Santiago Centro
80	Punitaqui	Santiago Centro	Santiago Centro	H			1997	7,1	2			-33,620	-71,600	Punitaqui	Santiago Centro	Santiago Centro
81	Punitaqui	Santiago Centro	Santiago Centro	V			1997	7,1	2			-33,620	-71,600	Punitaqui	Santiago Centro	Santiago Centro
82	South of Perú	Arica	Arica	H			2001	8,4	3			-18,482	-70,313	South of Perú	Arica	Arica
83	South of Perú	Arica	Arica	H			2001	8,4	3			-18,482	-70,313	South of Perú	Arica	Arica
84	South of Perú	Arica	Arica	V			2001	8,4	3			-18,482	-70,313	South of Perú	Arica	Arica
85	South of Perú	Arica Cementerio	Arica Cementerio	H			2001	8,4	3			-18,479	-70,308	South of Perú	Arica Cementerio	Arica Cementerio
86	South of Perú	Arica Cementerio	Arica Cementerio	H			2001	8,4	3			-18,479	-70,308	South of Perú	Arica Cementerio	Arica Cementerio
87	South of Perú	Arica Cementerio	Arica Cementerio	V			2001	8,4	3			-18,479	-70,308	South of Perú	Arica Cementerio	Arica Cementerio
88	South of Perú	Arica Costanera	Arica Costanera	H			2001	8,4	3			-18,471	-70,313	South of Perú	Arica Costanera	Arica Costanera
89	South of Perú	Arica Costanera	Arica Costanera	H			2001	8,4	3			-18,471	-70,313	South of Perú	Arica Costanera	Arica Costanera
90	South of Perú	Arica Costanera	Arica Costanera	V			2001	8,4	3			-18,471	-70,313	South of Perú	Arica Costanera	Arica Costanera
91	South of Perú	Cuya	Cuya	H			2001	8,4	3			-19,160	-70,180	South of Perú	Cuya	Cuya
92	South of Perú	Cuya	Cuya	H			2001	8,4	3			-19,160	-70,180	South of Perú	Cuya	Cuya
93	South of Perú	Cuya	Cuya	V			2001	8,4	3			-19,160	-70,180	South of Perú	Cuya	Cuya
94	South of Perú	Pisagua	Pisagua	H			2001	8,4	3			-19,595	-70,211	South of Perú	Pisagua	Pisagua
95	South of Perú	Pisagua	Pisagua	H			2001	8,4	3			-19,595	-70,211	South of Perú	Pisagua	Pisagua
96	South of Perú	Pisagua	Pisagua	V			2001	8,4	3			-19,595	-70,211	South of Perú	Pisagua	Pisagua
97	South of Perú	Poconchile	Poconchile	H			2001	8,4	3			-18,453	-70,067	South of Perú	Poconchile	Poconchile
98	South of Perú	Poconchile	Poconchile	H			2001	8,4	3			-18,453	-70,067	South of Perú	Poconchile	Poconchile
99	South of Perú	Poconchile	Poconchile	V			2001	8,4	3			-18,453	-70,067	South of Perú	Poconchile	Poconchile
100	South of Perú	Putre	Putre	H			2001	8,4	2			-18,195	-69,559	South of Perú	Putre	Putre
101	South of Perú	Putre	Putre	H			2001	8,4	2			-18,195	-69,559	South of Perú	Putre	Putre
102	South of Perú	Putre	Putre	V			2001	8,4	2			-18,195	-69,559	South of Perú	Putre	Putre
103	Tarapacá	Arica	Arica	H			2005	7,8	3			-18,479	-70,308	Tarapacá	Arica Cementerio	Arica Cementerio

		Cementerio	Cementerio													
104	Tarapacá	Arica Cementerio	Arica Cementerio	H			2005	7,8	3			-18,479	-70,308	Tarapacá	Arica Cementerio	Arica Cementerio
105	Tarapacá	Arica Cementerio	Arica Cementerio	V			2005	7,8	3			-18,479	-70,308	Tarapacá	Arica Cementerio	Arica Cementerio
106	Tarapacá	Arica Cerro La Cruz	Arica Cerro La Cruz	H			2005	7,8	3			-18,491	-70,311	Tarapacá	Arica Cerro La Cruz	Arica Cerro La Cruz
107	Tarapacá	Arica Cerro La Cruz	Arica Cerro La Cruz	H			2005	7,8	3			-18,491	-70,311	Tarapacá	Arica Cerro La Cruz	Arica Cerro La Cruz
108	Tarapacá	Arica Cerro La Cruz	Arica Cerro La Cruz	V			2005	7,8	3			-18,491	-70,311	Tarapacá	Arica Cerro La Cruz	Arica Cerro La Cruz
109	Tarapacá	Arica Costanera	Arica Costanera	H			2005	7,8	3			-18,471	-70,313	Tarapacá	Arica Costanera	Arica Costanera
110	Tarapacá	Arica Costanera	Arica Costanera	H			2005	7,8	3			-18,471	-70,313	Tarapacá	Arica Costanera	Arica Costanera
111	Tarapacá	Arica Costanera	Arica Costanera	V			2005	7,8	3			-18,471	-70,313	Tarapacá	Arica Costanera	Arica Costanera
112	Tarapacá	Calama	Calama	H			2005	7,8	2			-22,459	-68,930	Tarapacá	Calama	Calama
113	Tarapacá	Calama	Calama	H			2005	7,8	2			-22,459	-68,930	Tarapacá	Calama	Calama
114	Tarapacá	Calama	Calama	V			2005	7,8	2			-22,459	-68,930	Tarapacá	Calama	Calama
115	Tarapacá	Cuya	Cuya	H			2005	7,8	3			-19,160	-70,180	Tarapacá	Cuya	Cuya
116	Tarapacá	Cuya	Cuya	H			2005	7,8	3			-19,160	-70,180	Tarapacá	Cuya	Cuya
117	Tarapacá	Cuya	Cuya	V			2005	7,8	3			-19,160	-70,180	Tarapacá	Cuya	Cuya
118	Tarapacá	El Loa	El Loa	H			2005	7,8	2			-21,425	-70,057	Tarapacá	El Loa	El Loa
119	Tarapacá	El Loa	El Loa	H			2005	7,8	2			-21,425	-70,057	Tarapacá	El Loa	El Loa
120	Tarapacá	El Loa	El Loa	V			2005	7,8	2			-21,425	-70,057	Tarapacá	El Loa	El Loa
121	Tarapacá	Iquique	Iquique	H			2005	7,8	3			-20,214	-70,138	Tarapacá	Iquique	Iquique
122	Tarapacá	Iquique	Iquique	H			2005	7,8	3			-20,214	-70,138	Tarapacá	Iquique	Iquique
123	Tarapacá	Iquique	Iquique	V			2005	7,8	3			-20,214	-70,138	Tarapacá	Iquique	Iquique
124	Tarapacá	Iquique IDIEM	Iquique IDIEM	H			2005	7,8	3			-20,220	-70,142	Tarapacá	Iquique IDIEM	Iquique IDIEM
125	Tarapacá	Iquique IDIEM	Iquique IDIEM	H			2005	7,8	3			-20,220	-70,142	Tarapacá	Iquique IDIEM	Iquique IDIEM
126	Tarapacá	Iquique IDIEM	Iquique IDIEM	V			2005	7,8	3			-20,220	-70,142	Tarapacá	Iquique IDIEM	Iquique IDIEM
127	Tarapacá	Iquique Plaza	Iquique Plaza	H			2005	7,8	3			-20,213	-70,149	Tarapacá	Iquique Plaza	Iquique Plaza
128	Tarapacá	Iquique Plaza	Iquique Plaza	H			2005	7,8	3			-20,213	-70,149	Tarapacá	Iquique Plaza	Iquique Plaza
129	Tarapacá	Iquique Plaza	Iquique Plaza	V			2005	7,8	3			-20,213	-70,149	Tarapacá	Iquique Plaza	Iquique Plaza
130	Tarapacá	Mejillones	Mejillones	H			2005	7,8	3			-23,100	-70,450	Tarapacá	Mejillones	Mejillones
131	Tarapacá	Mejillones	Mejillones	H			2005	7,8	3			-23,100	-70,450	Tarapacá	Mejillones	Mejillones
132	Tarapacá	Mejillones	Mejillones	V			2005	7,8	3			-23,100	-70,450	Tarapacá	Mejillones	Mejillones
133	Tarapacá	Pica	Pica	H			2005	7,8	2			-20,492	-69,330	Tarapacá	Pica	Pica
134	Tarapacá	Pica	Pica	H			2005	7,8	2			-20,492	-69,330	Tarapacá	Pica	Pica
135	Tarapacá	Pica	Pica	V			2005	7,8	2			-20,492	-69,330	Tarapacá	Pica	Pica
136	Tarapacá	Pisagua	Pisagua	H			2005	7,8	3			-19,595	-70,211	Tarapacá	Pisagua	Pisagua
137	Tarapacá	Pisagua	Pisagua	H			2005	7,8	3			-19,595	-70,211	Tarapacá	Pisagua	Pisagua

138	Tarapacá	Pisagua	Pisagua	V			2005	7,8	3			-19,595	-70,211	Tarapacá	Pisagua	Pisagua
139	Tarapacá	Poconchile	Poconchile	H			2005	7,8	3			-18,453	-70,067	Tarapacá	Poconchile	Poconchile
140	Tarapacá	Poconchile	Poconchile	H			2005	7,8	3			-18,453	-70,067	Tarapacá	Poconchile	Poconchile
141	Tarapacá	Poconchile	Poconchile	V			2005	7,8	3			-18,453	-70,067	Tarapacá	Poconchile	Poconchile
142	Tarapacá	Putre	Putre	H			2005	7,8	2			-18,195	-69,559	Tarapacá	Putre	Putre
143	Tarapacá	Putre	Putre	H			2005	7,8	2			-18,195	-69,559	Tarapacá	Putre	Putre
144	Tarapacá	Putre	Putre	V			2005	7,8	2			-18,195	-69,559	Tarapacá	Putre	Putre
145	Tocopilla	Alto Hospicio	Alto Hospicio	H			2007	7,7	3			-20,265	-70,101	Tocopilla	Alto Hospicio	Alto Hospicio
146	Tocopilla	Alto Hospicio	Alto Hospicio	H			2007	7,7	3			-20,265	-70,101	Tocopilla	Alto Hospicio	Alto Hospicio
147	Tocopilla	Alto Hospicio	Alto Hospicio	V			2007	7,7	3			-20,265	-70,101	Tocopilla	Alto Hospicio	Alto Hospicio
148	Tocopilla	Antofagasta UCN	Antofagasta UCN	H			2007	7,7	3			-23,681	-70,411	Tocopilla	Antofagasta UCN	Antofagasta UCN
149	Tocopilla	Antofagasta UCN	Antofagasta UCN	H			2007	7,7	3			-23,681	-70,411	Tocopilla	Antofagasta UCN	Antofagasta UCN
150	Tocopilla	Antofagasta UCN	Antofagasta UCN	V			2007	7,7	3			-23,681	-70,411	Tocopilla	Antofagasta UCN	Antofagasta UCN
151	Tocopilla	Calama	Calama	H			2007	7,7	2			-22,459	-68,930	Tocopilla	Calama	Calama
152	Tocopilla	Calama	Calama	H			2007	7,7	2			-22,459	-68,930	Tocopilla	Calama	Calama
153	Tocopilla	Calama	Calama	V			2007	7,7	2			-22,459	-68,930	Tocopilla	Calama	Calama
154	Tocopilla	Copiapó	Copiapó	H	C	III	2007	7,7	3	349		-27,374	-70,322	Tocopilla	Copiapó	Copiapó
155	Tocopilla	Copiapó	Copiapó	H	C	III	2007	7,7	3	349		-27,374	-70,322	Tocopilla	Copiapó	Copiapó
156	Tocopilla	Copiapó	Copiapó	V	C	III	2007	7,7	3	349		-27,374	-70,322	Tocopilla	Copiapó	Copiapó
157	Tocopilla	El Loa	El Loa	H			2007	7,7	2			-21,425	-70,057	Tocopilla	El Loa	El Loa
158	Tocopilla	El Loa	El Loa	H			2007	7,7	2			-21,425	-70,057	Tocopilla	El Loa	El Loa
159	Tocopilla	El Loa	El Loa	V			2007	7,7	2			-21,425	-70,057	Tocopilla	El Loa	El Loa
160	Tocopilla	Fuerte Baquedano	Fuerte Baquedano	H			2007	7,7	1			-19,996	-69,767	Tocopilla	Fuerte Baquedano	Fuerte Baquedano
161	Tocopilla	Fuerte Baquedano	Fuerte Baquedano	H			2007	7,7	1			-19,996	-69,767	Tocopilla	Fuerte Baquedano	Fuerte Baquedano
162	Tocopilla	Fuerte Baquedano	Fuerte Baquedano	V			2007	7,7	1			-19,996	-69,767	Tocopilla	Fuerte Baquedano	Fuerte Baquedano
163	Tocopilla	Iquique	Iquique	H			2007	7,7	3			-20,214	-70,138	Tocopilla	Iquique	Iquique
164	Tocopilla	Iquique	Iquique	H			2007	7,7	3			-20,214	-70,138	Tocopilla	Iquique	Iquique
165	Tocopilla	Iquique	Iquique	V			2007	7,7	3			-20,214	-70,138	Tocopilla	Iquique	Iquique
166	Tocopilla	Iquique Esc Chapana	Iquique Esc Chapana	H			2007	7,7	2			-20,252	-70,126	Tocopilla	Iquique Esc Chapana	Iquique Esc Chapana
167	Tocopilla	Iquique Esc Chapana	Iquique Esc Chapana	H			2007	7,7	2			-20,252	-70,126	Tocopilla	Iquique Esc Chapana	Iquique Esc Chapana
168	Tocopilla	Iquique Esc Chapana	Iquique Esc Chapana	V			2007	7,7	2			-20,252	-70,126	Tocopilla	Iquique Esc Chapana	Iquique Esc Chapana
169	Tocopilla	Mejillones	Mejillones	H			2007	7,7	3			-23,100	-70,450	Tocopilla	Mejillones	Mejillones
170	Tocopilla	Mejillones	Mejillones	H			2007	7,7	3			-23,100	-70,450	Tocopilla	Mejillones	Mejillones
171	Tocopilla	Mejillones	Mejillones	V			2007	7,7	3			-23,100	-70,450	Tocopilla	Mejillones	Mejillones
172	Tocopilla	Puerto Patache	Puerto Patache	H			2007	7,7	3			-20,810	-70,200	Tocopilla	Puerto Patache	Puerto Patache
173	Tocopilla	Puerto	Puerto	H			2007	7,7	3			-20,810	-70,200	Tocopilla	Puerto Patache	Puerto Patache

		Patache	Patache													
174	Tocopilla	Puerto Patache	Puerto Patache	V			2007	7,7	3			-20,810	-70,200	Tocopilla	Puerto Patache	Puerto Patache
175	Tocopilla	Pica	Pica	H			2007	7,7	2			-20,492	-69,330	Tocopilla	Pica	Pica
176	Tocopilla	Pica	Pica	H			2007	7,7	2			-20,492	-69,330	Tocopilla	Pica	Pica
177	Tocopilla	Pica	Pica	V			2007	7,7	2			-20,492	-69,330	Tocopilla	Pica	Pica
178	Tocopilla	Pisagua	Pisagua	H			2007	7,7	3			-19,595	-70,211	Tocopilla	Pisagua	Pisagua
179	Tocopilla	Pisagua	Pisagua	H			2007	7,7	3			-19,595	-70,211	Tocopilla	Pisagua	Pisagua
180	Tocopilla	Pisagua	Pisagua	V			2007	7,7	3			-19,595	-70,211	Tocopilla	Pisagua	Pisagua
181	Tocopilla	Poconchile	Poconchile	H			2007	7,7	3			-18,453	-70,067	Tocopilla	Poconchile	Poconchile
182	Tocopilla	Poconchile	Poconchile	H			2007	7,7	3			-18,453	-70,067	Tocopilla	Poconchile	Poconchile
183	Tocopilla	Poconchile	Poconchile	V			2007	7,7	3			-18,453	-70,067	Tocopilla	Poconchile	Poconchile
184	Tocopilla	San Pedro de Atacama	San Pedro de Atacama	H			2007	7,7	1			-22,911	-68,200	Tocopilla	San Pedro de Atacama	San Pedro de Atacama
185	Tocopilla	San Pedro de Atacama	San Pedro de Atacama	H			2007	7,7	1			-22,911	-68,200	Tocopilla	San Pedro de Atacama	San Pedro de Atacama
186	Tocopilla	San Pedro de Atacama	San Pedro de Atacama	V			2007	7,7	1			-22,911	-68,200	Tocopilla	San Pedro de Atacama	San Pedro de Atacama
187	Tocopilla	Tocopilla	Tocopilla	H			2007	7,7	3			-22,090	-70,201	Tocopilla	Tocopilla	Tocopilla
188	Tocopilla	Tocopilla	Tocopilla	H			2007	7,7	3			-22,090	-70,201	Tocopilla	Tocopilla	Tocopilla
189	Tocopilla	Tocopilla	Tocopilla	V			2007	7,7	3			-22,090	-70,201	Tocopilla	Tocopilla	Tocopilla
190	Tocopilla	Puerto de Tocopilla	Puerto de Tocopilla	H			2007	7,7	3			-22,094	-70,209	Tocopilla	Puerto de Tocopilla	Puerto de Tocopilla
191	Tocopilla	Puerto de Tocopilla	Puerto de Tocopilla	H			2007	7,7	3			-22,094	-70,209	Tocopilla	Puerto de Tocopilla	Puerto de Tocopilla
192	Tocopilla	Puerto de Tocopilla	Puerto de Tocopilla	V			2007	7,7	3			-22,094	-70,209	Tocopilla	Puerto de Tocopilla	Puerto de Tocopilla
193	Maule	Angol	Angol	H	C	III	2010	8,8	3	353	0,182	-37,790	-72,710	Maule	Angol	Angol
194	Maule	Angol	Angol	H	C	III	2010	8,8	3	353	0,182	-37,790	-72,710	Maule	Angol	Angol
195	Maule	Angol	Angol	V	C	III	2010	8,8	3	353	0,182	-37,790	-72,710	Maule	Angol	Angol
196	Maule	Concepción	Concepción	H	C	II	2010	8,8	3	423	1,316	-36,828	-73,048	Maule	Concepción	Concepción
197	Maule	Concepción	Concepción	H	C	II	2010	8,8	3	423	1,316	-36,828	-73,048	Maule	Concepción	Concepción
198	Maule	Concepción	Concepción	V	C	II	2010	8,8	3	423	1,316	-36,828	-73,048	Maule	Concepción	Concepción
199	Maule	Constitución	Constitución	H	C	III	2010	8,8	3	339	0,431	-35,340	-72,400	Maule	Constitución	Constitución
200	Maule	Constitución	Constitución	H	C	III	2010	8,8	3	339	0,431	-35,340	-72,400	Maule	Constitución	Constitución
201	Maule	Constitución	Constitución	V	C	III	2010	8,8	3	339	0,431	-35,340	-72,400	Maule	Constitución	Constitución
202	Maule	Copiapó	Copiapó	H	C	III	2010	8,8	3	349		-27,374	-70,322	Maule	Copiapó	Copiapó
203	Maule	Copiapó	Copiapó	H	C	III	2010	8,8	3	349		-27,374	-70,322	Maule	Copiapó	Copiapó
204	Maule	Copiapó	Copiapó	V	C	III	2010	8,8	3	349		-27,374	-70,322	Maule	Copiapó	Copiapó
205	Maule	Curicó	Curicó	H	B	II	2010	8,8	2	561		-34,991	-71,237	Maule	Curicó	Curicó
206	Maule	Curicó	Curicó	H	B	II	2010	8,8	2	561		-34,991	-71,237	Maule	Curicó	Curicó
207	Maule	Curicó	Curicó	V	B	II	2010	8,8	2	561		-34,991	-71,237	Maule	Curicó	Curicó
208	Maule	Hualañé	Hualañé	H	B	II	2010	8,8	3	541	0,408	-34,976	-71,806	Maule	Hualañé	Hualañé
209	Maule	Hualañé	Hualañé	H	B	II	2010	8,8	3	541	0,408	-34,976	-71,806	Maule	Hualañé	Hualañé
210	Maule	Hualañé	Hualañé	V	B	II	2010	8,8	3	541	0,408	-34,976	-71,806	Maule	Hualañé	Hualañé

211	Maule	Llolleo	Llolleo	H	C	III	2010	8,8	3	360		-33,616	-71,615	Maule	Llolleo	Llolleo
212	Maule	Llolleo	Llolleo	H	C	III	2010	8,8	3	360		-33,616	-71,615	Maule	Llolleo	Llolleo
213	Maule	Llolleo	Llolleo	V	C	III	2010	8,8	3	360		-33,616	-71,615	Maule	Llolleo	Llolleo
214	Maule	Matanzas	Matanzas	H	C	III	2010	8,8	3	370	0,290	-33,964	-71,876	Maule	Matanzas	Matanzas
215	Maule	Matanzas	Matanzas	H	C	III	2010	8,8	3	370	0,290	-33,964	-71,876	Maule	Matanzas	Matanzas
216	Maule	Matanzas	Matanzas	V	C	III	2010	8,8	3	370	0,290	-33,964	-71,876	Maule	Matanzas	Matanzas
217	Maule	Papudo	Papudo	H	A	I	2010	8,8	3	982	0,126	-32,520	-71,450	Maule	Papudo	Papudo
218	Maule	Papudo	Papudo	H	A	I	2010	8,8	3	982	0,126	-32,520	-71,450	Maule	Papudo	Papudo
219	Maule	Papudo	Papudo	V	A	I	2010	8,8	3	982	0,126	-32,520	-71,450	Maule	Papudo	Papudo
220	Maule	Santiago Centro	Santiago Centro	H			2010	8,8	2			-33,620	-71,600	Maule	Santiago Centro	Santiago Centro
221	Maule	Santiago Centro	Santiago Centro	H			2010	8,8	2			-33,620	-71,600	Maule	Santiago Centro	Santiago Centro
222	Maule	Santiago Centro	Santiago Centro	V			2010	8,8	2			-33,620	-71,600	Maule	Santiago Centro	Santiago Centro
223	Maule	Santiago La Florida	Santiago La Florida	H	B	II	2010	8,8	2	598		-33,514	-70,605	Maule	Santiago La Florida	Santiago La Florida
224	Maule	Santiago La Florida	Santiago La Florida	H	B	II	2010	8,8	2	598		-33,514	-70,605	Maule	Santiago La Florida	Santiago La Florida
225	Maule	Santiago La Florida	Santiago La Florida	V	B	II	2010	8,8	2	598		-33,514	-70,605	Maule	Santiago La Florida	Santiago La Florida
226	Maule	Santiago Maipú	Santiago Maipú	H	C	II	2010	8,8	2	430	0,336	-33,509	-70,771	Maule	Santiago Maipú	Santiago Maipú
227	Maule	Santiago Maipú	Santiago Maipú	H	C	II	2010	8,8	2	430	0,336	-33,509	-70,771	Maule	Santiago Maipú	Santiago Maipú
228	Maule	Santiago Maipú	Santiago Maipú	V	C	II	2010	8,8	2	430	0,336	-33,509	-70,771	Maule	Santiago Maipú	Santiago Maipú
229	Maule	Santiago Peñalolén	Santiago Peñalolén	H	C	III	2010	8,8	2	373		-33,501	-70,579	Maule	Santiago Peñalolén	Santiago Peñalolén
230	Maule	Santiago Peñalolén	Santiago Peñalolén	H	C	III	2010	8,8	2	373		-33,501	-70,579	Maule	Santiago Peñalolén	Santiago Peñalolén
231	Maule	Santiago Peñalolén	Santiago Peñalolén	V	C	III	2010	8,8	2	373		-33,501	-70,579	Maule	Santiago Peñalolén	Santiago Peñalolén
232	Maule	Santiago Puente Alto	Santiago Puente Alto	H			2010	8,8	2			-33,578	-70,581	Maule	Santiago Puente Alto	Santiago Puente Alto
233	Maule	Santiago Puente Alto	Santiago Puente Alto	H			2010	8,8	2			-33,578	-70,581	Maule	Santiago Puente Alto	Santiago Puente Alto
234	Maule	Santiago Puente Alto	Santiago Puente Alto	V			2010	8,8	2			-33,578	-70,581	Maule	Santiago Puente Alto	Santiago Puente Alto
235	Maule	Talca	Talca	H	B	II	2010	8,8	3	648		-35,430	-71,630	Maule	Talca	Talca
236	Maule	Talca	Talca	H	B	II	2010	8,8	3	648		-35,430	-71,630	Maule	Talca	Talca
237	Maule	Talca	Talca	V	B	II	2010	8,8	3	648		-35,430	-71,630	Maule	Talca	Talca
238	Maule	Valdivia	Valdivia	H	C	II	2010	8,8	3	454	1,250	-39,831	-73,239	Maule	Valdivia	Valdivia
239	Maule	Valdivia	Valdivia	H	C	II	2010	8,8	3	454	1,250	-39,831	-73,239	Maule	Valdivia	Valdivia
240	Maule	Valdivia	Valdivia	V	C	II	2010	8,8	3	454	1,250	-39,831	-73,239	Maule	Valdivia	Valdivia
241	Maule	Vallenar	Vallenar	H	B	II	2010	8,8	3	561		-28,577	-70,755	Maule	Vallenar	Vallenar
242	Maule	Vallenar	Vallenar	H	B	II	2010	8,8	3	561		-28,577	-70,755	Maule	Vallenar	Vallenar

243	Maule	Vallenar	Vallenar	V	B	II	2010	8,8	3	561		-28,577	-70,755	Maule	Vallenar	Vallenar
244	Maule	Valparaíso Almendral	Valparaíso Almendral	H	C	II	2010	8,8	3	454		-33,030	-71,620	Maule	Valparaíso Almendral	Valparaíso Almendral
245	Maule	Valparaíso Almendral	Valparaíso Almendral	H	C	II	2010	8,8	3	454		-33,030	-71,620	Maule	Valparaíso Almendral	Valparaíso Almendral
246	Maule	Valparaíso Almendral	Valparaíso Almendral	V	C	II	2010	8,8	3	454		-33,030	-71,620	Maule	Valparaíso Almendral	Valparaíso Almendral
247	Maule	Valparaíso (U.T.F.S.M.)	Valparaíso (U.T.F.S.M.)	H	A	I	2010	8,8	3	926		-33,030	-71,620	Maule	Valparaíso (U.T.F.S.M.)	Valparaíso (U.T.F.S.M.)
248	Maule	Valparaíso (U.T.F.S.M.)	Valparaíso (U.T.F.S.M.)	H	A	I	2010	8,8	3	926		-33,030	-71,620	Maule	Valparaíso (U.T.F.S.M.)	Valparaíso (U.T.F.S.M.)
249	Maule	Valparaíso (U.T.F.S.M.)	Valparaíso (U.T.F.S.M.)	V	A	I	2010	8,8	3	926		-33,030	-71,620	Maule	Valparaíso (U.T.F.S.M.)	Valparaíso (U.T.F.S.M.)
250	Maule	Viña del Mar Centro	Viña del Mar Centro	H	C	III	2010	8,8	3	289		-33,025	-71,553	Maule	Viña del Mar Centro	Viña del Mar Centro
251	Maule	Viña del Mar Centro	Viña del Mar Centro	H	C	III	2010	8,8	3	289		-33,025	-71,553	Maule	Viña del Mar Centro	Viña del Mar Centro
252	Maule	Viña del Mar Centro	Viña del Mar Centro	V	C	III	2010	8,8	3	289		-33,025	-71,553	Maule	Viña del Mar Centro	Viña del Mar Centro
253	Maule	Viña del Mar El Salto	Viña del Mar El Salto	H	C	III	2010	8,8	3	260	0,775	-33,047	-71,510	Maule	Viña del Mar El Salto	Viña del Mar El Salto
254	Maule	Viña del Mar El Salto	Viña del Mar El Salto	H	C	III	2010	8,8	3	260	0,775	-33,047	-71,510	Maule	Viña del Mar El Salto	Viña del Mar El Salto
255	Maule	Viña del Mar El Salto	Viña del Mar El Salto	V	C	III	2010	8,8	3	260	0,775	-33,047	-71,510	Maule	Viña del Mar El Salto	Viña del Mar El Salto
256	Constitución	CCSP	Concepción	H	C	III	2012	7,0	3	332	0,441	-36,844	-73,109	Constitución	CCSP	Concepción
257	Constitución	CCSP	Concepción	H	C	III	2012	7,0	3	332	0,441	-36,844	-73,109	Constitución	CCSP	Concepción
258	Constitución	CCSP	Concepción	V	C	III	2012	7,0	3	332	0,441	-36,844	-73,109	Constitución	CCSP	Concepción
259	Constitución	GO05	Hualañé	H	B	II	2012	7,0	3	541	0,408	-35,010	-71,930	Constitución	GO05	Hualañé
260	Constitución	GO05	Hualañé	H	B	II	2012	7,0	3	541	0,408	-35,010	-71,930	Constitución	GO05	Hualañé
261	Constitución	GO05	Hualañé	V	B	II	2012	7,0	3	541	0,408	-35,010	-71,930	Constitución	GO05	Hualañé
262	Constitución	LMEL	Las Melosas	H			2012	7,0	2			-33,848	-70,207	Constitución	LMEL	Las Melosas
263	Constitución	LMEL	Las Melosas	H			2012	7,0	2			-33,848	-70,207	Constitución	LMEL	Las Melosas
264	Constitución	LMEL	Las Melosas	V			2012	7,0	2			-33,848	-70,207	Constitución	LMEL	Las Melosas
265	Constitución	ROC1	Cerro El Roble	H	A	I	2012	7,0	3	1951		-32,976	-71,016	Constitución	ROC1	Cerro El Roble
266	Constitución	ROC1	Cerro El Roble	H	A	I	2012	7,0	3	1951		-32,976	-71,016	Constitución	ROC1	Cerro El Roble
267	Constitución	ROC1	Cerro El Roble	V	A	I	2012	7,0	3	1951		-32,976	-71,016	Constitución	ROC1	Cerro El Roble
268	Iquique	AP01	Aeropuerto Chacalluta	H			2014	7,7	3			-18,371	-70,342	Iquique	AP01	Aeropuerto Chacalluta
269	Iquique	AP01	Aeropuerto Chacalluta	H			2014	7,7	3			-18,371	-70,342	Iquique	AP01	Aeropuerto Chacalluta
270	Iquique	AP01	Aeropuerto Chacalluta	V			2014	7,7	3			-18,371	-70,342	Iquique	AP01	Aeropuerto Chacalluta
271	Iquique	GO01	Chusmiza	H			2014	7,7	2		0,593	-19,669	-69,194	Iquique	GO01	Chusmiza

272	Iquique	GO01	Chusmiza	H			2014	7,7	2		0,593	-19,669	-69,194	Iquique	GO01	Chusmiza
273	Iquique	GO01	Chusmiza	V			2014	7,7	2		0,593	-19,669	-69,194	Iquique	GO01	Chusmiza
274	Iquique	HMBCX	Humberstone	H	B	II	2014	7,7	3	677	0,613	-20,278	-69,888	Iquique	HMBCX	Humberstone
275	Iquique	HMBCX	Humberstone	H	B	II	2014	7,7	3	677	0,613	-20,278	-69,888	Iquique	HMBCX	Humberstone
276	Iquique	HMBCX	Humberstone	V	B	II	2014	7,7	3	677	0,613	-20,278	-69,888	Iquique	HMBCX	Humberstone
277	Iquique	MNMCX	Miñi Miñi	H			2014	7,7	2			-19,131	-69,596	Iquique	MNMCX	Miñi Miñi
278	Iquique	MNMCX	Miñi Miñi	H			2014	7,7	2			-19,131	-69,596	Iquique	MNMCX	Miñi Miñi
279	Iquique	MNMCX	Miñi Miñi	V			2014	7,7	2			-19,131	-69,596	Iquique	MNMCX	Miñi Miñi
280	Iquique	PB01	Huatacondo	H			2014	7,7	2			-21,043	-69,487	Iquique	PB01	Huatacondo
281	Iquique	PB01	Huatacondo	H			2014	7,7	2			-21,043	-69,487	Iquique	PB01	Huatacondo
282	Iquique	PB01	Huatacondo	V			2014	7,7	2			-21,043	-69,487	Iquique	PB01	Huatacondo
283	Iquique	PB02	Salar Grande	H			2014	7,7	3			-21,320	-69,896	Iquique	PB02	Salar Grande
284	Iquique	PB02	Salar Grande	H			2014	7,7	3			-21,320	-69,896	Iquique	PB02	Salar Grande
285	Iquique	PB02	Salar Grande	V			2014	7,7	3			-21,320	-69,896	Iquique	PB02	Salar Grande
286	Iquique	PB03	El Tigre	H			2014	7,7	3			-22,048	-69,753	Iquique	PB03	El Tigre
287	Iquique	PB03	El Tigre	H			2014	7,7	3			-22,048	-69,753	Iquique	PB03	El Tigre
288	Iquique	PB03	El Tigre	V			2014	7,7	3			-22,048	-69,753	Iquique	PB03	El Tigre
289	Iquique	PB04	Mantos de Luna	H			2014	7,7	3			-22,334	-70,149	Iquique	PB04	Mantos de Luna
290	Iquique	PB04	Mantos de Luna	H			2014	7,7	3			-22,334	-70,149	Iquique	PB04	Mantos de Luna
291	Iquique	PB04	Mantos de Luna	V			2014	7,7	3			-22,334	-70,149	Iquique	PB04	Mantos de Luna
292	Iquique	PB07	Cerro Tatas	H			2014	7,7	3			-21,727	-69,886	Iquique	PB07	Cerro Tatas
293	Iquique	PB07	Cerro Tatas	H			2014	7,7	3			-21,727	-69,886	Iquique	PB07	Cerro Tatas
294	Iquique	PB07	Cerro Tatas	V			2014	7,7	3			-21,727	-69,886	Iquique	PB07	Cerro Tatas
295	Iquique	PB08	Macaya	H			2014	7,7	2			-20,141	-69,153	Iquique	PB08	Macaya
296	Iquique	PB08	Macaya	H			2014	7,7	2			-20,141	-69,153	Iquique	PB08	Macaya
297	Iquique	PB08	Macaya	V			2014	7,7	2			-20,141	-69,153	Iquique	PB08	Macaya
298	Iquique	PB09	Quillagua	H			2014	7,7	2			-21,796	-69,242	Iquique	PB09	Quillagua
299	Iquique	PB09	Quillagua	H			2014	7,7	2			-21,796	-69,242	Iquique	PB09	Quillagua
300	Iquique	PB09	Quillagua	V			2014	7,7	2			-21,796	-69,242	Iquique	PB09	Quillagua
301	Iquique	PB11	Quebrada Aricilda	H			2014	7,7	2		1,285	-19,761	-69,656	Iquique	PB11	Quebrada Aricilda
302	Iquique	PB11	Quebrada Aricilda	H			2014	7,7	2		1,285	-19,761	-69,656	Iquique	PB11	Quebrada Aricilda
303	Iquique	PB11	Quebrada Aricilda	V			2014	7,7	2		1,285	-19,761	-69,656	Iquique	PB11	Quebrada Aricilda
304	Iquique	PB12	Arica Cerro Camaraca	H			2014	7,7	3			-18,614	-70,328	Iquique	PB12	Arica Cerro Camaraca
305	Iquique	PB12	Arica Cerro Camaraca	H			2014	7,7	3			-18,614	-70,328	Iquique	PB12	Arica Cerro Camaraca
306	Iquique	PB12	Arica Cerro Camaraca	V			2014	7,7	3			-18,614	-70,328	Iquique	PB12	Arica Cerro Camaraca
307	Iquique	PB15	Sierra Gorda	H			2014	7,7	2			-23,208	-69,471	Iquique	PB15	Sierra Gorda

308	Iquique	PB15	Sierra Gorda	H			2014	7,7	2			-23,208	-69,471	Iquique	PB15	Sierra Gorda
309	Iquique	PB15	Sierra Gorda	V			2014	7,7	2			-23,208	-69,471	Iquique	PB15	Sierra Gorda
310	Iquique	PSGCX	Pisagua	H	A	I	2014	7,7	3	1558	0,491	-19,597	-70,123	Iquique	PSGCX	Pisagua
311	Iquique	PSGCX	Pisagua	H	A	I	2014	7,7	3	1558	0,491	-19,597	-70,123	Iquique	PSGCX	Pisagua
312	Iquique	PSGCX	Pisagua	V	A	I	2014	7,7	3	1558	0,491	-19,597	-70,123	Iquique	PSGCX	Pisagua
313	Iquique	T03A	Regimiento Granaderos	H			2014	7,7	3		0,345	-20,230	-70,146	Iquique	T03A	Regimiento Granaderos
314	Iquique	T03A	Regimiento Granaderos	H			2014	7,7	3		0,345	-20,230	-70,146	Iquique	T03A	Regimiento Granaderos
315	Iquique	T03A	Regimiento Granaderos	V			2014	7,7	3		0,345	-20,230	-70,146	Iquique	T03A	Regimiento Granaderos
316	Iquique	T05A	Iquique SERVIU	H	B	II	2014	7,7	3	811	0,378	-20,210	-70,150	Iquique	T05A	Iquique SERVIU
317	Iquique	T05A	Iquique SERVIU	H	B	II	2014	7,7	3	811	0,378	-20,210	-70,150	Iquique	T05A	Iquique SERVIU
318	Iquique	T05A	Iquique SERVIU	V	B	II	2014	7,7	3	811	0,378	-20,210	-70,150	Iquique	T05A	Iquique SERVIU
319	Iquique	T06A	Hospital Ernesto Torres G	H			2014	7,7	3			-20,214	-70,138	Iquique	T06A	Hospital Ernesto Torres G
320	Iquique	T06A	Hospital Ernesto Torres G	H			2014	7,7	3			-20,214	-70,138	Iquique	T06A	Hospital Ernesto Torres G
321	Iquique	T06A	Hospital Ernesto Torres G	V			2014	7,7	3			-20,214	-70,138	Iquique	T06A	Hospital Ernesto Torres G
322	Iquique	T07A	Pozo Almonte	H	C	III	2014	7,7	3	344	0,332	-20,256	-69,786	Iquique	T07A	Pozo Almonte
323	Iquique	T07A	Pozo Almonte	H	C	III	2014	7,7	3	344	0,332	-20,256	-69,786	Iquique	T07A	Pozo Almonte
324	Iquique	T07A	Pozo Almonte	V	C	III	2014	7,7	3	344	0,332	-20,256	-69,786	Iquique	T07A	Pozo Almonte
325	Iquique	T08A	Alto Hospicio	H	C	III	2014	7,7	3	277	0,709	-20,270	-70,094	Iquique	T08A	Alto Hospicio
326	Iquique	T08A	Alto Hospicio	H	C	III	2014	7,7	3	277	0,709	-20,270	-70,094	Iquique	T08A	Alto Hospicio
327	Iquique	T08A	Alto Hospicio	V	C	III	2014	7,7	3	277	0,709	-20,270	-70,094	Iquique	T08A	Alto Hospicio
328	Iquique	T09A	Pisagua Esmeralda	H			2014	7,7	3		0,036	-19,596	-70,211	Iquique	T09A	Pisagua Esmeralda
329	Iquique	T09A	Pisagua Esmeralda	H			2014	7,7	3		0,036	-19,596	-70,211	Iquique	T09A	Pisagua Esmeralda
330	Iquique	T09A	Pisagua Esmeralda	V			2014	7,7	3		0,036	-19,596	-70,211	Iquique	T09A	Pisagua Esmeralda
331	Iquique	T10A	Huara	H	C	II	2014	7,7	3	417	1,024	-19,995	-69,767	Iquique	T10A	Huara
332	Iquique	T10A	Huara	H	C	II	2014	7,7	3	417	1,024	-19,995	-69,767	Iquique	T10A	Huara
333	Iquique	T10A	Huara	V	C	II	2014	7,7	3	417	1,024	-19,995	-69,767	Iquique	T10A	Huara
334	Iquique	T12A	Mamiña	H			2014	7,7	2			-20,071	-69,217	Iquique	T12A	Mamiña
335	Iquique	T12A	Mamiña	H			2014	7,7	2			-20,071	-69,217	Iquique	T12A	Mamiña
336	Iquique	T12A	Mamiña	V			2014	7,7	2			-20,071	-69,217	Iquique	T12A	Mamiña
337	Iquique	T13A	Tenencia de Pica	H	C	III	2014	7,7	2	357	0,377	-20,496	-69,337	Iquique	T13A	Tenencia de Pica
338	Iquique	T13A	Tenencia de	H	C	III	2014	7,7	2	357	0,377	-20,496	-69,337	Iquique	T13A	Tenencia de Pica

			Pica												
339	Iquique	T13A	Tenencia de Pica	V	C	III	2014	7,7	2	357	0,377	-20,496	-69,337	Iquique	T13A	Tenencia de Pica
340	Iquique	TA01	Iquique Cerro Dragon	H			2014	7,7	3			-20,566	-70,181	Iquique	TA01	Iquique Cerro Dragon
341	Iquique	TA01	Iquique Cerro Dragon	H			2014	7,7	3			-20,566	-70,181	Iquique	TA01	Iquique Cerro Dragon
342	Iquique	TA01	Iquique Cerro Dragon	V			2014	7,7	3			-20,566	-70,181	Iquique	TA01	Iquique Cerro Dragon
343	Coquimbo	AC04	Llanos de Challe	H			2015	8,3	3			-28,205	-71,074	Coquimbo	AC04	Llanos de Challe
344	Coquimbo	AC04	Llanos de Challe	H			2015	8,3	3			-28,205	-71,074	Coquimbo	AC04	Llanos de Challe
345	Coquimbo	AC04	Llanos de Challe	V			2015	8,3	3			-28,205	-71,074	Coquimbo	AC04	Llanos de Challe
346	Coquimbo	C01O	Serena 6ta Comisaria	H			2015	8,3	3			-29,877	-71,238	Coquimbo	C01O	Serena 6ta Comisaria
347	Coquimbo	C01O	Serena 6ta Comisaria	H			2015	8,3	3			-29,877	-71,238	Coquimbo	C01O	Serena 6ta Comisaria
348	Coquimbo	C01O	Serena 6ta Comisaria	V			2015	8,3	3			-29,877	-71,238	Coquimbo	C01O	Serena 6ta Comisaria
349	Coquimbo	C09O	Consistoria La Higuera	H			2015	8,3	3			-29,511	-71,200	Coquimbo	C09O	Consistoria La Higuera
350	Coquimbo	C09O	Consistoria La Higuera	H			2015	8,3	3			-29,511	-71,200	Coquimbo	C09O	Consistoria La Higuera
351	Coquimbo	C09O	Consistoria La Higuera	V			2015	8,3	3			-29,511	-71,200	Coquimbo	C09O	Consistoria La Higuera
352	Coquimbo	C10O	Andacoyo	H			2015	8,3	3			-30,234	-71,082	Coquimbo	C10O	Andacoyo
353	Coquimbo	C10O	Andacoyo	H			2015	8,3	3			-30,234	-71,082	Coquimbo	C10O	Andacoyo
354	Coquimbo	C10O	Andacoyo	V			2015	8,3	3			-30,234	-71,082	Coquimbo	C10O	Andacoyo
355	Coquimbo	C11O	Monte Patria	H			2015	8,3	3			-30,696	-70,959	Coquimbo	C11O	Monte Patria
356	Coquimbo	C11O	Monte Patria	H			2015	8,3	3			-30,696	-70,959	Coquimbo	C11O	Monte Patria
357	Coquimbo	C11O	Monte Patria	V			2015	8,3	3			-30,696	-70,959	Coquimbo	C11O	Monte Patria
358	Coquimbo	C14O	Paihuano	H			2015	8,3	3			-30,123	-70,491	Coquimbo	C14O	Paihuano
359	Coquimbo	C14O	Paihuano	H			2015	8,3	3			-30,123	-70,491	Coquimbo	C14O	Paihuano
360	Coquimbo	C14O	Paihuano	V			2015	8,3	3			-30,123	-70,491	Coquimbo	C14O	Paihuano
361	Coquimbo	C18O	Rio Hurtado	H			2015	8,3	3			-30,278	-70,669	Coquimbo	C18O	Rio Hurtado
362	Coquimbo	C18O	Rio Hurtado	H			2015	8,3	3			-30,278	-70,669	Coquimbo	C18O	Rio Hurtado
363	Coquimbo	C18O	Rio Hurtado	V			2015	8,3	3			-30,278	-70,669	Coquimbo	C18O	Rio Hurtado
364	Coquimbo	C19O	Totoralillo	H			2015	8,3	3			-30,093	-71,369	Coquimbo	C19O	Totoralillo
365	Coquimbo	C19O	Totoralillo	H			2015	8,3	3			-30,093	-71,369	Coquimbo	C19O	Totoralillo
366	Coquimbo	C19O	Totoralillo	V			2015	8,3	3			-30,093	-71,369	Coquimbo	C19O	Totoralillo
367	Coquimbo	C20O	Hospital San Pablo Coquimbo	H			2015	8,3	3			-29,968	-71,337	Coquimbo	C20O	Hospital San Pablo Coquimbo
368	Coquimbo	C20O	Hospital San Pablo	H			2015	8,3	3			-29,968	-71,337	Coquimbo	C20O	Hospital San Pablo Coquimbo

			Coquimbo												
369	Coquimbo	C20O	Hospital San Pablo Coquimbo	V			2015	8,3	3			-29,968	-71,337	Coquimbo	C20O	Hospital San Pablo Coquimbo
370	Coquimbo	C22O	Coquimbo UCN	H			2015	8,3	3			-29,966	-71,351	Coquimbo	C22O	Coquimbo UCN
371	Coquimbo	C22O	Coquimbo UCN	H			2015	8,3	3			-29,966	-71,351	Coquimbo	C22O	Coquimbo UCN
372	Coquimbo	C22O	Coquimbo UCN	V			2015	8,3	3			-29,966	-71,351	Coquimbo	C22O	Coquimbo UCN
373	Coquimbo	C26O	Tongoy	H			2015	8,3	3			-30,259	-71,490	Coquimbo	C26O	Tongoy
374	Coquimbo	C26O	Tongoy	H			2015	8,3	3			-30,259	-71,490	Coquimbo	C26O	Tongoy
375	Coquimbo	C26O	Tongoy	V			2015	8,3	3			-30,259	-71,490	Coquimbo	C26O	Tongoy
376	Coquimbo	C27O	La Higuera	H			2015	8,3	3			-29,384	-70,745	Coquimbo	C27O	La Higuera
377	Coquimbo	C27O	La Higuera	H			2015	8,3	3			-29,384	-70,745	Coquimbo	C27O	La Higuera
378	Coquimbo	C27O	La Higuera	V			2015	8,3	3			-29,384	-70,745	Coquimbo	C27O	La Higuera
379	Coquimbo	C28O	Los Choros	H			2015	8,3	3			-29,291	-71,308	Coquimbo	C28O	Los Choros
380	Coquimbo	C28O	Los Choros	H			2015	8,3	3			-29,291	-71,308	Coquimbo	C28O	Los Choros
381	Coquimbo	C28O	Los Choros	V			2015	8,3	3			-29,291	-71,308	Coquimbo	C28O	Los Choros
382	Coquimbo	C33O	Estadio La Portada	H			2015	8,3	3			-29,911	-71,251	Coquimbo	C33O	Estadio La Portada
383	Coquimbo	C33O	Estadio La Portada	H			2015	8,3	3			-29,911	-71,251	Coquimbo	C33O	Estadio La Portada
384	Coquimbo	C33O	Estadio La Portada	V			2015	8,3	3			-29,911	-71,251	Coquimbo	C33O	Estadio La Portada
385	Coquimbo	CO03	El Pedregal	H			2015	8,3	3			-30,839	-70,689	Coquimbo	CO03	El Pedregal
386	Coquimbo	CO03	El Pedregal	H			2015	8,3	3			-30,839	-70,689	Coquimbo	CO03	El Pedregal
387	Coquimbo	CO03	El Pedregal	V			2015	8,3	3			-30,839	-70,689	Coquimbo	CO03	El Pedregal
388	Coquimbo	CO06	Fray Jorge	H			2015	8,3	3			-30,674	-71,635	Coquimbo	CO06	Fray Jorge
389	Coquimbo	CO06	Fray Jorge	H			2015	8,3	3			-30,674	-71,635	Coquimbo	CO06	Fray Jorge
390	Coquimbo	CO06	Fray Jorge	V			2015	8,3	3			-30,674	-71,635	Coquimbo	CO06	Fray Jorge
391	Coquimbo	GO04	Tololo Vicuña	H			2015	8,3	3			-30,173	-70,799	Coquimbo	GO04	Tololo Vicuña
392	Coquimbo	GO04	Tololo Vicuña	H			2015	8,3	3			-30,173	-70,799	Coquimbo	GO04	Tololo Vicuña
393	Coquimbo	GO04	Tololo Vicuña	V			2015	8,3	3			-30,173	-70,799	Coquimbo	GO04	Tololo Vicuña
394	Coquimbo	LMEL	Las Melosas	H			2015	8,3	2			-33,848	-70,207	Coquimbo	LMEL	Las Melosas
395	Coquimbo	LMEL	Las Melosas	H			2015	8,3	2			-33,848	-70,207	Coquimbo	LMEL	Las Melosas
396	Coquimbo	LMEL	Las Melosas	V			2015	8,3	2			-33,848	-70,207	Coquimbo	LMEL	Las Melosas
397	Coquimbo	M02L	Los Quenes	H			2015	8,3	2			-35,000	-70,812	Coquimbo	M02L	Los Quenes
398	Coquimbo	M02L	Los Quenes	H			2015	8,3	2			-35,000	-70,812	Coquimbo	M02L	Los Quenes
399	Coquimbo	M02L	Los Quenes	V			2015	8,3	2			-35,000	-70,812	Coquimbo	M02L	Los Quenes
400	Coquimbo	M03L	Curicó	H	B	II	2015	8,3	2	651	0,476	-34,976	-71,231	Coquimbo	M03L	Curicó
401	Coquimbo	M03L	Curicó	H	B	II	2015	8,3	2	651	0,476	-34,976	-71,231	Coquimbo	M03L	Curicó
402	Coquimbo	M03L	Curicó	V	B	II	2015	8,3	2	651	0,476	-34,976	-71,231	Coquimbo	M03L	Curicó
403	Coquimbo	M09L	Empedrados	H			2015	8,3	3			-35,591	-72,281	Coquimbo	M09L	Empedrados
404	Coquimbo	M09L	Empedrados	H			2015	8,3	3			-35,591	-72,281	Coquimbo	M09L	Empedrados

405	Coquimbo	M09L	Empedrados	V			2015	8,3	3			-35,591	-72,281	Coquimbo	M09L	Empedrados
406	Coquimbo	M11L	Talca	H	B	II	2015	8,3	2	648		-35,440	-71,632	Coquimbo	M11L	Talca
407	Coquimbo	M11L	Talca	H	B	II	2015	8,3	2	648		-35,440	-71,632	Coquimbo	M11L	Talca
408	Coquimbo	M11L	Talca	V	B	II	2015	8,3	2	648		-35,440	-71,632	Coquimbo	M11L	Talca
409	Coquimbo	MT01	Los Guindos	H			2015	8,3	1			-33,864	-71,251	Coquimbo	MT01	Los Guindos
410	Coquimbo	MT01	Los Guindos	H			2015	8,3	1			-33,864	-71,251	Coquimbo	MT01	Los Guindos
411	Coquimbo	MT01	Los Guindos	V			2015	8,3	1			-33,864	-71,251	Coquimbo	MT01	Los Guindos
412	Coquimbo	MT05	Cerro Colorado	H			2015	8,3	2			-33,392	-70,738	Coquimbo	MT05	Cerro Colorado
413	Coquimbo	MT05	Cerro Colorado	H			2015	8,3	2			-33,392	-70,738	Coquimbo	MT05	Cerro Colorado
414	Coquimbo	MT05	Cerro Colorado	V			2015	8,3	2			-33,392	-70,738	Coquimbo	MT05	Cerro Colorado
415	Coquimbo	MT09	Isla Maipo	H			2015	8,3	2			-33,776	-70,989	Coquimbo	MT09	Isla Maipo
416	Coquimbo	MT09	Isla Maipo	H			2015	8,3	2			-33,776	-70,989	Coquimbo	MT09	Isla Maipo
417	Coquimbo	MT09	Isla Maipo	V			2015	8,3	2			-33,776	-70,989	Coquimbo	MT09	Isla Maipo
418	Coquimbo	R02M	Centro de Justicia	H			2015	8,3	2			-33,473	-70,660	Coquimbo	R02M	Centro de Justicia
419	Coquimbo	R02M	Centro de Justicia	H			2015	8,3	2			-33,473	-70,660	Coquimbo	R02M	Centro de Justicia
420	Coquimbo	R02M	Centro de Justicia	V			2015	8,3	2			-33,473	-70,660	Coquimbo	R02M	Centro de Justicia
421	Coquimbo	R05M	Campo Militar La Reina	H			2015	8,3	2			-33,443	-70,534	Coquimbo	R05M	Campo Militar La Reina
422	Coquimbo	R05M	Campo Militar La Reina	H			2015	8,3	2			-33,443	-70,534	Coquimbo	R05M	Campo Militar La Reina
423	Coquimbo	R05M	Campo Militar La Reina	V			2015	8,3	2			-33,443	-70,534	Coquimbo	R05M	Campo Militar La Reina
424	Coquimbo	R12M	Ciudad Empresarial	H			2015	8,3	2			-33,389	-70,622	Coquimbo	R12M	Ciudad Empresarial
425	Coquimbo	R12M	Ciudad Empresarial	H			2015	8,3	2			-33,389	-70,622	Coquimbo	R12M	Ciudad Empresarial
426	Coquimbo	R12M	Ciudad Empresarial	V			2015	8,3	2			-33,389	-70,622	Coquimbo	R12M	Ciudad Empresarial
427	Coquimbo	R13M	Panamericana Norte	H			2015	8,3	2			-33,216	-70,767	Coquimbo	R13M	Panamericana Norte
428	Coquimbo	R13M	Panamericana Norte	H			2015	8,3	2			-33,216	-70,767	Coquimbo	R13M	Panamericana Norte
429	Coquimbo	R13M	Panamericana Norte	V			2015	8,3	2			-33,216	-70,767	Coquimbo	R13M	Panamericana Norte
430	Coquimbo	R14M	Hospital FACH	H			2015	8,3	2			-33,397	-70,546	Coquimbo	R14M	Hospital FACH
431	Coquimbo	R14M	Hospital FACH	H			2015	8,3	2			-33,397	-70,546	Coquimbo	R14M	Hospital FACH
432	Coquimbo	R14M	Hospital	V			2015	8,3	2			-33,397	-70,546	Coquimbo	R14M	Hospital FACH

			FACH													
433	Coquimbo	R18M	Estadio Santiago Bueras	H			2015	8,3	2			-33,508	-70,749	Coquimbo	R18M	Estadio Santiago Bueras
434	Coquimbo	R18M	Estadio Santiago Bueras	H			2015	8,3	2			-33,508	-70,749	Coquimbo	R18M	Estadio Santiago Bueras
435	Coquimbo	R18M	Estadio Santiago Bueras	V			2015	8,3	2			-33,508	-70,749	Coquimbo	R18M	Estadio Santiago Bueras
436	Coquimbo	R19M	Estadio Roberto Bravo	H			2015	8,3	3			-33,699	-71,217	Coquimbo	R19M	Estadio Roberto Bravo
437	Coquimbo	R19M	Estadio Roberto Bravo	H			2015	8,3	3			-33,699	-71,217	Coquimbo	R19M	Estadio Roberto Bravo
438	Coquimbo	R19M	Estadio Roberto Bravo	V			2015	8,3	3			-33,699	-71,217	Coquimbo	R19M	Estadio Roberto Bravo
439	Coquimbo	R20M	Talagante	H			2015	8,3	2			-33,665	-70,929	Coquimbo	R20M	Talagante
440	Coquimbo	R20M	Talagante	H			2015	8,3	2			-33,665	-70,929	Coquimbo	R20M	Talagante
441	Coquimbo	R20M	Talagante	V			2015	8,3	2			-33,665	-70,929	Coquimbo	R20M	Talagante
442	Coquimbo	R21M	AMB	H			2015	8,3	2			-33,381	-70,796	Coquimbo	R21M	AMB
443	Coquimbo	R21M	AMB	H			2015	8,3	2			-33,381	-70,796	Coquimbo	R21M	AMB
444	Coquimbo	R21M	AMB	V			2015	8,3	2			-33,381	-70,796	Coquimbo	R21M	AMB
445	Coquimbo	R22M	INACAP Ñuñoa	H			2015	8,3	2			-33,453	-70,592	Coquimbo	R22M	INACAP Ñuñoa
446	Coquimbo	R22M	INACAP Ñuñoa	H			2015	8,3	2			-33,453	-70,592	Coquimbo	R22M	INACAP Ñuñoa
447	Coquimbo	R22M	INACAP Ñuñoa	V			2015	8,3	2			-33,453	-70,592	Coquimbo	R22M	INACAP Ñuñoa
448	Coquimbo	ROC1	Cerro El Roble	H	A	I	2015	8,3	3	1951		-32,976	-71,016	Coquimbo	ROC1	Cerro El Roble
449	Coquimbo	ROC1	Cerro El Roble	H	A	I	2015	8,3	3	1951		-32,976	-71,016	Coquimbo	ROC1	Cerro El Roble
450	Coquimbo	ROC1	Cerro El Roble	V	A	I	2015	8,3	3	1951		-32,976	-71,016	Coquimbo	ROC1	Cerro El Roble
451	Coquimbo	V01A	8va Comisaria Valparaíso	H			2015	8,3	3			-33,053	-71,622	Coquimbo	V01A	8va Comisaria Valparaíso
452	Coquimbo	V01A	8va Comisaria Valparaíso	H			2015	8,3	3			-33,053	-71,622	Coquimbo	V01A	8va Comisaria Valparaíso
453	Coquimbo	V01A	8va Comisaria Valparaíso	V			2015	8,3	3			-33,053	-71,622	Coquimbo	V01A	8va Comisaria Valparaíso
454	Coquimbo	V02A	5ta Comisaria Viña del Mar	H			2015	8,3	3			-33,023	-71,518	Coquimbo	V02A	5ta Comisaria Viña del Mar
455	Coquimbo	V02A	5ta Comisaria Viña del Mar	H			2015	8,3	3			-33,023	-71,518	Coquimbo	V02A	5ta Comisaria Viña del Mar
456	Coquimbo	V02A	5ta Comisaria	V			2015	8,3	3			-33,023	-71,518	Coquimbo	V02A	5ta Comisaria Viña del

			Viña del Mar													Mar
457	Coquimbo	V09A	Congreso Nacional	H			2015	8,3	3			-33,048	-71,604	Coquimbo	V09A	Congreso Nacional
458	Coquimbo	V09A	Congreso Nacional	H			2015	8,3	3			-33,048	-71,604	Coquimbo	V09A	Congreso Nacional
459	Coquimbo	V09A	Congreso Nacional	V			2015	8,3	3			-33,048	-71,604	Coquimbo	V09A	Congreso Nacional
460	Coquimbo	VA01	Faro Punta Ángeles	H			2015	8,3	3			-33,023	-71,637	Coquimbo	VA01	Faro Punta Ángeles
461	Coquimbo	VA01	Faro Punta Ángeles	H			2015	8,3	3			-33,023	-71,637	Coquimbo	VA01	Faro Punta Ángeles
462	Coquimbo	VA01	Faro Punta Ángeles	V			2015	8,3	3			-33,023	-71,637	Coquimbo	VA01	Faro Punta Ángeles
463	Coquimbo	VA03	San Esteban	H			2015	8,3	2			-32,764	-70,551	Coquimbo	VA03	San Esteban
464	Coquimbo	VA03	San Esteban	H			2015	8,3	2			-32,764	-70,551	Coquimbo	VA03	San Esteban
465	Coquimbo	VA03	San Esteban	V			2015	8,3	2			-32,764	-70,551	Coquimbo	VA03	San Esteban
466	Coquimbo	VA05	Aeródromo Santo Domingo	H			2015	8,3	3			-33,657	-71,614	Coquimbo	VA05	Aeródromo Santo Domingo
467	Coquimbo	VA05	Aeródromo Santo Domingo	H			2015	8,3	3			-33,657	-71,614	Coquimbo	VA05	Aeródromo Santo Domingo
468	Coquimbo	VA05	Aeródromo Santo Domingo	V			2015	8,3	3			-33,657	-71,614	Coquimbo	VA05	Aeródromo Santo Domingo
469	Coquimbo	VA06	Catapilco	H			2015	8,3	3			-32,561	-71,298	Coquimbo	VA06	Catapilco
470	Coquimbo	VA06	Catapilco	H			2015	8,3	3			-32,561	-71,298	Coquimbo	VA06	Catapilco
471	Coquimbo	VA06	Catapilco	V			2015	8,3	3			-32,561	-71,298	Coquimbo	VA06	Catapilco
472	Chiloé	AY01	Puyuhuapi	H			2016	7,6	1			-44,421	-72,648	Chiloé	AY01	Puyuhuapi
473	Chiloé	AY01	Puyuhuapi	H			2016	7,6	1			-44,421	-72,648	Chiloé	AY01	Puyuhuapi
474	Chiloé	AY01	Puyuhuapi	V			2016	7,6	1			-44,421	-72,648	Chiloé	AY01	Puyuhuapi
475	Chiloé	GO07	Quellón	H			2016	7,6	2			-43,114	-73,664	Chiloé	GO07	Quellón
476	Chiloé	GO07	Quellón	H			2016	7,6	2			-43,114	-73,664	Chiloé	GO07	Quellón
477	Chiloé	GO07	Quellón	V			2016	7,6	2			-43,114	-73,664	Chiloé	GO07	Quellón
478	Chiloé	L05L	Municipalidad Fresia	H			2016	7,6	3			-41,154	-73,417	Chiloé	L05L	Municipalidad Fresia
479	Chiloé	L05L	Municipalidad Fresia	H			2016	7,6	3			-41,154	-73,417	Chiloé	L05L	Municipalidad Fresia
480	Chiloé	L05L	Municipalidad Fresia	V			2016	7,6	3			-41,154	-73,417	Chiloé	L05L	Municipalidad Fresia
481	Chiloé	L06R	La Unión	H			2016	7,6	3			-40,293	-73,084	Chiloé	L06R	La Unión
482	Chiloé	L06R	La Unión	H			2016	7,6	3			-40,293	-73,084	Chiloé	L06R	La Unión
483	Chiloé	L06R	La Unión	V			2016	7,6	3			-40,293	-73,084	Chiloé	L06R	La Unión
484	Chiloé	L07R	Futrono	H			2016	7,6	2			-40,128	-72,394	Chiloé	L07R	Futrono
485	Chiloé	L07R	Futrono	H			2016	7,6	2			-40,128	-72,394	Chiloé	L07R	Futrono
486	Chiloé	L07R	Futrono	V			2016	7,6	2			-40,128	-72,394	Chiloé	L07R	Futrono

487	Chiloé	L09L	Ancud	H			2016	7,6	3			-41,865	-73,826	Chiloé	L09L	Ancud
488	Chiloé	L09L	Ancud	H			2016	7,6	3			-41,865	-73,826	Chiloé	L09L	Ancud
489	Chiloé	L09L	Ancud	V			2016	7,6	3			-41,865	-73,826	Chiloé	L09L	Ancud
490	Chiloé	L10R	Paillaco	H			2016	7,6	2			-40,070	-72,873	Chiloé	L10R	Paillaco
491	Chiloé	L10R	Paillaco	H			2016	7,6	2			-40,070	-72,873	Chiloé	L10R	Paillaco
492	Chiloé	L10R	Paillaco	V			2016	7,6	2			-40,070	-72,873	Chiloé	L10R	Paillaco
493	Chiloé	LL01	San Ignacio de Yungay	H			2016	7,6	1			-42,379	-72,412	Chiloé	LL01	San Ignacio de Yungay
494	Chiloé	LL01	San Ignacio de Yungay	H			2016	7,6	1			-42,379	-72,412	Chiloé	LL01	San Ignacio de Yungay
495	Chiloé	LL01	San Ignacio de Yungay	V			2016	7,6	1			-42,379	-72,412	Chiloé	LL01	San Ignacio de Yungay
496	Chiloé	LL03	Puerto Varas	H			2016	7,6	2			-41,138	-72,403	Chiloé	LL03	Puerto Varas
497	Chiloé	LL03	Puerto Varas	H			2016	7,6	2			-41,138	-72,403	Chiloé	LL03	Puerto Varas
498	Chiloé	LL03	Puerto Varas	V			2016	7,6	2			-41,138	-72,403	Chiloé	LL03	Puerto Varas
499	Chiloé	LL04	Puerto Octay	H			2016	7,6	2			-40,910	-72,408	Chiloé	LL04	Puerto Octay
500	Chiloé	LL04	Puerto Octay	H			2016	7,6	2			-40,910	-72,408	Chiloé	LL04	Puerto Octay
501	Chiloé	LL04	Puerto Octay	V			2016	7,6	2			-40,910	-72,408	Chiloé	LL04	Puerto Octay
502	Chiloé	LL06	Dalcahue	H			2016	7,6	2			-42,215	-73,628	Chiloé	LL06	Dalcahue
503	Chiloé	LL06	Dalcahue	H			2016	7,6	2			-42,215	-73,628	Chiloé	LL06	Dalcahue
504	Chiloé	LL06	Dalcahue	V			2016	7,6	2			-42,215	-73,628	Chiloé	LL06	Dalcahue
505	Chiloé	LL07	Queilen	H			2016	7,6	2			-42,832	-73,478	Chiloé	LL07	Queilen
506	Chiloé	LL07	Queilen	H			2016	7,6	2			-42,832	-73,478	Chiloé	LL07	Queilen
507	Chiloé	LL07	Queilen	V			2016	7,6	2			-42,832	-73,478	Chiloé	LL07	Queilen
508	Chiloé	LR02	Universidad Austral	H			2016	7,6	3			-39,806	-73,250	Chiloé	LR02	Universidad Austral
509	Chiloé	LR02	Universidad Austral	H			2016	7,6	3			-39,806	-73,250	Chiloé	LR02	Universidad Austral
510	Chiloé	LR02	Universidad Austral	V			2016	7,6	3			-39,806	-73,250	Chiloé	LR02	Universidad Austral

H: Horizontal; V: Vertical; V_{s30}: shear propagation velocity; T_{nak}: Nakamura period

Equivalence of the classification of defined soils defined by the Chilean Highway Manual and the decree DS 61 of seismic design of buildings in Chile.

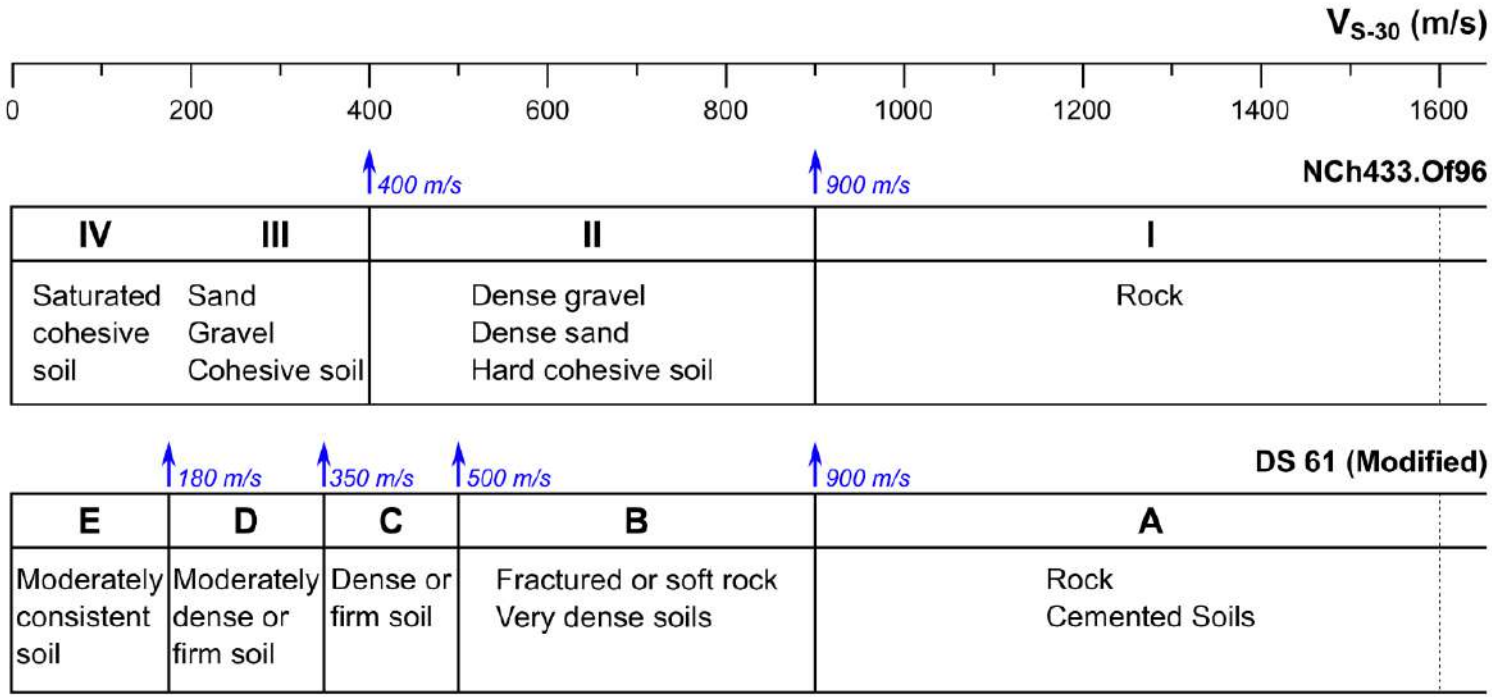

APPENDIX B

Summarizes the formulas and the main analytical results obtained in the proposed self-centering shear key model.

Equations

Degrees of freedom

$$\dot{x}_d^t = \dot{x}_g + \dot{u}_d$$
$$\dot{z}_d^t = \dot{z}_g$$
$$\dot{x}_u^t = \dot{x}_g + \dot{u}_d + \dot{u}_u$$
$$\dot{z}_u^t = \dot{z}_g + \dot{u}_u \tan\alpha \,\mathrm{sign} u_u$$

Virtual displacements

$$\delta x_d^t = \delta x_g + \delta u_d$$
$$\delta z_d = \delta z_g$$
$$\delta x_u^t = \delta x_g + \delta u_d + \delta u_u$$
$$\delta z_u^t = \delta z_g + \delta u_u \tan\alpha \,\mathrm{sign} u_u$$

Virtual work

$$\delta\widetilde{W}_d = (f\cos\alpha + N\sin\alpha - f_c)\big(\delta x_g + \delta u_d\big) + (f\sin\alpha - N\cos\alpha - W_d + N_c)\delta z_g$$
$$\delta\widetilde{W}_u = (-f\cos\alpha - N\sin\alpha)\big(\delta x_g + \delta u_d + \delta u_u\big) + (N\cos\alpha - f\sin\alpha - W_u)(\delta z_g + \delta u_u \tan\alpha \,\mathrm{sign} u_u)$$
$$\delta\widetilde{W} = (-f_c)\delta x_g + (-W_d + N_c - W_u)\delta z_g + (-f_c)\delta u_d + \left(-\sum_{i=1}^{16}\frac{1}{\cos\alpha} f_i - W_u \tan\alpha \,\mathrm{sign} u_u\right)\delta u_u$$

Generalized forces:

$$F_{u_d} = -f_c$$
$$F_{u_u} = -\sum_{i=1}^{16}\frac{1}{\cos\alpha} f_i - W_u \tan\alpha \,\mathrm{sign} u_u = -\boldsymbol{L}^T\boldsymbol{f} - W_u \tan\alpha \,\mathrm{sign} u_u$$

Force – deformation relationships

$$f_c = k_c u_d + c_c \dot{u}_d$$

Kinetic energy

$$T = \frac{1}{2}m_d\left[\left(\dot{x}_g + \dot{u}_d\right)^2 + \dot{z}_g^2\right] + \frac{1}{2}\left[\left(\dot{x}_g + \dot{u}_d + \dot{u}_u\right)^2 + \left(\dot{z}_g + \dot{u}_u \tan\alpha \operatorname{sign} u_u\right)^2\right]$$

Euler-Lagrange equations

$$\frac{d}{dt}\left(\frac{\partial T}{\partial \dot{u}_d}\right) - \frac{\partial T}{\partial u_d} = F_{u_d}$$

$$(m_d + m_u)\ddot{u}_d + m_u\ddot{u}_u + k_c u_d + c_c\dot{u}_d = -(m_d + m_u)\ddot{x}_g$$

$$\frac{d}{dt}\left(\frac{\partial T}{\partial \dot{u}_u}\right) - \frac{\partial T}{\partial u_u} = F_{u_u}$$

$$m_u\ddot{u}_d + m_u(1 + \tan^2\alpha)\ddot{u}_u + \boldsymbol{L}^T\boldsymbol{f} = -m_u\ddot{x}_g - m_u \tan\alpha \operatorname{sign} u_u\ddot{z}_g - W_u \tan\alpha \operatorname{sign} u_u$$

Equation of motion

$$\begin{bmatrix} m_d + m_u & m_u \\ m_u & m_u(1 + \tan^2\alpha) \end{bmatrix}\begin{bmatrix} \ddot{u}_d \\ \ddot{u}_u \end{bmatrix} + \begin{bmatrix} c_c & 0 \\ 0 & 0 \end{bmatrix}\begin{bmatrix} \dot{u}_d \\ \dot{u}_u \end{bmatrix} + \begin{bmatrix} k_c & 0 \\ 0 & 0 \end{bmatrix}\begin{bmatrix} u_d \\ u_u \end{bmatrix} + \begin{bmatrix} 0 \\ \boldsymbol{L}^T\boldsymbol{f} \end{bmatrix}$$
$$= -\begin{bmatrix} m_d + m_u \\ m_u \end{bmatrix}\ddot{x}_g - \begin{bmatrix} 0 \\ m_u \tan\alpha \operatorname{sign} u_u \end{bmatrix} - \begin{bmatrix} 0 \\ W_u \tan\alpha \operatorname{sign} u_u \end{bmatrix}$$

APPENDIX C

Analytical results: Time-history analysis

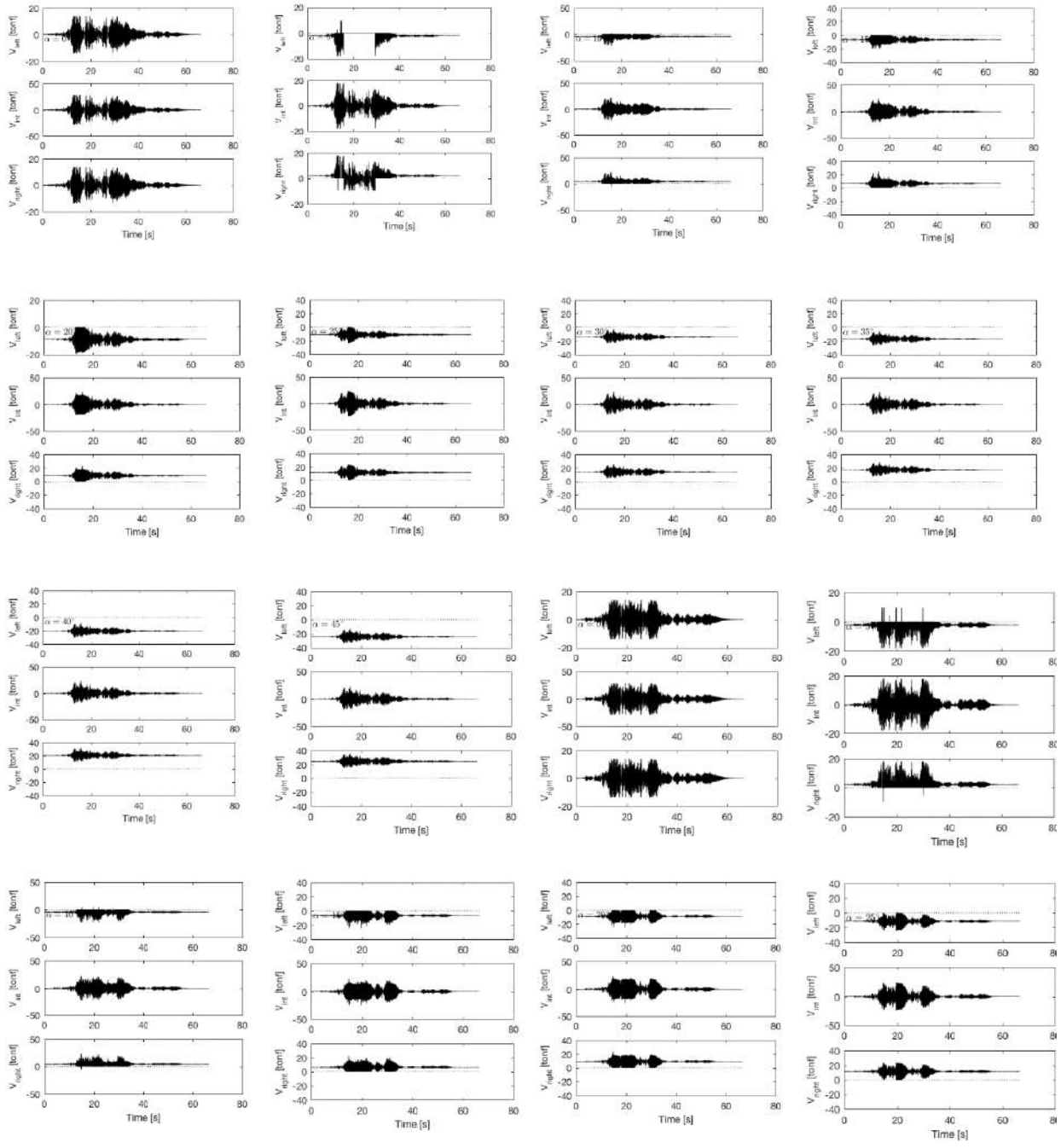

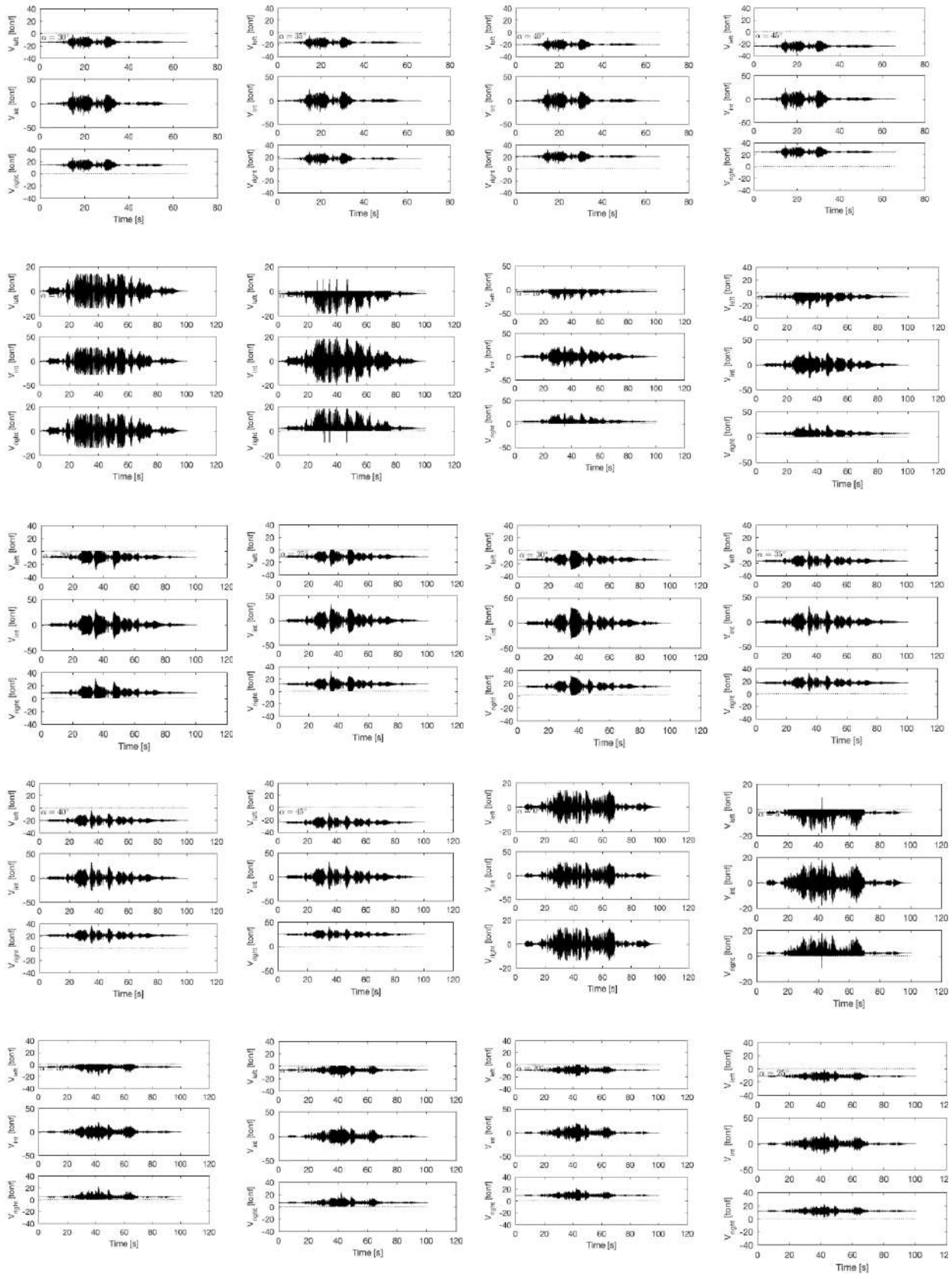

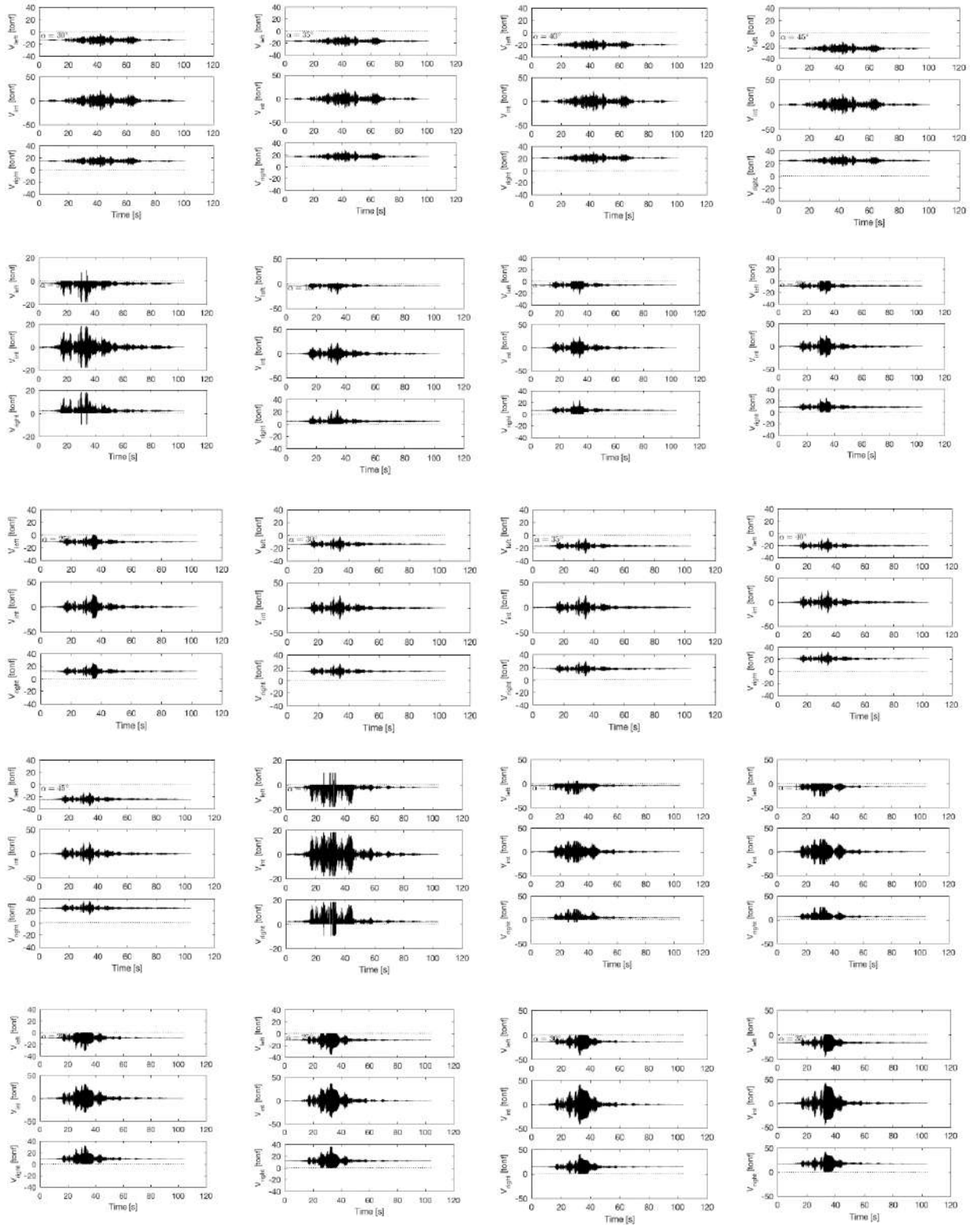

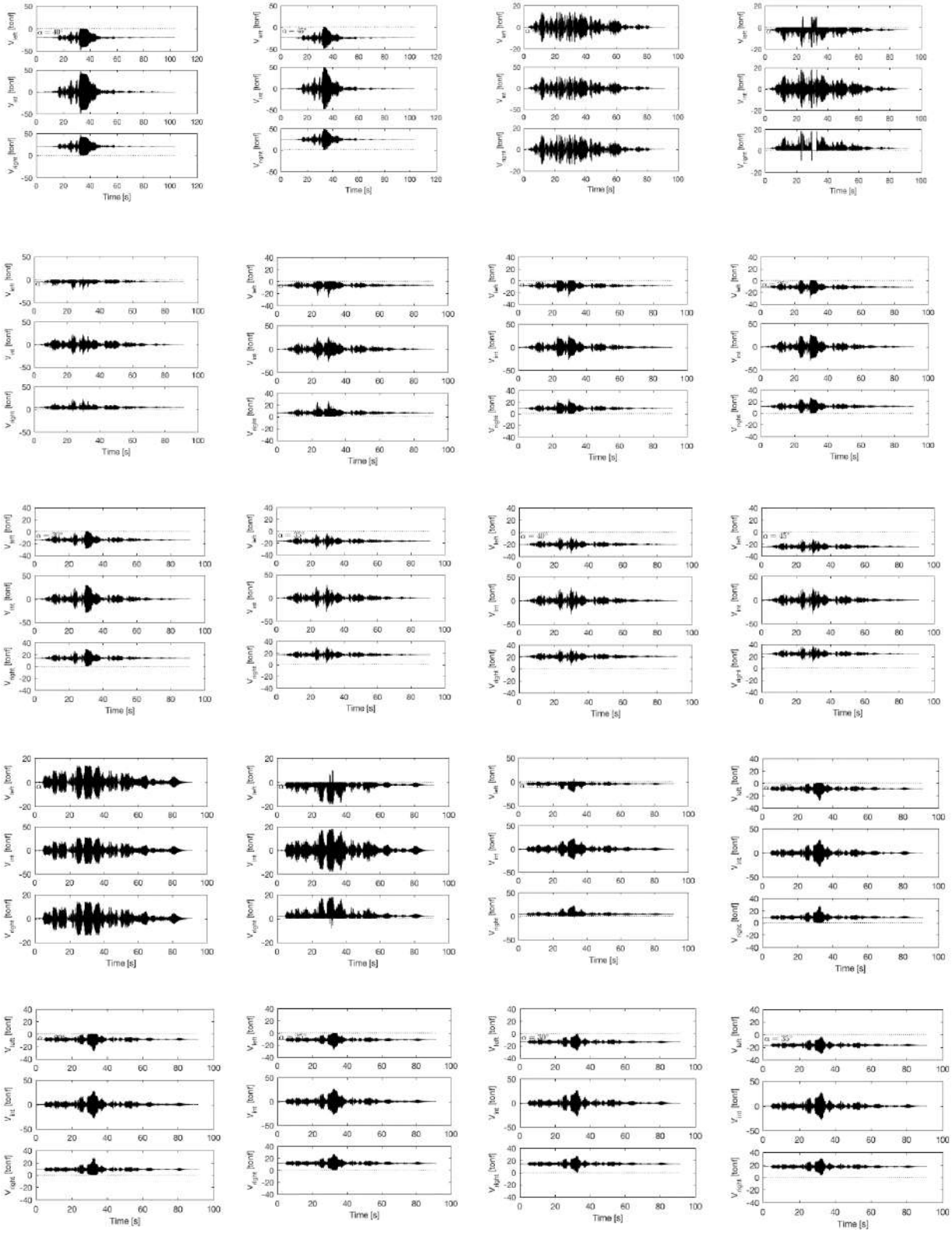
Time [s]

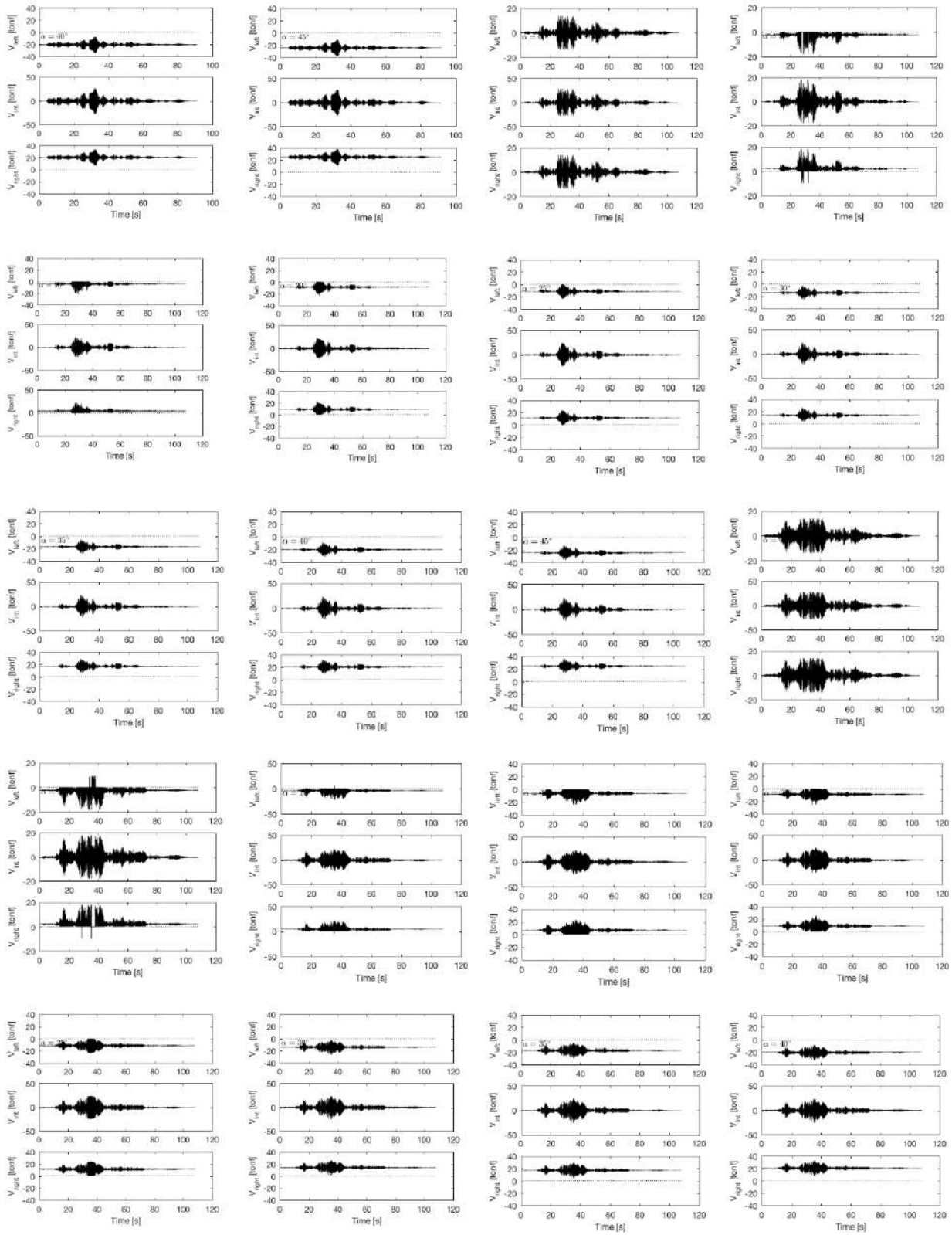

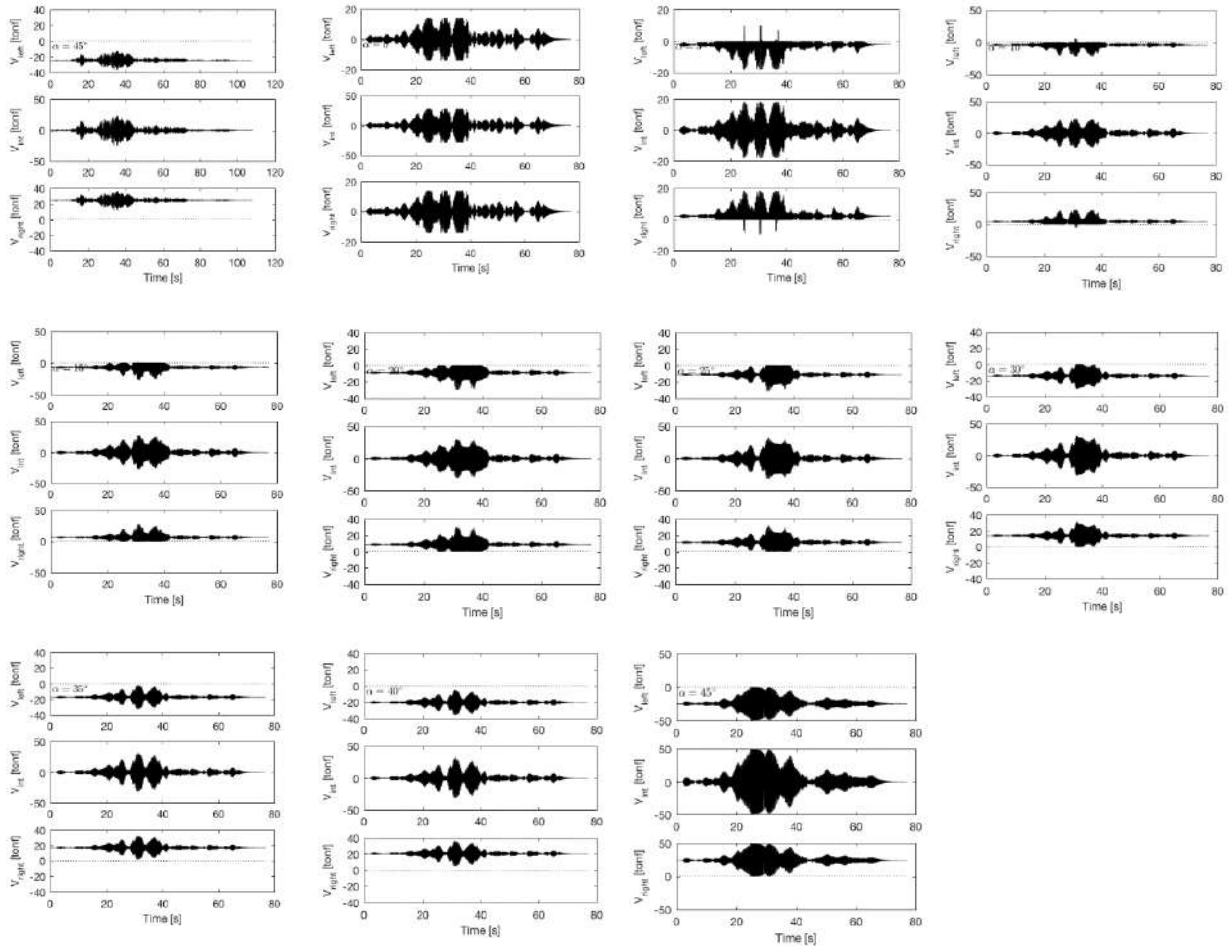
Time [s]

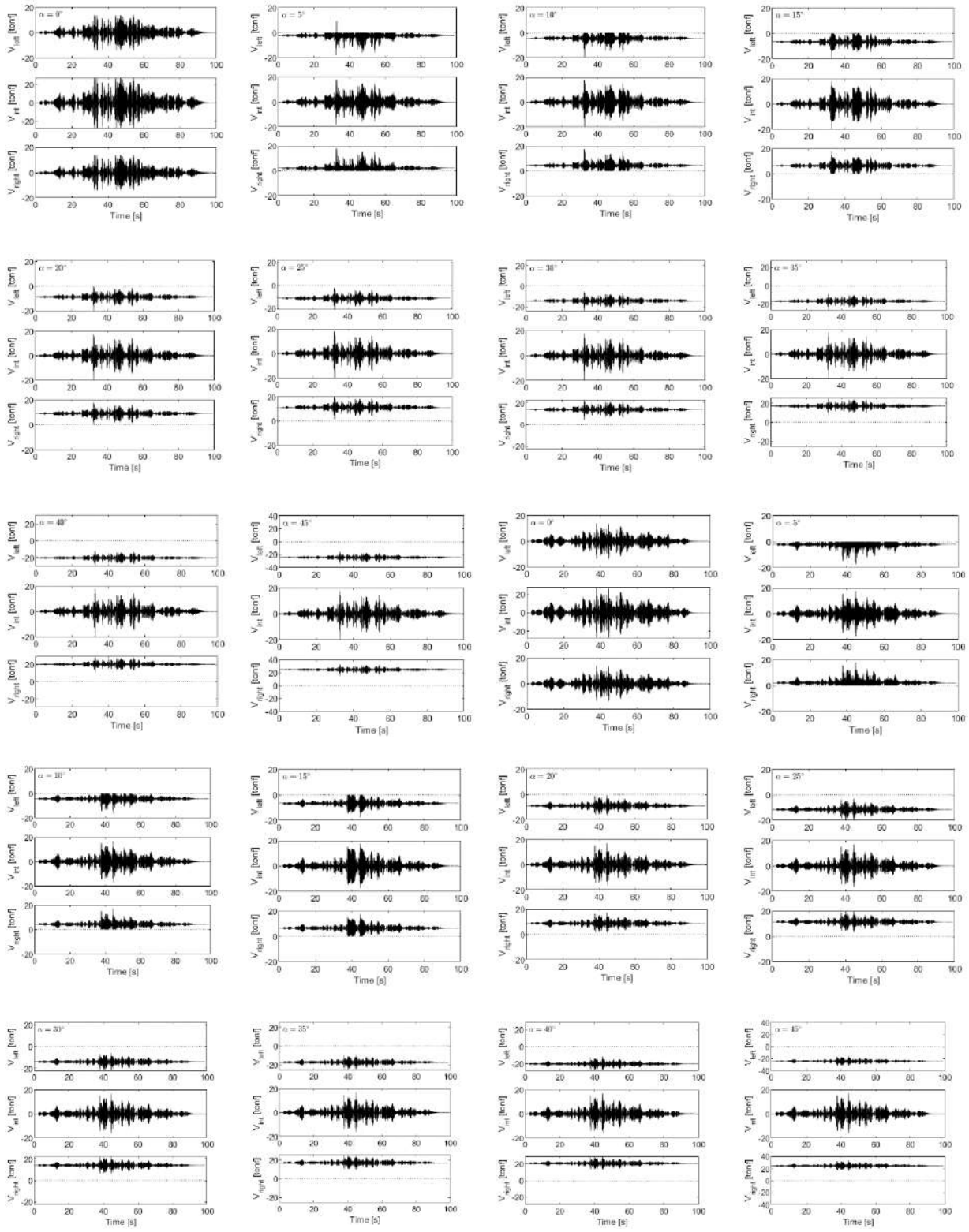

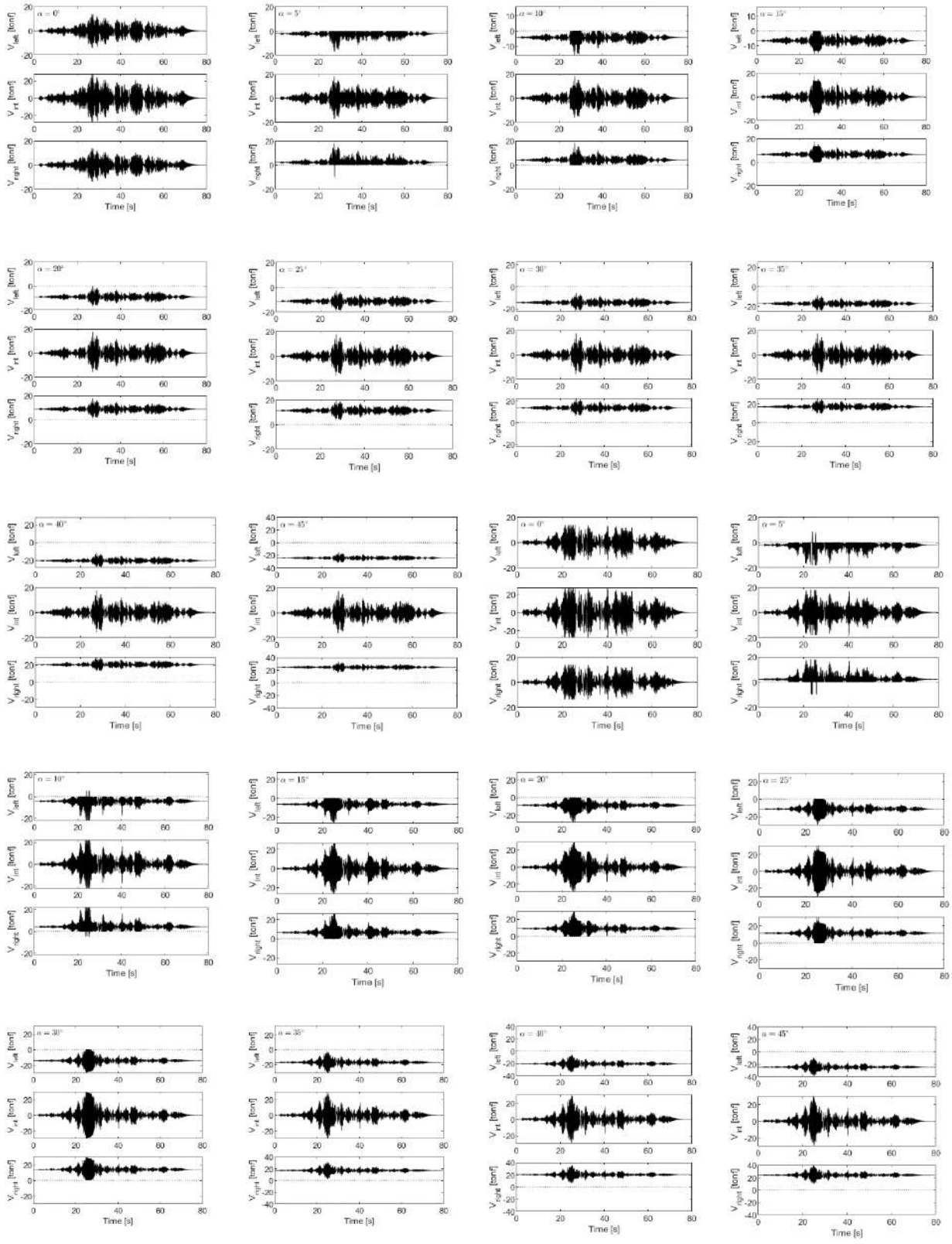
α = 0°
α = 5°
α = 10°
α = 15°
α = 20°
α = 25°
α = 30°
α = 35°
α = 40°
α = 45°
Time [s]

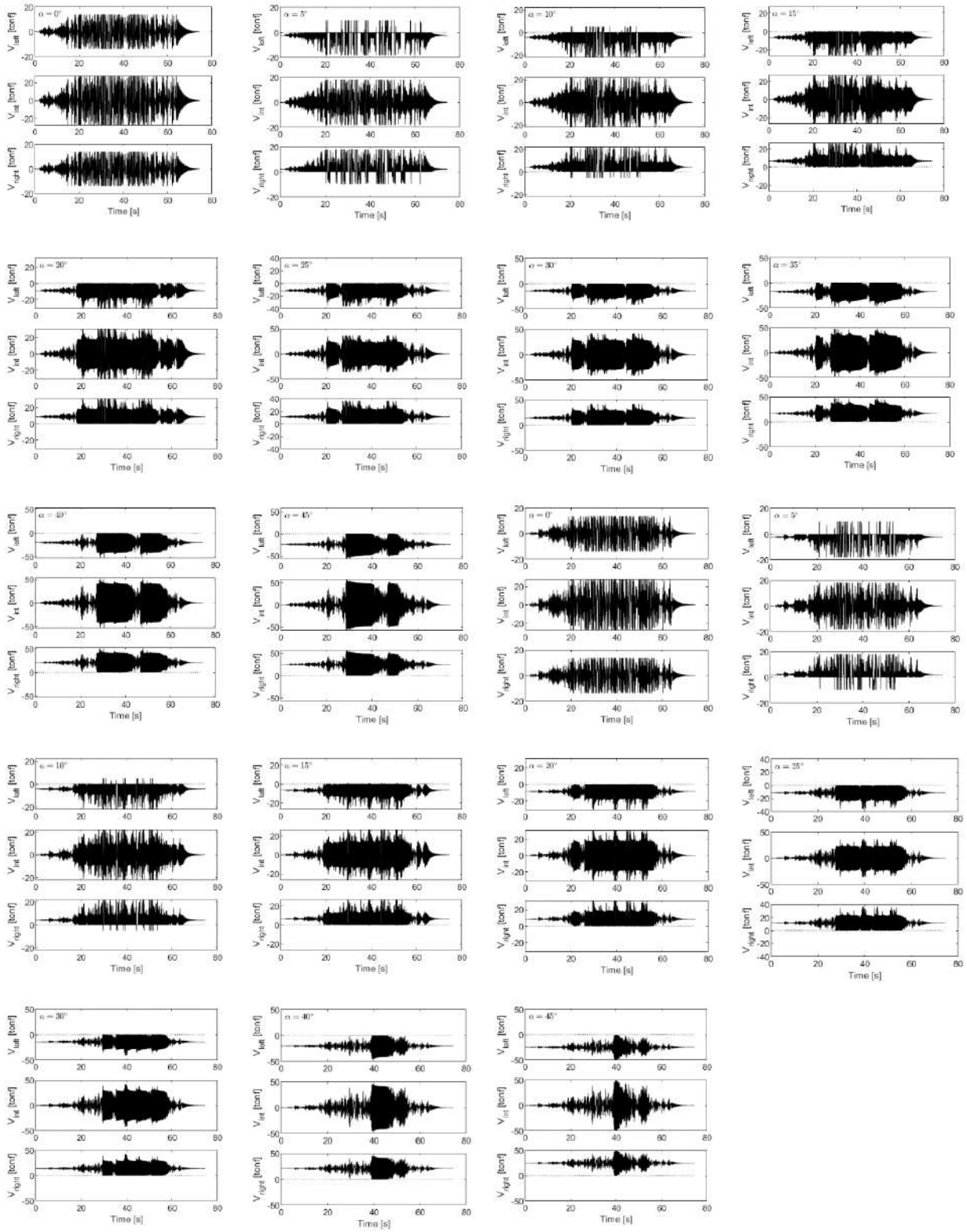
α = 0°
α = 5°
α = 10°
α = 15°
α = 20°
α = 25°
α = 30°
α = 35°
α = 40°
α = 45°
V_left [ton]
V_int [ton]
V_right [ton]
Time [s]